Characteristics of Diesel Sprays at High Temperatures and Pressures

LACOSTE Julien

Ph.D 2006

Characteristics of Diesel Sprays at High Temperatures and Pressures

LACOSTE Julien

A thesis submitted in partial fulfilment of the requirement of the
University of Brighton for the degree of
Doctor of philosophy

School of Engineering, University of Brighton
In collaboration with
Ricardo Consulting Engineers

COPYRIGHT

ABSTRACT

A high-speed video camera was used to obtain photographs of a transient spray. The spray images were analysed to provide spray characteristics which include the spray tip penetration length, initial spray hesitation, nozzle opening time delay, hole-to-hole spray variation and spray structure. Both single and multi-hole nozzles were used to study these parameters.

Fuel droplet characteristics within dense Diesel sprays were studied using Phase Doppler Anemometry (PDA) in an optical rapid compression machine. A comprehensive study of the PDA operating parameters was conducted. Additionally, the effects of injection pressure and in-cylinder pressure and temperature upon spray properties were studied.

PDA has proved to be a valuable technique in providing an understanding of the structure and characteristics of sprays. However, the application of PDA to dense sprays is difficult. The results obtained are not always reliable and the accuracy of the results is often questionable. Phase Doppler Anemometers are not immune to errors and by carefully identifying these errors, the accuracy of the technique can be significantly improved.

The effects of the PDA system parameters on the measurement accuracy have been studied. It was found that a thorough study of the operating parameters was required to tailor the system to the measurements of dense sprays. The photomultipliers voltages, the laser beam power and the size of the measurement volume all show significant effects on measured droplet diameters. Spray produced from a common-rail injection system proved to be a challenging environment for the PDA.

Following the calibration of the PDA, investigations were conducted to study the effects of various parameters on spray characteristics including injection pressure, in-cylinder pressure and temperature. Results are presented for in-cylinder pressures ranging from 1.6 to 6 MPa and injection pressures from 60 to 160 MPa. The highest injection pressure produced faster droplets and improved the spray atomisation.

TABLE OF CONTENTS

LIST OF FIGURES

LIST OF TABLES

ACKNOWLEDGEMENTS

I am most grateful to my thesis supervisors, Professor Morgan Heikal, Dr Dave Kennaird, Dr Cyril Crua from the University of Brighton and Dr Martin Gold from Ricardo CE, for all their expert guidance, insight and valuable professional advice they have given me throughout my report. It has been a challenge, a learning unique experience and a pleasure to work with them.

I would like to express my thanks and appreciation to Dr Martin Gold for his help and Steve Begg for his support on the PDA tests and set-up of laser systems. Special thanks also to the various members of the technical staff who have aided with the construction of various testing rigs, specifically: Bill, Dave, Ken, George and Tony.

Many members of the internal combustion engine group have helped me during the past months, but in particular I would like to thank Cyril, Paul, Guillaume, Kourosh and Dave.

I would like to express my deepest gratitude to my parents, my brother and Jenni for their encouragement.

This work is supported by Ricardo UK Ltd and the internal combustion engine group at the University of Brighton, and sponsored by the EPSRC.

DECLARATION

I hereby certify that this report is my own work except where otherwise indicated. I have identified my sources of information, and in particular have put in quotation marks any passages that have been quoted word for word and identified their origins.

Signed: Date:

NOMENCLATURE

Roman symbols

A .....Constant varying for each nozzle type

$A_{p.S/2}$ ..... Projected area of the upstream half of the spray [m^2]

B_d.....Beam diameter [mm]

d.....Droplet diameter [m]

d_{10}..... Arithmetic mean diameter

d_{32}..... Sauter mean diameter

D .....Nozzle orifice diameter [m]

D_e..... Equivalent nozzle diameter [m]

Do..... Sack chamber diameter of the nozzle [m]

E ..... Eykman constant

E_R .....Expander ratio

F ..... Focal length [mm]

f..... Doppler shift frequency [Hz]

L.....Nozzle length [m]

L_B.....Break-up length [m]

P_a..... Ambient pressure [Pa]

n..... Refractive index

n_{rel}..... Relative index of refraction

Q.....Amount of fuel delivery [mm^3/stroke]

r..... Round radius of nozzle [m]

S .....Spray penetration length [m]

s..... Distance between fringes [m]

T .....Temperature [°C]

t.....Injection time [s]

T_D..... Doppler period [s]

T_{phase}.....

. Period between the zero crossing of the signals from detectors 1 and 2 [s]

t_B ..... Characteristics break-up time [s]

u_d ..... Droplet velocity [m s^{-1}]

U .....Velocity component of particle normal to the fringes [m s^{-1}]

U_B ..... Penetration velocity in break-up zone [m s^{-1}]
U_{inj} ..... Velocity in nozzle orifice [m s^{-1}]
V_i ..... Initial spray velocity [m s^{-1}]
y ..... Number of particles passing through the measurement volume

Greek symbols

α ..... Beam intersection angle [deg]
? ..... Spray angle [deg]
$?_1$ ..... Angle of the incident laser beam [deg]
$?_2$ ..... Angle of the refractive laser beam [deg]
? ..... Wavelength [m]
μ ..... Viscosity [Pa.s]
? ..... Kinematic viscosity [m^2/s]
? ..... Density [kg m^{-3}]
ϕ ..... Polarisation angle [deg]
s ..... Surface tension [N/m]
? ..... Scattering angle [deg]
? ..... Phase shift [deg]
? P ..... Difference between injection pressure and ambient pressure

Subscripts

a ..... Ambient
B ..... Break-up
g ..... Gas
l ..... Liquid

Acronyms

AMD ..... Arithmetic mean diameter
ASOIP ..... After start of injection pulse
ATDC ..... After top dead centre
BK7 ..... Borosilicate
BTDC ..... Before top dead centre

CA ..... Crank angle
CCD ..... Charge coupled device
CFD ..... Computational fluid dynamic
CO ..... Carbon monoxide
DI ..... Direct injection
ECU ..... Electronically control unit
EPA ..... Environmental Protection Agency
FIE ..... Fuel injection equipment
HC ..... Hydrocarbons
HDPI ..... High-pressure direct injection
HS ..... Complete spray
ICP ..... In-cylinder pressure
LDA ..... Laser Doppler anemometry
LIF ..... Laser induced fluorescence
LS ..... Incomplete spray
LSD ..... Laser sheet dropsizing
MIE ..... Mie scatter
NO_X ..... Oxides of nitrogen
PIV ..... Particle image Velocimetry
PDA ..... Phase Doppler Anemometry
PMT ..... Photomultiplier
PTV ..... Particle Tracking Velocimetry
VCO ..... Valve covered orifice
Re ..... Reynolds number
SMD ..... Sauter mean diameter
SSMD ..... Spatial Sauter mean diameter
TDC ..... Top dead centre
We ..... Weber number
Z ..... Ohnesorge number

1 INTRODUCTION

1.1 General statement of the problem and objectives

The compression ignition (Diesel) engine, due to its associated fuel consumption efficiency, longevity and durability, has become a popular power source for many vehicles. It is the most globally accepted form of internal combustion engine for agricultural, industrial, and construction equipment along with marine propulsion engines. Concerning fuel consumption rates, Diesel engines are approximately 35% more fuel efficient than their gasoline fuelled counterparts. With advances in fuel injection control technologies, improvements in manufacturing process (such as electrical discharge machining for nozzle design) and the adoption of certain features such as turbocharging and exhaust gas recirculation (EGR), today's high-speed direct injection engines (HSDI) have become very competitive in the passenger car market. The market share for Diesel powered passenger cars is increasing in Europe and more than a third of the car buyers choose Diesel-powered cars. The performance of the current HSDI Diesel engine for passenger cars has increased to such a degree that it is now considered superior than equivalent gasoline engines.

Unfortunately, compared to the conventional, catalyst equipped, gasoline engine, the Diesel engine is notorious for being a source of particulate matter and nitrogen oxides (NO_X) emissions, which have undesired impacts on health and the environment. According to the Environmental Protection Agency (EPA) NO_X and particulate matter are responsible for:

- Respiratory problems (particulates accumulate in the respiratory system).
- Acidification and global warming.
- Deterioration of water quality.
- Formation of toxic chemicals.

In order to improve air quality, legislations on emissions from mobile sources have tightened considerably over the recent years, in the U.S.A., in Japan and in Europe. Table 1-1 shows the existing and proposed European legislation for Diesel passenger cars in Europe.

Legislation/year	CO (g/km)	HC+NO_X (g/km)	NO_X (g/km)	PM (mg/km)
Euro 1 / 1992	2.72	0.97	-	140
Euro 2 (IDI) / 1996	1.0	0.70	-	80
Euro 2 (DI) / 1999	1.0	0.90	-	100
Euro 3 / 2000	0.64	0.56	0.50	50
Euro 4 / 2005	0.50	0.30	0.25	25
Euro 5 (proposal) / 2008	-	-	*0.08*	*2.5*

Table 1-1: Overview of European emissions legislation for Diesel passenger cars. (Dieselnet.com).

As can been seen in Table 1-1, carbon monoxides (CO) and hydrocarbons (HC) are also regulated exhaust components. Carbon monoxides particularly affect children, elderly persons and individuals with respiratory diseases. Hydrocarbons react in the sunlight with nitrogen oxides to form ground-level ozone, a major component of smog.

High-pressure direct injection seems to be one of the most efficient ways to tackle stringent emission standards of Diesel engines. High injection pressures were demonstrated by Kato et al. (1989) as a way of decreasing smoke emissions without an increase in nitrogen oxide (NO_x) emissions. The use of high-pressure common rail systems in recent vehicles illustrates this efficiency. High pressures seem to induce a very different spray structure than that of earlier low pressure sprays (Baritaud et al., 1994). This is mainly due to cavitation phenomena created in the nozzle at high pressures, which result in a much faster atomisation (Tamaki et al., 1998). Recent studies (Bruneaux et al., 1999 and Dec, 1997) show that this causes better mixing followed by faster combustion, which affect pollutant formation.

A detailed understanding of the fuel injection and combustion processes of the engines is required in order to reduce these products of combustion within the engine cylinder, while not compromising the engine fuel economy. In recent years, comprehensive research studies have been carried out in the field of Diesel injection and Diesel spray characterisation. Numerical, theoretical and experimental studies all achieved important results that provide guidelines for the design of injection and combustion systems (Ficarella et al., 1998). Each of the approaches has its own unique role and contributions. With this improved understanding, cleaner combustion systems can be designed.

An experimental approach has been chosen to be the main theme of this study. The Phase Doppler Anemometer (PDA) technique was used to provide velocity and diameter measurements of individual droplets at single point location within the spray. The aim of this study was to provide injection and spray characteristics information of modern high-pressure injection systems to enhance and optimise their applications to future engine, and provide experimental data to allow the validation of CFD (Computational Fluid Dynamic) spray modelling program. In addition the data were acquired in a format that could be used to develop new models for the spray break-up process.

Phase Doppler anemometers are among the most accurate flow measurement devices. However, the technique is complicated and care must be taken to avoid errors during measurements. It is important to identify the sources of error when making PDA measurements. Hence, an appropriate phase Doppler system has to be tailored and tested under real injection conditions. Historically, as shown in Figure 1-1, most of the PDA research investigating Diesel spray properties, so far, have been undertaken at unrealistic engine conditions (Koo and Martin, 1990; Hardalupas et al., 1992; Ficarella et al., 1997). This may be attributed to the associated difficulties with measurements in dense sprays such as multiple occupancy of the measurement volume, non-spherical particles generated by aerodynamic load or viscous stresses, beam and signal attenuation. Hosoya and Obokata (1993) undertook laser Doppler anemometer (LDA) and PDA measurements on Diesel spray injected at 9.8 MPa and obtained droplet diameters up to 500 µm. Koo et al. (1997) reduced the

chamber pressure from 21 MPa to 0.6 MPa in order to avoid the aforementioned problems with dense spray measurement. Araneo and Tropea (2000) used injection durations of 8 ms in order to obtain quasi-stationary sprays. Ficarella et al. (1997) had to reduce the probe volume by cutting it with a spatial filter and increase the laser power up to 5W to ensure that reliable results were obtained. Additionally, the injection pressure was reduced to 15 MPa for the acquisition of results. At these conditions the spray no longer represented that found under real engine conditions.

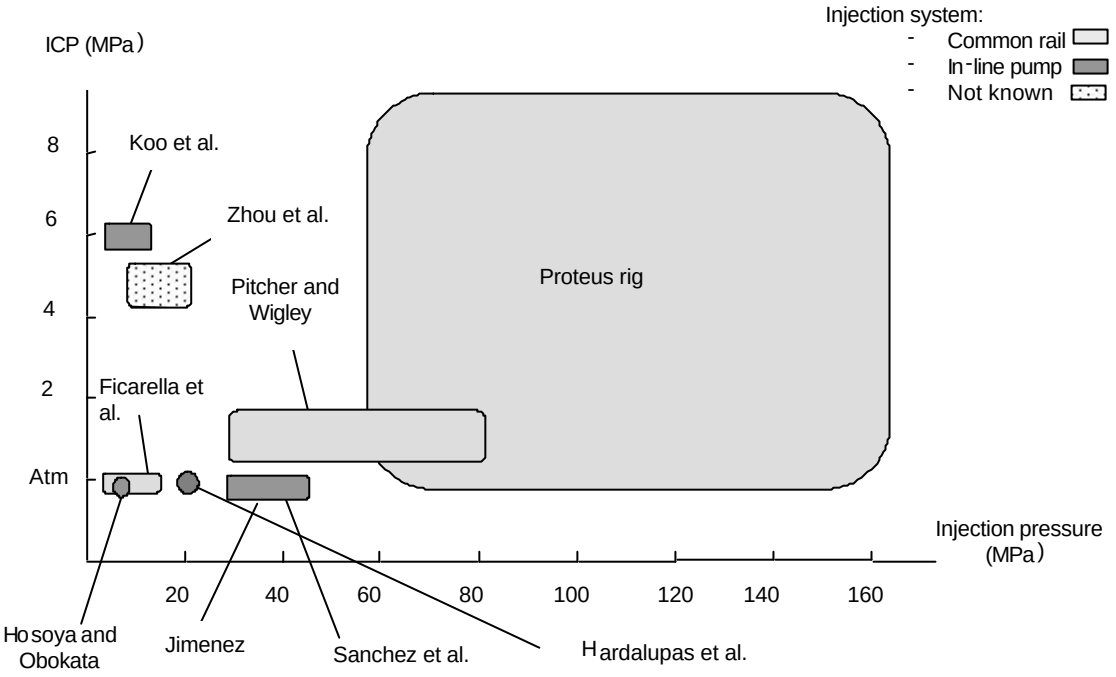

Figure 1-1: Comparison between the testing conditions of the Proteus (rapid compression machine used to gather data in this study) and those from the literature for PDA.

The difficulties in obtaining measurements in the dense spray environment within a Diesel engine mean a different approach to that classically used in LDA/PDA measurements needed to be adopted. In conjunction with flow measurement (tests will be performed at engine conditions in a pressurised chamber at ambient or heated temperature) in this project development of the measuring technique and study the sources of uncertainties such as changes of air and fuel refractive index, attenuation of the scattered light were undertaken.

1.2 General background

1.2.1 The compression ignition engine

The principle operation of Diesel engines relies on the heat within the compressed air to cause an ignition of the fuel charge. The chemical energy stored in the fuel is then converted into mechanical energy, which can be used to power tractors, locomotives and freight trucks. As no ignition device is employed, it is often called a compression-ignition engine. The idea of using compression ignition appears to have been first mentioned by French physicist Sadi Carnot in 1824. The principle on which modern automobile engines operate was invented in 1862 by Alphonse Beau de Rochas; however, it was not applied to practical engines until 1876, when the German Engineer Nikolaus Otto built the first engine in which the charge (fuel–air mixture) was compressed in the cylinder before burning. This was the engine that Rudolf Diesel, a German engineer, decided to improve when he started the experiments that led to the Diesel engine. The Diesel engine can operate either in 4 or 2 stroke principles. In automotive application, Diesels are practically always based on the 4 stroke model.

The technical characteristics of the Proteus (engine used in this study) and a DI Diesel engine are shown in Table 1-2.

Proteus		DI Diesel engine	
Compression ratio	9:1	Compression ratio	19:1
Specific heat ratio	1.3	Specific heat ratio	1.3
Intake air temperature	373 K	Intake air temperature	313 K
Intake air pressure	0.8 MPa	Intake air pressure	0.2 MPa
Temperature at TDC	721 K	Temperature at TDC	757 K
Pressure at TDC	13.9 MPa	Pressure at TDC	9.2 MPa

Table 1-2: Comparison between a modern Diesel engine and the Proteus (Crua, 2002).

1.2.2 The common-rail fuel injection equipment

The purpose of the fuel injection equipment (FIE) is to provide the engine with the adequate quantity of fuel needed in proportion to the power required and timed with a good accuracy, so that the engine will deliver that power within the

limit prescribed for fuel consumption, exhaust smoke and noise. The FIE ensures that the engine not only runs smoothly but also economically. The fuel is injected through one or several holes, located at the tip of the injector, at pressures high enough to cause the required degree of atomisation in the combustion chamber and ensure that it mixes properly with sufficient air to complete the combustion.

The fuel injection equipment includes a fuel pump, a common high pressure rail, an injector, an electric motor and an electronic control unit. The injector is mainly constructed of a triggering element (solenoid valve), a valve spring, a valve control plunger, a valve ball, a bleed orifice, a feed orifice and a needle (Figure 1-2).

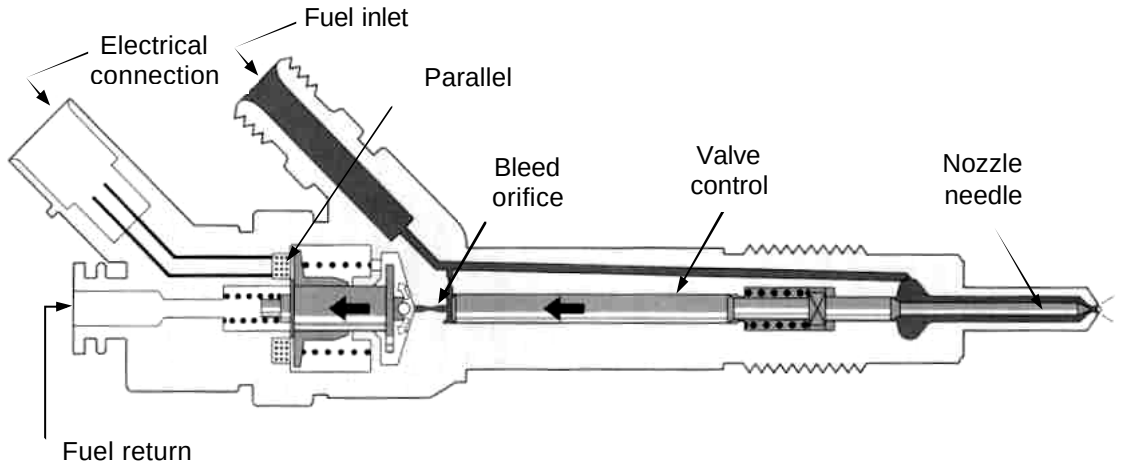

Figure 1-2: Bosch common rail injector (Bosch, 1999).

A voltage applied to the solenoid as a shaped pulse activates the coil, because the force exerted by the triggered solenoid is now higher than that of the valve spring, which then opens the bleed orifice. The lower pressure in the valve-control chamber causing a reduction in the force exerted on the control plunger will open the needle. The fuel is then injected as the pressure difference between ambient and fuel line pressure.

The Diesel fuel injection system has the most dominant effect on flow processes in the combustion of compression ignition engines; because it controls the process of fuel atomisation, and the subsequent fuel/air mixing, mixture ignition, combustion and pollutant formation (Figure 1-3).

The characteristics of Diesel spray usually include spray tip penetration, spray angle, droplet velocities, droplet sizes and distributions, and global spray structure. These characteristics in time and space form are used to describe the performance of the fuel injection system. A good understanding of these characteristics is essential for raising the combustion efficiency and reducing environmental pollution. For instance, size distribution of droplets in a spray has a fundamental effect on compression-ignition engines. Smaller fuel droplets vaporise much more quickly than large ones, but their penetration is shorter and therefore the size distribution must be optimised. Factors that may influence the droplet size distribution include the injection and cylinder pressures, geometry of the injector nozzle and speed operation of the needle (Birch, 2000). To study the droplet formation from an injector effectively, very finely resolved time measurements are essential.

The different studies previously reported attempt to explore the results of such strategies upon droplet distributions and behaviour with the emphasis on data from the core of the spray. Understanding the droplet behaviour will help explain the benefits of these injection strategies and aid in improving the mixture formation process in Diesel engines.

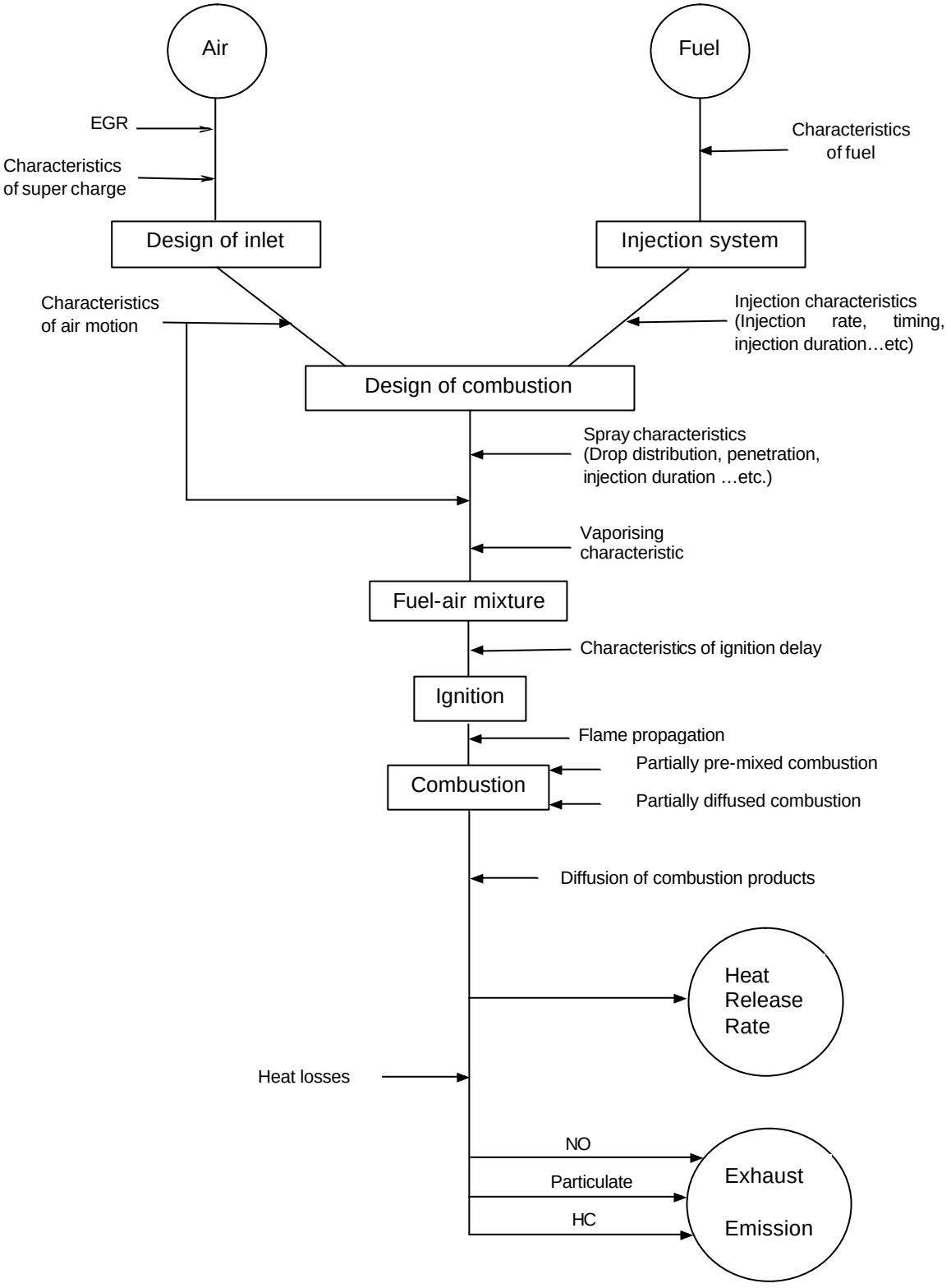

Figure 1-3: Diagram of the Diesel combustion system (adapted from Hiroyasu & Arai, 1990).

1.3 Thesis layout

Chapter two describes sprays in general and provides some background about Diesel spray research. Chapter three provides an overview of the PDA system and discusses errors specific to Diesel spray measurements. Additionally, the literature regarding PDA measurements of Diesel sprays is covered.

The characterisations of the high injection pressure spray is described in chapter 4, in which all the characteristics required to proceed to the visualisation of the spray is established and analysed. Chapter 5 provides an overview of the PDA system and some of the aspects that affect data acquisition. Chapter 6 provides phase Doppler results for the common rail injection system. Effects of in-cylinder temperature, injection and in-cylinder pressures are studied.

Finally, the conclusions and recommendations for future work are summarised in chapter 7.

2 REVIEW OF DROP SIZING TECHNIQUES AND SPRAY CHARACTERISTICS

2.1 Introduction

The atomisation of liquids is a process of great practical importance. It finds application in many branches of industry: mechanical, chemical, aerospace, metallurgy, medicine, agriculture. (Chigier, 1993). For different applications, people attempt to manipulate the spray by changing the operating conditions to satisfy their own demands. In order to understand how and why changes in operating conditions change spray characteristics, studies on the spray characterisation and the basic physical mechanisms involved in the formation of spray have to be carried out while the application is considered. Currently, the physical mechanisms of the Diesel spray formation are not completely understood. Also, in response to the demand on improving the performance of the sprays, new technologies are being explored. The sprays generated by these new technologies need to be characterised to provide necessary information for their applications.

In this study, sprays generated by a technically advanced injection system (common-rail injection system) are examined. Investigations into Diesel sprays characteristics have concentrated on the effect of the injection system parameters and ambient conditions (pressure, temperature, density, viscosity) and on global parameters such as the spray tip penetration, break-up length and droplet size and velocity distributions (Figure 2-1).

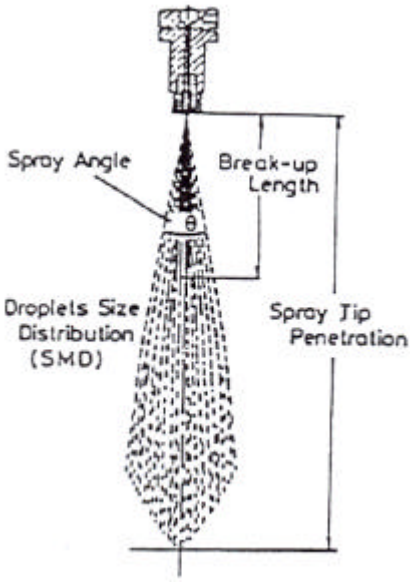

Figure 2-1: Spray parameters (Hiroyasu & Arai, 1990).

A list of works investigating Diesel sprays would be an extensive list. Therefore, in this chapter and the following one, a review of the literature to provide background about Diesel sprays, sprays in general and phase Doppler systems is undertaken.

2.2 Review of spray sizing techniques

Various techniques can be employed in spray measurement; they can be grouped into three broad categories: mechanical, electrical and optical (Lefebvre, 1989). The first category involves the capture of the spray on a solid surface (glass slide) or in a cell containing a special liquid (molten wax). The droplets are then photographed or observed with a microscope. Hiroyasu and Kadota (1974) used liquid immersion technique to determine spray droplet size in a Diesel engine. It consists of collecting a sample of the spray in cell containing a suitable immersion liquid and making a microscopic size count of droplets. This method has the advantages of keeping spherical drops and preventing evaporation. However the detection of break-up and coalescence of droplets is difficult to achieve. Mechanical methods also have the virtues of simplicity and low cost. Their main problem lies in the extraction and collection of representative spray samples.

The second category consists of the detection and analysis of electronic pulses produced by drops for calculating size distributions. The device can only be operated at relatively low velocities (<10 m s^{-1}) (Lefebvre, 1989).
The last category can be divided into imaging and non-imaging techniques and has the main advantage of being non-intrusive.

2.2.1 Direct imaging method

Direct imaging methods attempt to image droplets or particles in a plane and determine size or other parameters by analysing the recorded images (from photographic film or CCD camera). A laser sheet illuminates a plane of spray, and particles images are collected orthogonal to the illuminating sheet (Figure 2-2). The main advantages of direct imaging method are that they require relatively inexpensive equipment and the optical path arrangement is easy to set-up. However, imaging methods can be problematic when analysing dense sprays: focus issues, image overlap, and particle tracking difficulties can affect measurements.

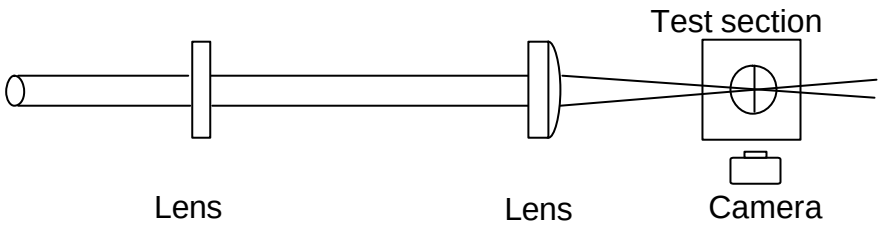

Figure 2-2: Optical set-up for direct imaging of spray (Farrell, 1999).

2.2.2 Fraunhofer diffraction method (forward scattering method)

Some droplets sizing techniques (Malvern particle sizer, diffraction-based sizing diagnostic) are based on the analysis of the Fraunhofer diffraction pattern. When a drop interacts with the laser beam, a diffraction pattern is formed in which some of the light is scattered in the near-forward direction and has an angular distribution with a width inversely proportional to the particle diameter (Figure 2-3). This technique is used to evaluate the droplet size distribution in a

spray, but it has a limited application in Diesel spray investigation due to complicated system layout and high cost. The Fraunhofer diffraction theory applies to droplets whose diameter is much larger than the incident light wavelength. This means that inaccuracies may happen when measuring particles below 5 μm in diameter (Lefebvre, 1989). Moreover, if the concentration of droplets is too high, multiple scattering occurs and alters the diffraction pattern so that Fraunhofer theory no longer applies. Dodge (1984) found that if the spray obscures more than 50% of the light, the measurement accuracy significantly reduces. Non-spherical droplets can also result in measurement errors. For further discussion on these issues the reader is referred to Lefebvre (1989).

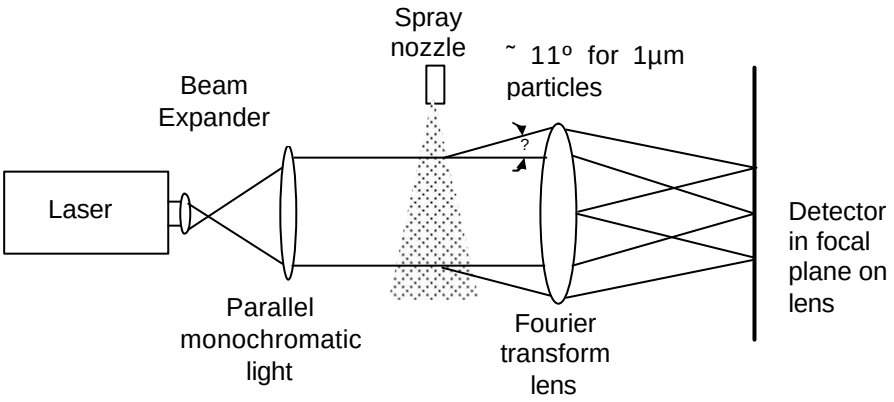

Figure 2-3: Optical arrangement employed in Malvern particle arrangement (Lefebvre, 1989).

2.2.3 Particle Imaging Velocimetry (PIV) and Particle Tracking Velocimetry (PTV)

Particle Image Velocimetry (PIV) is an application of the laser sheet technique. A laser sheet is pulsed to enable fuel particles of the spray field to be illuminated and the Mie-scattering signal produced will be then photographed by a camera. The laser light sheet is double pulsed (Faure, 1997) or triple pulsed (Farrugia et al., 1995) at a known time interval. The first pulse of the laser freezes images of the initial positions of these particles onto the first frame of the camera. The camera frame is advanced and the second frame of the

camera is exposed to the light scattered by the particles from the second laser pulse. Hence two images are acquired, the first showing the initial position of the particles and the second their final position due to the movement of the flow field. The velocity vector is then calculated by measuring the particle displacement in the known time interval. PIV technique may also utilise multiple exposed single images strategy, where each particle appears several times at different locations on the same picture. Whereas PIV performs an average of the vector velocity field over the area of interrogation using autocorrelation or the cross correlation between two separate images, the Particle Tracking Velocimetry (PTV) methods uses randomly located tracked velocity vectors obtained from the individual particles. The PTV technique has the advantage of not being biased by gradients, because individual particles are tracked. Signal amplitude dynamic range and the ability to track particles over a dynamic velocity range of more than a factor of 10 will be the limiting factors (Bachalo, 2000).

2.2.4 Laser Sheet Dropsizing (LSD)

Laser sheet dropsizing produces two-dimensional images of the Sauter mean diameter (SMD) by combining the laser sheet techniques of Mie scatter and Laser Induced Fluorescence (LIF) (Le Gal et al., 1999 and Sankar et al. 1999). These techniques can be used for qualitative and rapid measurement of fuel mass, spray geometry, and Sauter Mean Diameter. LSD allows a rapid spray characterisation. When a particle is illuminated by a laser light source, a portion of the incident light energy is absorbed by the excitable molecule that is then radiated as fluorescence. The remaining portion of the incident light experiences elastic light scattering. A laser induced fluorescence image is taken, of fluorescence from a fluorophor added to the spray. The LIF signal S_{LIF} will be given by:

$$S_{LIF} = C_{LIF} \sum_{i=o}^{N} d_i^3 , \qquad (2.1)$$

where d_i is the diameter of the droplet i and C_{LIF} is a calibration constant, which depends on the imaging system. An image is also taken using the elastic Mie scattering from the droplets. Since the fluorescence is red shifted, the two

images can be taken without interference from the other scattering process. The elastic signal S_{MIE} is given by:

$$S_{MIE} = C_{MIE} \sum_{i=0}^{N} d_i^2 , \tag{2.2}$$

providing all the droplets scatter in the Mie regime. The ratio of intensity measured by one pixel in the LIF image, to the intensity measured by the same pixel in the Mie image is then given by:

$$\frac{S_{LIF}}{S_{MIE}} = \frac{C_{LIF}}{C_{MIE}} \frac{\sum_{i=0}^{N} d_i^3}{\sum_{i=0}^{N} d_i^2} , \tag{2.3}$$

which is proportional to the Sauter mean diameter, defined by:

$$SMD = \frac{\sum_{i=0}^{N} d_i^3}{\sum_{i=0}^{N} d_i^2} \tag{2.4}$$

Thus by ratioing the two images and dividing by a calibration constant, a map of SMD in the image plane is generated with high spatial resolution. The principle advantage of the laser sheet drop sizing technique is its ability to characterise dense sprays (Le Gal et al., 1999 and Domann & Hardalupas, 2002). However, PDA measurements of known size droplets are required for its calibration. Since it is a laser sheet technique, mapping of the spray can be realised rapidly. Nevertheless, this technique is only capable of measuring Sauter mean diameter and the maximum measurable diameter is around 20 μm.

2.2.5 Holography

The spray is illuminated with a coherent beam of light in the form of a short pulse. As the duration of the laser pulse is very short, the drops contained within the measurement volume are “frozen”. Then an entire holographic image of the spray can be constructed in three-dimension. The main disadvantage of the holographic technique is that it is restricted to fairly dilute sprays (Jones, 1977) because it relies on the preservation of phase differences in the light scattered from the droplets. Moreover, it is a relatively complicated optical system that requires delicate manipulation of the lighting sources. However, it has the

advantages of measuring droplets as small as 1 μm and picture of the width of the spray can be instantaneously obtained.

2.2.6 Limitations of the present techniques

None of the sizing techniques previously described is totally satisfactory. Many useful techniques have been developed, each with its own advantages and limitations. Of the optical methods discussed, phase Doppler anemometry presents the advantage of obtaining simultaneous measurements of single particles size and velocity. Furthermore PDA is ideally suited to applications requiring high spatial resolution. Besides, Fraunhofer diffraction, holography, particle imaging velocimetry and particle tracking velocimetry are not considered as reliable techniques to undertake measurements in regions of sprays with high droplet number density.

2.3 Formation of liquid sprays

In the most basic sense, a spray is simply the introduction of liquid into a gaseous environment through a nozzle such that the liquid, through its interaction with the surrounding gas and by its own instability, breaks-up into droplets. The formation of a spray begins with the detaching of droplets from the outer surface of a continuous liquid core extending from the orifice of the injection nozzle (Figure 2-4).

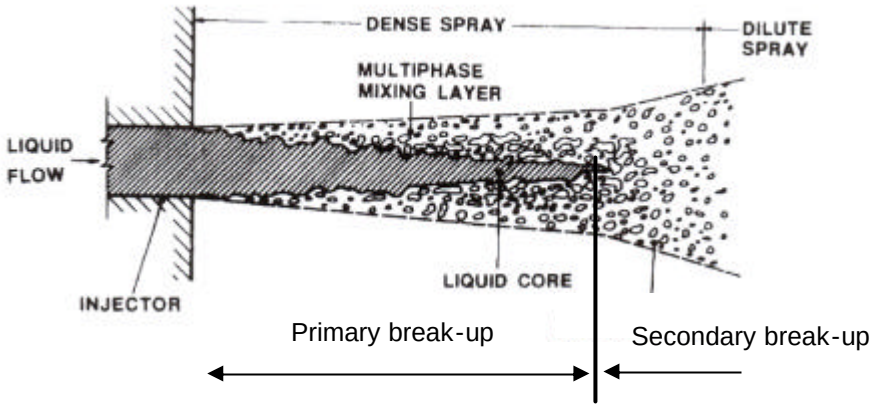

Figure 2-4: Sketch of the flow pattern of a pressure-atomised spray near the nozzle tip region (Faeth et al., 1995).

The detaching of the liquid core into ligaments or large droplets is called primary break-up, which involves the action of forces internal to the liquid jet. The liquid ligaments and large droplets will further break-up into small droplets due to the interactions between the liquid ambient gas or droplet collisions. The process of this further break-up is called secondary break-up. The near nozzle region, where the volume fraction of the liquid is usually larger than that of the ambient gas is called the dense spray region. Correspondingly, the downstream region where the volume fraction of the liquid is relatively low is called the dilute spray region.

2.4 Atomisation process

2.4.1 Dimensionless criteria of the atomisation process

To achieve a fuller understanding of the atomisation process, a number of non-dimensional numbers have been derived as follows:

- Weber number (We): expresses the ratio of dynamic forces of an ambient gas to the surface tension. It defines the effect of external factors on the drop development.

$$We = \frac{Inertia}{SurfaceTension} = \frac{?_g d u_d^2}{s_l}, \quad (2.5)$$

where $?_g$ is the gas density, d the droplet diameter, u_d the droplet relative velocity and s_l the liquid surface tension.

- Reynolds number (Re): denotes the ratio of inertial force to viscous force.

$$Re = \frac{Inertia}{Viscosity} = \frac{?_l u_d L}{\mu_l} = \frac{u_d L}{?_l}, \quad (2.6)$$

where ν_l is the kinematic viscosity, $?_l$ the liquid density and L the nozzle length.

- Ohnesorge number (Oh): defines the ratio of internal viscous forces to surface tension forces.

$$Z = \frac{Viscosity}{Tension} = \frac{\sqrt{We}}{Re} \quad (2.7)$$

These dimensionless numbers will be used in the structure of Diesel spray section to describe the break-up and the penetration length.

2.4.2 Mechanisms of atomisation

The process of atomisation is one in which liquid is disintegrated into drops and ligaments by the action of internal and external forces; it leads to the spray formation. It proceeds more easily if the liquid is present in a form that is more susceptible to disintegration: thin jets or liquid sheets, because they have the highest surface energy and thus the greatest instability (Lefebvre, 1989). Atomisation plays a major role in the combustion process, where a large amount of droplets are required for better vaporisation, mixing and combustion.
The atomisation processes, as shown in Figure 2-5, can be divided into incomplete (laminar flow regime in the injection hole) and complete sprays (cavitating flow regime).

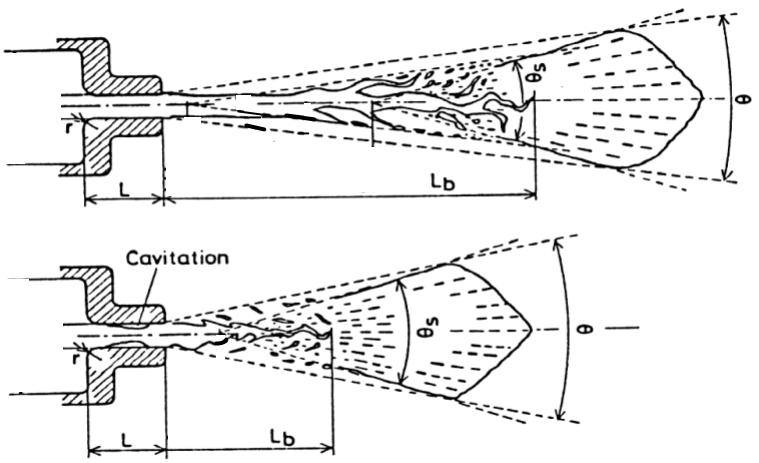

Figure 2-5: Internal structures of complete and incomplete sprays (Hiroyasu & Arai, 1990).

The atomisation process depends mainly on the injection velocity in the nozzle hole. The spray cannot be formed correctly (incomplete spray) for low injection velocities, causing an insufficient atomisation, with a long transformation process from liquid column to droplets. However, when cavitation (complete spray) is initiated in the injection holes, by increasing the injection velocity, dramatic changes occur in the spray structure. A rapid disintegration process from jet to fine spray appears.

Soteriou et al. (1995) reported that cavitation in the nozzle holes is the predominant mechanism causing atomisation in the sprays. The cavitation is beneficial to spray atomisation and causes atomisation of the jet immediately on the nozzle hole exit. Two different mechanisms causing cavitation in Diesel fuel injection equipment have been reported: dynamically induced cavitation and geometry induced cavitation. The cavitation occurring in the holes of standard direct injection nozzles is categorised as geometry induced cavitation which could occur in steady state as well as in transient flow. It is initiated by local high velocities within a separated boundary. The high velocities could result in sufficiently large reduction in local pressure to cause the formation of vapour bubbles. This type of cavitation produces an homogeneous opaque foam, rather than large voids. The intensity of geometry induced cavitation of an orifice could

be indicated by a cavitation number which is defined as the ratio of a factor tending to create cavitation, such as an average flow velocity or pressure drop across the orifice, to a factor tending to suppress it, such as downstream pressure. The jet from each nozzle hole diverges and atomises when cavitation first occurs within the hole. The spray angle increases significantly once the cavitation spreads across and down to the bottom of the hole.

Arcoumanis et al. (1997) reported three different atomisation models:

- Aerodynamic-induced atomisation: waves develop on the surface of the liquid jet, caused by relative motion between the injected fuel and the gas. The Weber number is used to determine the growth rate of these waves and the disintegration of the jet into smaller droplets and the Ohnesorge number for the liquid viscosity effects.
- Jet turbulence-induced atomisation: at fully turbulent flow conditions in the injector nozzle holes, the radial velocity component in the jet soon leads to disruption of the surface film, followed by general disintegration of the jet. Even when injected into vacuum, the jet will disintegrate under the influence of its own turbulence.
- Cavitation-induced atomisation: the liquid jet emerging from the injection hole disintegrates due to the collapsing of the cavitation bubbles present at the exit of the holes. Since the pressure around the emerging jet is much higher than the pressure inside the cavitating bubbles, these bubbles gradually collapse while they are circulated by the internal jet turbulence. This process causes perturbation on the surface of the liquid jet. The perturbations lead to jet disintegration and formation of smaller droplets at the time of total bubble collapse or at the time the bubble reach the jet surface.

A recent review from Smallwood and Gülder (2000) provided more in-depth investigation into the mechanism of atomisation. The authors showed that the spray is completely atomised at or near the nozzle tip, where nozzle cavitation and turbulence-driven instabilities are the dominant break-up mechanisms. The influence of cavitation on jet break-up is dual:

- Bursting and collapsing of vapour cavities contribute to the disintegration of liquid masses at the exit of the nozzle hole, resulting in a mixture of bubbles and liquid occupying most of the cross-sectional area.
- Cavitation increases the turbulence of the flow through the nozzle, thus contributing to the instability of the liquid jet. The instability, along with the pressure fluctuations in the nozzle, cause variation in the exit velocity of the droplets, resulting in temporal and spatial clustering droplets in the plume.

2.4.3 Effects of injection pressure and nozzle shape on atomisation

As previously mentioned, high injection pressures combined with small nozzle hole diameters can provide better spray formation, better air entrainment, better air-fuel mixing, and more homogeneous mixture with lower equivalence ratio and fewer over-rich regions. In a study of a 250 MPa high injection pressure Diesel spray, Minami et al. (1990) concluded that fuel droplets in the spray became finer with an increase in injection pressure, and even finer by using a smaller diameter nozzle hole. However, there are other ways to improve the spray atomisation, such as improvement of the nozzle configuration. Su et al. (1995) pointed out that the nozzle configuration has an important effect on the fuel atomisation. The configuration includes the following factors: the surface area of the nozzle hole, the entrance shape of the hole, the number of holes, the length to diameter ratio, the orientation of the nozzle holes with respect to the nozzle axis and the sac volume. The authors used a mini-sac injector with two types of nozzle hole entrances: sharp-edged and round-edged inlet. Higher injection pressures resulted in longer spray tip penetrations, narrower spray angles and smaller particle sizes for both nozzle entrance shapes. The sharp-edged inlet nozzle produced a wider spray dispersion angle, smaller SMD and a smaller value of particulate emission, compared to the round-edged inlet tip.

Atomisation can also be improved by increasing the fuel flow velocity in the nozzle hole. Yoda and Tsuda (1997) found that an increase of the fuel flow velocity enabled the improvement of the atomisation without increasing the

injection pressure. The atomisation can also be improved by enlarging the chamfer at the spray hole inlet, which also improved the fuel flow velocity at the spray hole outlet.

2.5 Structure of Diesel sprays

2.5.1 Break-up length

The break-up length characterises a point of discontinuity, where the spray changes from a densely packed zone of liquid (bulk liquid, or interconnected ligaments and droplets), to a finely atomised regime of droplets. After the disintegration of the liquid column emerging from the nozzle, the generated droplets may further break-up into smaller ones as they move into the surrounding gas. Due to a relative velocity between the droplets and the gas, a surrounding non-uniform pressure develops, causing the particles to deform. Development of this deformation leads to break-up into smaller droplets. The forces associated with dynamic pressure, surface tension and viscosity control the break-up of a drop. To achieve a fuller understanding a dimensional analysis can be carried out.

Shimizu et al. (1984) measured the break-up length in the spray flow region by measuring an electrical resistance between the nozzle and a fine wire net located in the spray jet. The researchers found that the break-up length decreased with an increase in injection velocity, finally reaching a constant value. The same technique was applied by Hiroyasu and Arai (1990) for the effects of injection velocity, ambient pressure and nozzle geometry on the jet break-up length. Figure 2-6 displays the effects of these parameters on the break-up length. The injected liquid did not break-up instantly after the start of injection. There is about 10-30 mm of break-up length; even when the injection pressure is higher than 20 MPa.

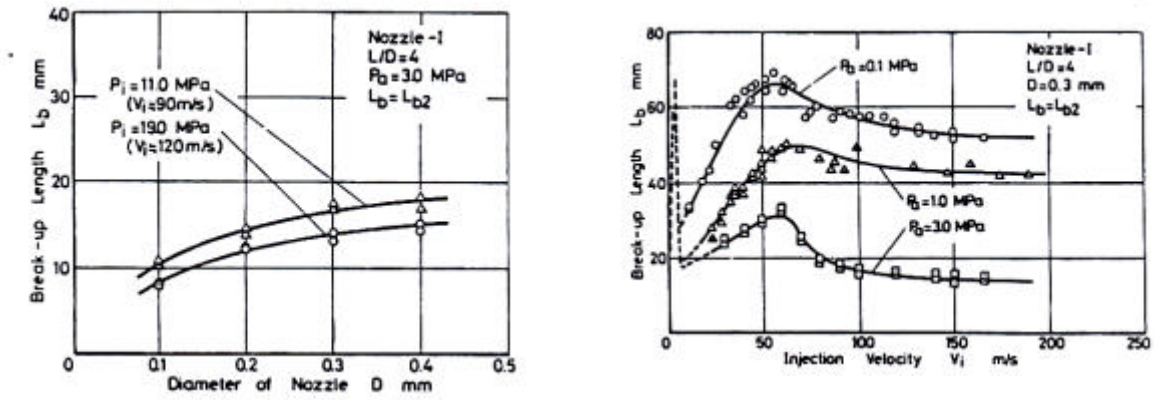

Figure 2-6: Effect of nozzle diameter and injection velocity on break-up length (Hiroyasu & Arai, 1990)

The authors also found that the break-up length varied inversely with ambient pressure, but its dependence on injection velocity is more complicated. Break-up processes and momentum both contribute to determine the break-up length, resulting in a non-linear dependence on injection velocity (Figure 2-7).

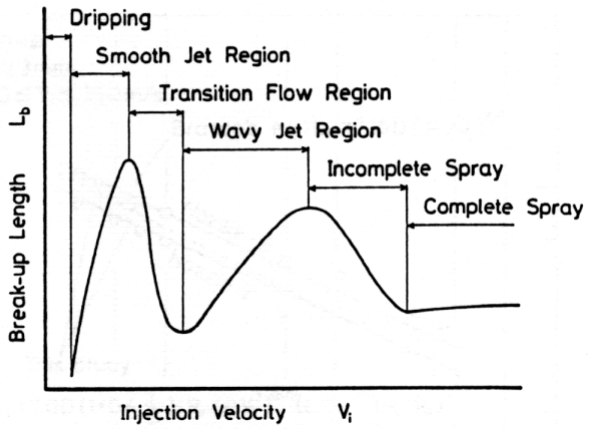

Figure 2-7: Break-up behaviour of a liquid jet (Hiroyasu & Arai, 1990).

A correlation valid for any complete region was developed considering the effect of the nozzle shape and the cavitation number on the break-up length.

$$L_B = 7D_N\left(1+0.4\frac{r}{D}\right)\left(\frac{P_a}{?_l V_i^2}\right)^{0.05}\left(\frac{L}{D}\right)^{0.13}\left(\frac{?_l}{?_g}\right)^{0.5}, \qquad (2.8)$$

Yule and Filipovic (1992) measured the break-up zone characteristics of Diesel sprays injected into a high-pressure gas. Three different single-hole nozzle diameters were used: 0.265, 0.213 and 0.46 mm with L/D ratio of 2, 3.6 and 1.65 respectively. The mean injection pressures during full opening pressure were 21, 31.2 and 25.4 MPa and the injection durations were 1.36, 1.5 and 1.9 ms correspondingly. The authors estimated the break-up length with indirect techniques which included the computation of the overall void fraction of the spray, as a function of time, and curve fitting a new penetration correlation that incorporated break-up time as an adjustable empirical constant. With curve fitting of the correlation to the measured spray tip penetration length, the break-up time, the break-up length and the characteristic velocity in the break-up zone were obtained:

$$\frac{L_B}{D_N} = 2.8 \times 10^4 \, We_B^{-0.46} \tag{2.9}$$

$$t_B = 8.9 \times 10 We_B^{-0.46} Re_B^{-0.3} \frac{D}{U_{inj}} \tag{2.10}$$

$$\frac{U_{inj}}{U_B} = 31.7 Re_B^{-0.3}, \tag{2.11}$$

where $We_B = \frac{\rho_g U_B^2 D}{\sigma_l}$, $Re_B = \frac{U_B D_e}{\nu_l}$ and $D_e = D\left(\frac{\rho_l}{\rho_g}\right)^{0.5}$. These equations are applicable for $Re_B<10^5$. Note that the calculation of Re_B is based on derived diameter D_e.

Yule and Salters (1995) found, with a flat probe, that Diesel spray break-up length is of the order of 100 nozzle diameters at gas density corresponding to those found at realistic operating conditions. Also the break-up length increases with liquid viscosity. In addition, the authors discovered that the unbroken liquid structure appears to exist in significant portion as distributions of interconnected sheets and ligaments and not simply as a central column.

Hattori et al. (2002) conducted an experimental investigation to study the disintegration process from a liquid fuel to a Diesel spray. The visualisation of the initial break-up of the non-evaporative spray was undertaken by applying a

laser sheet scattering method and a high resolution microscopic photograph technique. The fuel spray was injected at 32 MPa into a constant volume chamber capable of reaching 3 MPa. The authors divided the break-up of the initial stage of injection into six stages. At the first stage, the spray is formed of an intact liquid pillar and begins to break-up at its tip towards stage two. During stage three the droplets spread in the radial direction to form a sphere cloud. At the fourth stage, the spray is lengthened with time and the tip changes its shape from the sphere to a triangular pyramid. At the following stage, the protruded liquid fuel is broken up and depressed by the resistance of the ambient gas. The number of droplets left around the liquid core increase with time. At the last stage, after 70 μs from the start of injection and at a distance of 3 mm from the nozzle tip, the break-up on the surface of the pillar begins and the whole spray is covered by the group of fuel droplets.

2.5.2 Spray Penetration

The spray penetration is defined as the maximum distance from the nozzle to the tip of the spray at any given time and is one of the most important characteristics of the combustion process. If the spray penetration is too long, there is a risk of impingement on the wall of the combustion chamber, which may lead to fuel wastage and the formation of soot. This normally occurs when the chamber wall is cold and where there is limited air motion. However, a short penetration will reduce mixing efficiency hence resulting in poor combustion. Hence the information of spray tip penetration would be useful for the design of the engine combustion chamber. The dependence of penetration on injection parameters differed significantly from one investigation to another.

Dent (1971) briefly reviewed some data previously published on spray penetration from studies on hot and cold bombs and engines. An empirical correlation Equation (2.12) based on gas jet theory was derived, which indicated that the spray penetration increases with the injection pressure, whereas the gas density and temperature had the reverse effect. He applied a factor of $(295/T_g)^{1/4}$ to correct the effect of the fluid temperature on the gas temperature at the nozzle.

$$S = 3.01\left[\sqrt{\frac{?P}{?_g}}tD\right]^{1/2}\left(\frac{295}{T_g}\right)^{1/4} \quad (2.12)$$

The comparison between theoretical and experimental data was generally good, except for the early stage of the injection, where the equation was found to over predict the tip penetration.

Hay and Jones (1972) carried out a review of the literature pertaining to theoretical or experimental correlation of spray penetration variables, twelve correlations were found. According to their research, Dent's correlation proved to give acceptable results with experimental data from several sources. However, they advised against its use for exceptionally large pressure chamber (P > 10 MPa).

Hiroyasu and Arai (1990) measured the spray tip penetration with the aid of photographic techniques at different conditions and suggested that it could be divided into two phases. During the first period, the spray behaved as a steady jet with a tip velocity equal to the jet exit velocity. After the break-up, the jet disintegrated to form a spray, with a tip penetration proportional to $t^{0.5}$.

$t < t_{break\text{-}up}$

$$S = 0.39 \times t\sqrt{\frac{2\Delta P}{?_l}} \quad (2.13)$$

$t > t_{break\text{-}up}$

$$S = 2.95\left(\frac{?P}{?_g}\right)^{1/4}\sqrt{Dt} \quad (2.14)$$

$$t_B = 28.65\frac{?_l D}{\sqrt{?_g ?P}} \quad (2.15)$$

Increasing the ambient pressure was shown to decrease the spray tip penetration as well as the break-up length. Changing the ambient temperature had a minor effect on the spray tip penetration, due to a corresponding reduction in ambient density. However, a reduction in the spray angle was observed at higher temperatures, suggesting that the evaporation of the droplets were confined to the region on the periphery of the spray.

Yule and Filipovic (1991) derived a new equation for sprays produced by simple orifice Diesel injectors, taking into account the transition from the nozzle to the downstream spray.

$$S = 3.8\left(\frac{?P}{?_g}\right)^{0.25} D_N^{0.5} t^{0.5} \tanh\left[\left(\frac{t}{t_B}\right)^{0.6}\right] \quad (2.16)$$

The break-up time is an adjustable constant, which is proportional to the time at which the spray penetration distance is the same as the break-up length. Moreover, the agreement with experimental data was found to be excellent.

Chang and Farrel (1997) investigated the effects of fuel viscosity and nozzle geometry on high injection pressure Diesel spray. The authors found that Hiroyasu's correlation (2.14) over predicted spray tip penetration except for case of high fuel viscosity and nozzles with rounded inlets.

The effects of ambient gas density and fuel vaporization on spray penetration were examined by Naber and Siebers (1996). The sprays were generated with an electronically controlled, common-rail, single-hole injector. The injection pressure was 137 MPa and the diameter of the nozzle hole was 0.257 mm. A high-speed camera was used to record the behaviour of the sprays in a constant-volume combustion chamber. The ambient density was varied between 3 and 200 kg m^{-3}. Figure 2-8 shows the ambient gas density effects on the penetration of non-vaporising and vaporising sprays respectively. The most noticeable trends are the decrease in penetration with an increase in ambient density and the decreasing rate of penetration with time. The effect of vaporisation was to reduce the penetration. The reduction is as much as 20% at the low density conditions. The effects of vaporisation became smaller for longer penetration distance and high gas density.

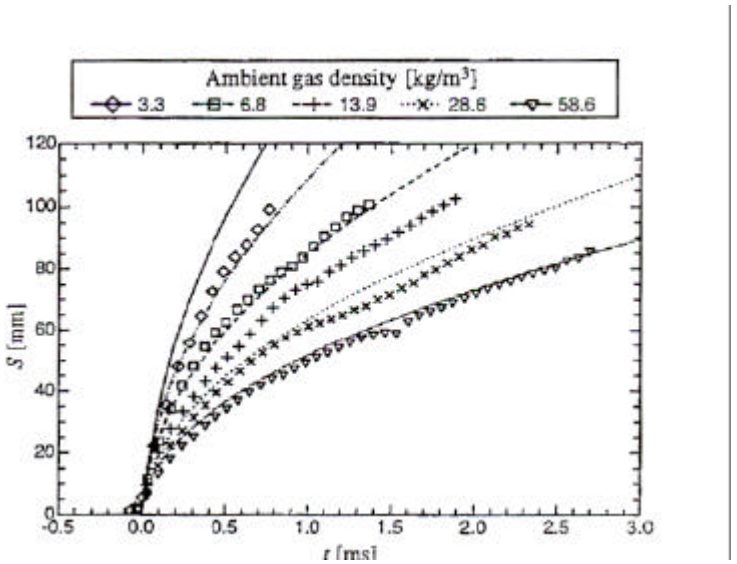

Figure 2-8: Vaporising spray penetration vs. time (Naber & Siebers, 1996).

The effects of gas density on liquid and vapour penetration were also investigated by Kennaird et al. (2002). Non-vaporising and vaporising sprays were studied for injection pressures varying between 60 and 160 MPa and densities varying between 14 and 49 kg m^{-3}. High injection pressure was found to produce a completely develop spray in a shorter period of time. The experimental data was compared with a spray penetration theory (Equation 2.10) proposed by Hiroyasu and Arai (1990) and a good agreement was found for a coefficient of 6.5. The vapour propagation was faster with an increase in injection pressure but became slower with higher gas densities.

System	Variable	Input	Effect on liquid spray penetration distance
Injector	Orifice diameter	decrease	Strong decrease
	Injection pressure	increase	Weak increase
	Nozzle aspect ratio	increase	No significant effect
Engine	Ambient density	increase	Strong decrease
	Ambient temperature	increase	Strong decrease
Fuel	Fuel temperature	increase	Linear decrease

Table 2-1: Parameters affecting the liquid spray penetration distance (from Smallwood & Gülder, 2000).

2.5.3 Spray cone angle

The spray cone angle is defined as the angle formed by two straight lines drawn from the injector tip to the outer periphery of the spray at 60 d_0 downstream from the nozzle (Lefebvre 1989). According to Naber and Siebers (1996), the definition of the spray angle and the spray penetration are dependent on each other. Therefore the spray angle can be defined as follow:

$$? = \tan^{-1}\left(\frac{A_{p.S/2}}{(S/2)^2}\right), \tag{2.17}$$

where $A_{p.S/2}$ is the projected area of the upstream half of the spray in an image. The spray cone angle is a qualitative indicator of how well the spray disperses. It is influenced by the nozzle dimensions, the liquid properties and the density of the medium in which the spray is introduced.

The influence of the nozzle aspect ratio (L/D) on the spray angle was examined by several researchers. Shimizu et al. (1984) showed that an L/D of approximately 4 or 5 gave the maximum cone angle and shortest break-up length and also that an increase and decrease of L/D gave respectively a smaller cone angle and longer break-up length. The effects of kinematic viscosity and injection pressure on the spray cone angle were examined by Hiroyasu et al. (1990, 1998). They found that spray angles were widened by a reduction in liquid viscosity and an increase in injection pressure (Figure 2-9), before stabilising after reaching a maximum value. An experimental correlation for the spray angle was developed from these observations:

$$? = \left(\frac{L}{D}\right)^{-0.22}\left(\frac{D}{D_0}\right)^{0.15}\left(\frac{?_g}{?_L}\right)^{0.26} \tag{2.18}$$

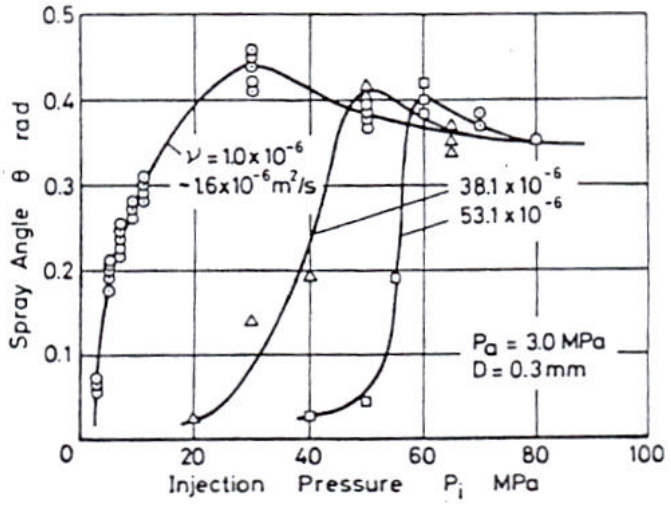

Figure 2-9: Effects of kinematic viscosity and injection pressure on the spray angle (Hiroyasu & Arai, 1990).

2.5.4 Droplet diameter and size distribution

A spray is occasionally defined as a system of droplets plunging through a gaseous continuous phase. The droplets usually do not exist at a uniform drop size throughout the spray due to the variety of atomisation processes, droplet-droplet interactions and their heterogeneous nature (Lefebvre 1989). Instead, droplets tend to fall within some distribution around some mean values.

Hence, looking at the microscopic structure of the spray is, in a sense, defining the degree of atomisation of the spray. Such microscopic details give clues to the fuel distribution processes involved and may help explain emissions and performance behaviour.

2.5.4.1 Mean diameters definition

Sprays are often described by the mean diameter of the droplets. Mean diameters are calculated using the general relationship proposed by Mugele and Evans (1951) and are summarised in Table 2-2.

$$d_{ab} = \left(\frac{\sum_{i=0}^{N} N_i d_i^a}{\sum_{i=0}^{N} N_i d_i^b} \right)^{\frac{1}{a-b}}, \qquad (2.19)$$

where d_i is the representative diameter of class i, N_i is the number of count of droplet in class i and a, b are integers.

a	b	Name of mean diameter	Symbol	Expression	Application
1	0	Length or arithmetic diameter (AMD)	d_{10}	$\frac{\sum N_i d_i}{\sum N_i}$	Comparisons
2	0	Surface area	d_{20}^2	$\left(\frac{\sum N_i d_i^2}{\sum N_i}\right)^{\frac{1}{2}}$	Surface area controlling
3	0	Volume	d_{30}^3	$\left(\frac{\sum N_i d_i^3}{\sum N_i}\right)^{\frac{1}{3}}$	Volume controlling
2	1	Surface area-length	d_{21}	$\frac{\sum N_i d_{1_i}^2}{\sum N_i d_i}$	Absorption
3	1	Volume-length	d_{31}^2	$\left(\frac{\sum N_i d_i^3}{\sum N_i d_i}\right)^{\frac{1}{2}}$	Evaporation
3	2	Sauter Mean Diameter (SMD)	d_{32}	$\frac{\sum N_i d_i^3}{\sum N_i d_{i_i}^2}$	Vaporisation
4	3	De Brouckere	d_{43}	$\frac{\sum N_i d_i^4}{\sum N_i d_{i_i}^3}$	Combustion equilibrium

Table 2-2: Mean diameters and their applications (Lefebvre, 1989).

Two different mean diameters are commonly used in PDA studies: the arithmetic mean diameter and the Sauter mean diameter. The Sauter mean diameter of a spray represents the diameter of the droplet that has the same volume / surface ratio as that of the total spray. It indicates the quality of the atomisation process. The smaller the SMD, the finer the spray droplets which mean the better the spray atomised. It is also the most useful value for determining the rate of evaporation.

2.5.4.2 Droplet size distribution of sprays

Although sprays are often characterised by their mean droplet diameter, this number can vary greatly depending on the location and time of the calculated measurement (Reitz & Diwakar, 1987; Hiroyasu & Kadota, 1974). Additionally, it

is possible to measure two different sprays with the same arithmetic mean diameter or Sauter mean diameter. Thus, it is more correct, although more tedious and complex, to describe sprays, by their local droplet size distribution. Droplet size data is often displayed as a histogram, which is a bar plot of the number of droplets for a given drop size bin.

In order to simplify the description of droplet size distribution, several researchers have tried to replace drop sizing data with mathematical expressions that are defined with one or more parameters. There are several functions used to represent droplet distribution for both size and velocity, among them:

- Normal distribution

The normal distribution function is based on the random occurrence of a given drop size. Its application is limited to processes that are random in nature and where no specific bias is present. It is usually expressed in terms of a number distribution function *f(d)* that gives the number of particles of a given diameter d:

$$f(d) = \frac{1}{s_n\sqrt{2p}}\exp\left[-\frac{1}{2s_n^2}\left(d-\bar{d}\right)^2\right], \tag{2.20}$$

where s_n is a measure of the deviation of values of d from a mean value $\bar{d}$. s_n is usually referred to as standard deviation, and s_n^2 is the variance.

- Log-Normal distribution

Many particle size distributions that occur in nature have been found to follow the Gaussian or normal distribution law if the logarithm of the particle diameter is used as the variable. With this modification, the Normal distribution Equation becomes:

$$f(d) = \frac{1}{ds_n\sqrt{2p}}\exp-\left[\frac{1}{2s_n^2}\left(\ln d - \ln\overline{d_{ng}}\right)^2\right], \tag{2.21}$$

where $\overline{d_{ng}}$ is the number geometric mean drop size and s_g is the geometric standard deviation.

A wide range of empirical functions have also been developed to characterise the droplet size distribution in a spray; among these are Rosin-Rammler, Nukiyama-Tanasawa and chi-square (Lefebvre, 1989; Koo & Martin, 1991). The main disadvantage of these functions come from the fact that they are specific to the single studied injector and cannot be used for evaluation of a new design.

2.5.4.3 Injection parameter effects on droplet size distribution

The effects of injection parameters like nozzle geometry, injection pressure, ambient conditions and fuel properties on droplet size distribution were studied by several researchers (Hiroyasu & Kadota, 1974; Arai et al., 1985 and Tabata et al., 1991).

Shimizu et al. (1984) examined how SMD varied with the injection pressure, ambient gas pressure, nozzle geometry and fuel viscosity. This was done through a broad set of experiments with a constant injection pressure and ambient conditions at steady state. It was found that for a spray to have a fine droplet distribution there was an upper limit for fluid viscosity and also a lower limit for injection pressure. Higher fuel viscosity resulted in higher SMD as did lower injection pressure. SMD was minimised for a L/D ratio of 4 at low injection pressure and also for increased ambient gas pressure. At higher injection pressures, SMD appeared independent of the ambient gas pressure. The spray SMD also increased with an increase of nozzle hole diameter and this trend held for those sprays under all injection pressures and ambient pressures.

Tabata et al. (1991) examined the effects of ambient temperature on Diesel spray drop size by using the Fraunhofer diffraction technique in a high pressure environment. The experiments were undertaken with an injection pressure of 22 MPa, ambient pressures from 0.1 MPa to 3 MPa and from ambient temperatures varying from 300 K to 800 K. Measurements of the droplet size were obtained 60 mm downstream from the nozzle. The authors found that the SMD increased with an increase of viscosity and surface tension. At high injection pressure (larger than 10 MPa), the SMD increased with an increase in

ambient pressure. However, at low injection pressure, the SMD decreased with increasing ambient pressure.

Farrar-Khan et al. (1992) studied the influence of the nozzle sac volume on spray penetration, atomisation and velocity. Four multi-hole nozzles with a sac volume varying from 0 to 1.34 mm^3 were investigated at an injection pressure of 21.5 MPa. A reduction in sac volume reduced the SMD by 3 to 4 µm.

SMD is not only a function of physical injection parameters but also of time and location within the spray. Hiroyasu and Kadota (1974) looked at SMD variation with sampling location. In terms of droplet size behaviour with radial distance from the spray axis, they discovered that droplets were small on the edge of the spray and large along the spray axis (Figure 2-10). Droplets were found to be large near the nozzle and small further along the spray axis. Although, the droplet size decreased rapidly downstream of the nozzle, there was an eventual increase in droplet size far downstream. This phenomenon was attributed to the collision and coalescence of droplets in the higher gas density environment found far from the nozzle.

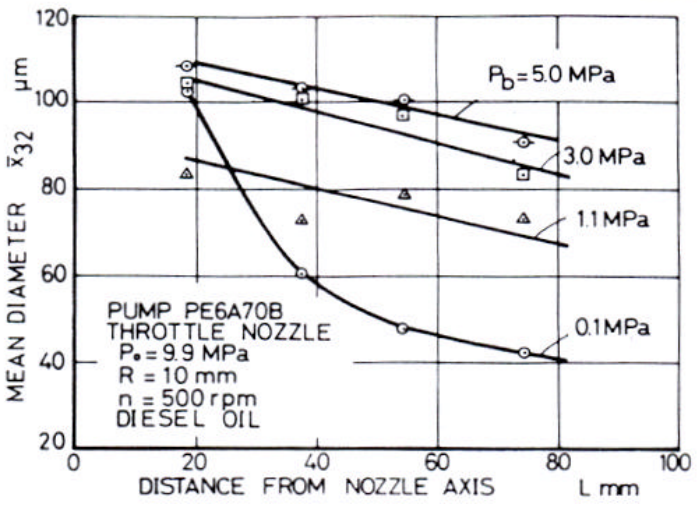

Figure 2-10: Sauter mean diameter a various sampling locations (Hiroyasu and Kadota, 1974).

The research previously reported in this chapter have been undertaken at low injection pressures; Minami et al. (1990) attempted to investigate high pressure Diesel spray using holography, high speed and shadow photography. The authors used high injection pressure equipment capable of producing injection pressure up to 280 MPa. The authors found that the SMD became finer with an increase in injection pressure and even finer with a reduction in hole diameter. The measurement undertaken in this study seemed to follow the trend observed by investigators at lower injection pressure; however the SMDs calculated were around 5 to10 µm smaller.

2.5.4.4 Equations for mean drop size

The physical processes involved in atomisation are not well understood for mean diameters to be expressed in terms of equation derived from first principles. Therefore, most of equations concerning the droplet size distribution have been empirical in nature and have resulted in empirical equations for mean droplet diameter. These equations are often express mean diameter (AMD or SMD) in terms of dimensionless group such as Reynolds number, Weber number or Ohnesorge number. The mean diameter equations presented below are only a small summary of what is available in the literature. More detailed information on drop size equations may be found in Lefebvre (1989).

By taking into account the effects of injection pressure, air density and the quantity of fuel delivered, Hiroyasu and Kadota (1974) developed their first experimental correlation for the Sauter mean diameter of spray droplets:

$$d_{32} = A(\Delta P^{-0.135}(?_g)^{0.121}(Q)^{0.131}), \qquad (2.22)$$

where A is a constant varying for each nozzle: 25.1 for pintle nozzle, 23.9 for hole nozzle, and 22.4 for throttling pintle nozzle.

Hiroyasu and Arai (1990) improved the measuring technique (liquid immersion sampling and Fraunhofer diffraction technique) previously used by Hiroyasu and

Kadota (1974) and they presented a new relationship, where the effect of fuel viscosity and surface tension are taken into account.

$$d_{32} = 2.33 \times 10^{3} (?P)^{-0.135} (?_{g})^{0.121} (Q)^{0.131} \quad (2.23)$$

$$\frac{d_{32}}{D} = MAX\left[\frac{d_{32}^{LS}}{D_N}, \frac{d_{32}^{HS}}{D_N}\right], \quad (2.24)$$

$$\frac{d_{32}^{LS}}{D} = 4.12 Re^{0.12} We^{-0.75} \left(\frac{\mu_l}{\mu_g}\right)^{0.54} \left(\frac{?_l}{?_g}\right)^{0.18}, \quad (2.25)$$

$$\frac{d_{32}^{HS}}{D} = 0.38 Re^{0.25} We^{-0.32} \left(\frac{\mu_l}{\mu_g}\right)^{0.37} \left(\frac{?_l}{?_g}\right)^{-0.47}, \quad (2.26)$$

where $MAX\left[\frac{d_{32}^{LS}}{D_N}, \frac{d_{32}^{HS}}{D_N}\right]$ represents the larger value of one of the following equations. Equation (2.24) is the Sauter mean diameter for an incomplete spray with low injection velocity, and Equation (2.25) for a complete spray.

Varde (1991) studied high injection pressure Diesel sprays of four different types of nozzle. Gas density was varied between 1.1 kg m^{-3} and 42 kg m^{-3}. The author showed that at a given density the SMD is proportional to Reynolds and Weber numbers:

$$\frac{d_{32}}{D_N} \propto (Re.We)^{0.28} \quad (2.27)$$

2.6 Summary

Some of the studies on spray atomisation spray formation and spray characteristics were reviewed. The main findings of individual investigations on Diesel sprays are summarised in Table 2-3. Many of the studies concerned with spray atomisation and spray characteristics dealt with either steady spray or low injection pressure sprays and at these conditions the spray no longer represented that found under real engine conditions.

Presently, the processes leading to the atomisation of high injection pressure transient sprays are not well understood. This is due to the difficulties in

characterising the atomisation experimentally and the influences of many factors in the atomisation process. In the current work, experimental research will be undertaken to provide injection and spray characteristics information of modern high-pressure injection systems to enhance and optimise their applications to future engines.

Table 2-3: Summary of Diesel spray characteristics

Author and Year	Technique used	Main results
Dent (1971)	Review of data from studies on spray penetration for cold and hot bombs and engines.	Developments of a spray tip penetration correlation for gas jet theory. Better results for the later stage of the injection.
Hay and Jones (1972)	Survey on spray literature. Diesel engine used to test the correlations.	Recommendation of two correlations: Dent (not valid for high-pressure chamber) and Wakuri et al. (valid under light load conditions).
Hiroyasu and Kadota (1974)	High-pressure chamber at room temperature. Liquid immersion technique for droplet size measurement.	Largest droplets found on the centreline of the spray. Increasing injection frequency produces larger SMD, due to droplet coalescence. Faster fuel delivery leads to lower SMD. Increasing ambient pressure increases SMD. Development of a correlation for SMD.
Shimizu et al. (1984)	High-pressure chamber. Testing of fourteen nozzles. Measurement of the break-up length with an electric circuit.	Increasing the injection velocity increases the break-up length in the turbulent flow region. Increasing the ambient pressure decreases the break-up length and increases the spray angle.
Arai et al. (1985)	Water jet in high pressure chamber. Different nozzles of various diameters and lengths. Electrical resistance method used to determine break-up length.	Break-up length shows discontinuous change at atmospheric condition in the turbulent flow region if L/D is small. In the spray flow region, the break-up length is elongated and the spray angle is reduced if the nozzle length is long sufficiently long.
Hiroyasu and Arai (1990)	Constant volume spray chamber. Electric resistance to measure break-up length. Photography & light interception method for spray penetration and cone angle. Fraunhofer diffraction technique to determine droplet size distribution.	Increasing the ambient pressure decreases the break-up length. Increasing the ratio L/D leads to a longer break-up. Penetration is linear with time until spray reaches break-up. Increasing the ambient gas pressure decreases the spray tip penetration. Spray penetration is not significantly affected by temperature changes. Increasing injection pressure decreases SMD. Increasing the viscosity of fuel increases SMD. Equations developed for spray tip penetration, SMD, spray angle and break-up length and time.

Author and Year	Technique used	Main results
Minami et al. (1990)	High injection pressure and high-pressure vessel. High speed photography (spray penetration), shadow photography analysis (SMD) and holography used for spray measurements.	As injection pressure increases, the fuel droplets become finer, which is enhanced further if a smaller nozzle hole diameter is used. Increasing the injection pressure tends to increase the spray volume.
Huh et al. (1991)	Injection from a single hole nozzle. Observation of the spray behaviour by shadowgraph technique.	Increasing the gas pressure decreases the spray penetration and increases the spray angle. Preheated fuel produces larger spray angle.
Tabata et al. (1991)	Elevated temperature and pressure environment. Fraunhofer diffraction method used to obtain SMD.	SMD increases with an increase of the surrounding pressure. Effect of the temperature on the SMD is stronger at the portion of the spray tip. Effect of fuel property on SMD.
Varde (1991)	High injection and chamber pressure. Drop size measurement by collection technique and direct photography.	SMD increases with an increase in nozzle diameter. Increasing the injection velocity reduces SMD. Increasing the gas density increases SMD. Development of a correlation that related SMD to Re, We and gas density.
Yule et al (1991)	Pressurised gas chamber. Single orifice Diesel injectors. High speed movie photography and spark photography to measure the penetration rate.	Development of a break-up length correlation, which covers the whole spray flow field.
Farrar-Khan et al. (1992)	4 multi-hole Diesel injectors. Atmospheric spray. Droplet sizing with Malvern Diesel spray analyser.	Reduction in sac volume reduces SMD. Spray development (penetration and break-up) is affected by the discharge hole upstream flow. Critical point in the reduction of the sac volume where design changes are necessary to maintain good spray regime.
Yule and Salters (1995)	Conductivity probes measurement of the break-up length of Diesel sprays.	Four phenomena influenced by the break-up process: penetration rate, ignition and combustion spray-swirl interaction and spray wall interaction.

Author and Year	Technique used	Main results
Naber and Siebers (1996)	Study of vaporising and non-vaporising spray. High-pressure fuel injection system (common-rail). Constant volume combustion chamber. Schlieren imaging system and high speed film camera.	Spray dispersion increases with an increase in gas density. A reduction in penetration length is observed with an increase of ambient gas density. Comparison of the data with spray penetration correlation from the literature. Development of a theoretical penetration correlation for non-vaporising spray.
Warrick et al (1996)	Multi-hole Diesel injector. Heated spray chamber. Nd:YAG laser and 35 mm camera used for spray visualisation. Two experiments: Static cold and warm tests.	Increasing the temperature of the spray environment decreases the hole-by-hole variations. Small effects of the spray temperature on the spray tip penetration. Increasing the chamber temperature increases the cone angle (vaporisation of the droplets situated on the edge of the spray plume).
Chang and Farrel (1997)	High-pressure constant volume chamber. 6-hole mini sac Diesel injector. Spray characteristics visualised using Cu-vapour laser and CCD camera.	Small effect of fuel viscosity on spray tip penetration for high injection pressure, non-evaporating sprays. Sharp inlet nozzle tends to generate smaller droplet size than round inlet nozzle. Sharp inlet nozzles create wide near spray cone angle.
Jawad (1997)	High-pressure chamber. Fraunhofer diffraction pattern analysis used to study the spray.	Finer spray produced when injection pressure increases. More effective spray atomisation at higher injection pressure. Increasing the chamber pressure increases the average drop sizes.
Yoda and Tsuda (1997)	Atmospheric spray. PDA measurement of droplet size and velocity. CCD camera for fuel sprays behaviour.	Enlarging the spray hole inlet enables to increase the fuel flow quantity by 20% and the fuel flow velocity by 18%. Increasing the fuel flow velocity at the spray hole improves atomisation. Enlarging the chamfer at the spray hole inlet improves atomisation.
Badock et al. (1999)	High-pressure chamber. Laser light sheet and shadowgraph technique used to observe cavitation.	No cavitation film into the internal flow of the injection nozzle. Intact liquid core leaving the nozzle at high injection pressure.

Author and Year	Technique used	Main results
Arcoumanis and Whitelaw (2000)	Observation of cavitation phenomenon on transparent acrylic large-scale nozzles and real-size nozzles. CCD camera used for cavitation visualisation.	Two types of cavitation observed in large scale VCO nozzle.
Cao et al. (2000)	Single-hole nozzle injecting into a high-pressure vessel. Visualisation of the internal structure of the spray with LIF. Droplet velocity measured with PIV technique.	Some droplets near the spray tip have large radial velocities. Some droplets in the spray core above the spray tip tend to have higher axial velocities and are event able to takeover the droplets on the spray tip.
Bae and Kang (2000)	Different VCO nozzle discharging in a high-pressure chamber. CCD camera and shadowgraph technique were used to observe the spray.	Hole-to-hole variation only observed for sac nozzle in terms of spray angle. Negligible hole-to-hole variation of spray for VCO nozzle. Droplets formed from the ligaments around the spray surface at the early stage.
Kennaird et al. (2002)	High-speed video camera and Schlieren technique. High-injection pressure common-rail system. Single, three and five hole VCO and mini-sac nozzle. High pressure spray rig.	No orifice variation of penetration for the multi-hole nozzles. Dependence of the vapour penetration on both injection pressure and in-cylinder density (an increase in injection pressure and a decrease in in-cylinder density resulted in a better vapour penetration). Faster liquid spray penetration at higher injection pressure.

3 PHASE DOPPLER ANEMOMETRY

3.1 Principles of operation

The Doppler shift was first considered by an Austrian physicist (1842), who observed a change of frequency due to movement of the source in any form of wave propagation. However, the idea of using the Doppler shift of laser light to measure velocity was described by Yeh and Cummins (1964), who observed the shift of light scattered from particles carried in a laminar pipe flow of water.

Phase Doppler anemometry (PDA) is a non-intrusive optical technique, used to simultaneously determine the drop size and velocity of particles at specific points in sprays. This method works specifically on single particles, thus allowing high spatial resolution to be obtained.

PDA can be used to measure the size and the velocity at a point in a flow using a very intense monochromatic light. It senses true velocity components (radial and axial), and measures the components in a sequence of near instantaneous samples, with very high accuracy.

3.1.1 Basic principle

The PDA technique is a combination of the laser Doppler anemometer technique used to define particle velocities in flows, with a particle sizing method. Particle sizing interferometry developed by Farmer was a significant attempt to achieve this goal. Figure 3-1 shows an optical configuration of a PDA system.

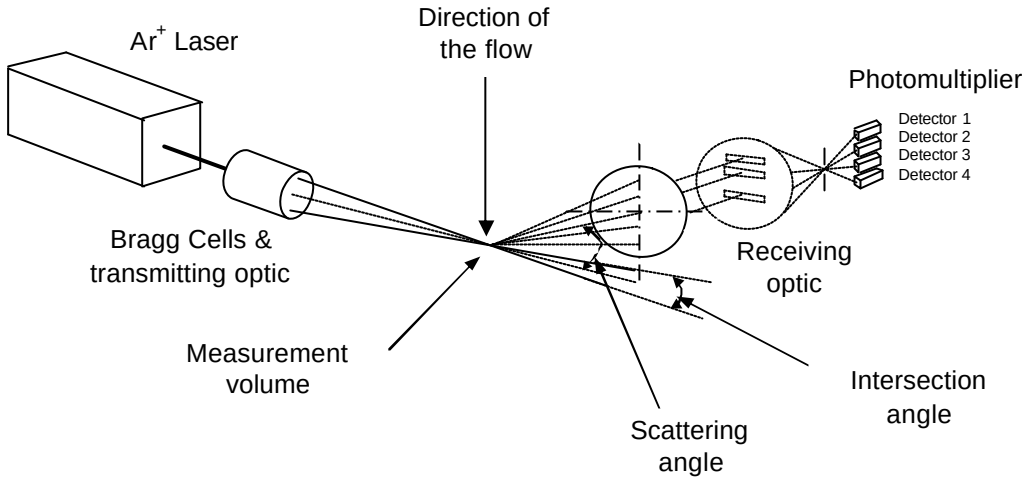

Figure 3-1: Schematic of the optical system of three receiver apertures and four detectors phase Doppler anemometer.

The output beam from a laser is split into two or more components of equal intensity. A lens is used to focus the beams at a point called the measuring volume. The interference of the light beams in the measurement volume creates a set of equally spaced fringes (bright and dark bands created by a difference of phase of the interfering light waves). Velocity and size measurements are made when a particle carried by the flow passes through these fringes. When a particle traverses the control volume, the amount of light received fluctuates with the fringes and is scattered in all directions. Some of the light is then collected by another lens and focussed onto a photodetector which converts the fluctuations of light intensity into fluctuations in a voltage signal. The frequency of this fluctuation is proportional to the velocity of the particle. This frequency is known as the Doppler shift frequency and can be calculated using the following formula:

$$f = \frac{2U\sin(a/2)}{?}, \qquad (3.1)$$

where U is the velocity component of the particle normal to the fringes, α is the beam intersection angle and ? is wavelength of the laser light (Durst et al., 1981).

The output signal of a PDA receiver is called a “Doppler burst” (raw signal) and is shown on Figure 3-2. The overall shape of the burst is caused by the fact that

the laser beams producing the measurement volume are stronger at their centre than at their edges (due to the Gaussian intensity profile of the laser beam). As the particle passes through the edge of the measurement volume where the fringes are weakly illuminated, the signal fluctuations are also weak. As the particle passes through the measurement volume centre the signal fluctuations become larger and then decay again. The signal can be split into two parts: a low frequency part called the "pedestal" and a high frequency part that actually contains the Doppler signal. The Doppler frequency *f* can be determined by measuring the period of the Doppler signal and knowing the laser wavelength and the angle of intersection of the two beams, the droplet velocity can then be calculated according to Equation 3.1.

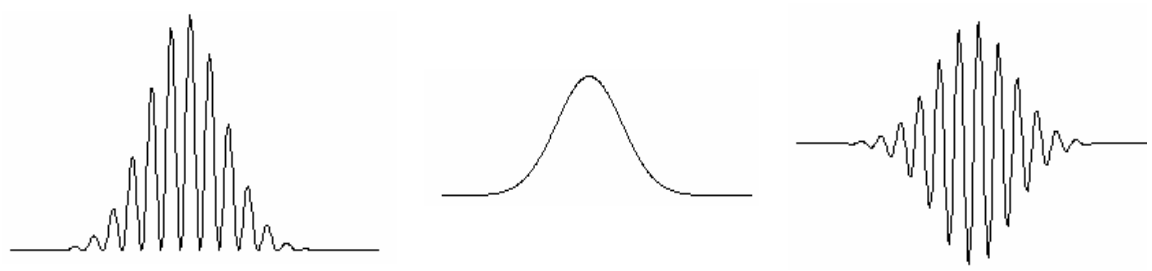

a: Doppler burst b: Gaussian pedestal c: Doppler signal

Figure 3-2: Anatomy of a typical LDA signal burst generated when a particle passes through the measurement volume.

The duration of the Doppler burst is inversely proportional to the velocity of the particles. Fast moving particles spend less time in the measuring volume and will produce short burst signals and thus slow moving particles cross the measuring volume in a longer period resulting in a longer burst.

Discussion on velocity measurements has assumed that the particle passes through the measurement volume from top to bottom (Figure 3-1). However this technique has some limitations; according to the Equation 3.1, a droplet travelling in the positive or negative direction through the fringes will produce the same frequency of signal. There is no embedded information in the signal to distinguish between positive and negative droplet direction. This problem is referred to as "directional ambiguity" and can be eliminated by shifting the

frequency of one of the laser beams. The frequency shift is usually obtained by using Bragg cells (acousto-optic devices), however other methods can be used (Durst et al., 1981). Therefore, a particle moving downwards will generate a signal at the Doppler frequency plus the frequency shift, while an upwards particles will generate a frequency of the shift frequency minus the Doppler frequency.

To determine the size of a particle, it is necessary to measure the spatial frequency of the interference fringe pattern produced by the scattered light. Bachalo and Houser (1984) showed that it could be achieved by using a second photodetector to collect light simultaneously from a different part of the interference pattern. A Doppler burst signal will be produced by each detector but with a phase shift between them, as illustrated in Figure 3-3. The signals from the two detectors have the same Doppler frequency *f* and similar amplitude, but are separated by a phase shift ϕ given by:

$$F = \frac{T_{phase}}{T_D} \times 360, \qquad (3.2)$$

where T_D is the Doppler period and T_{phase} is the period between the zero crossings of the signals from detectors 1 and 2.

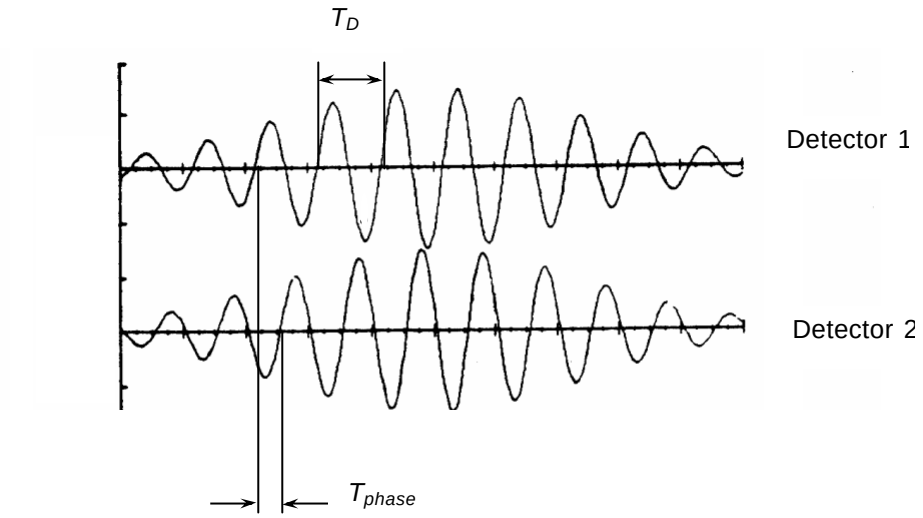

Figure 3-3: Doppler signal from detector 1 and 2 (from Bachalo and Houser, 1984).

For a given optical configuration, the phase shift is directly related to the particle size by a linear calibration curve shown in Figure 3-4. The slope of the linear response curve is dependent on optical parameters, which consist of the laser wavelength, the collection angle, the laser beam intersection angle and the refractive index of the particle. The theoretical relationships between the phase difference and particle diameter are given below for the two main scattering modes (Dantec, 2002).

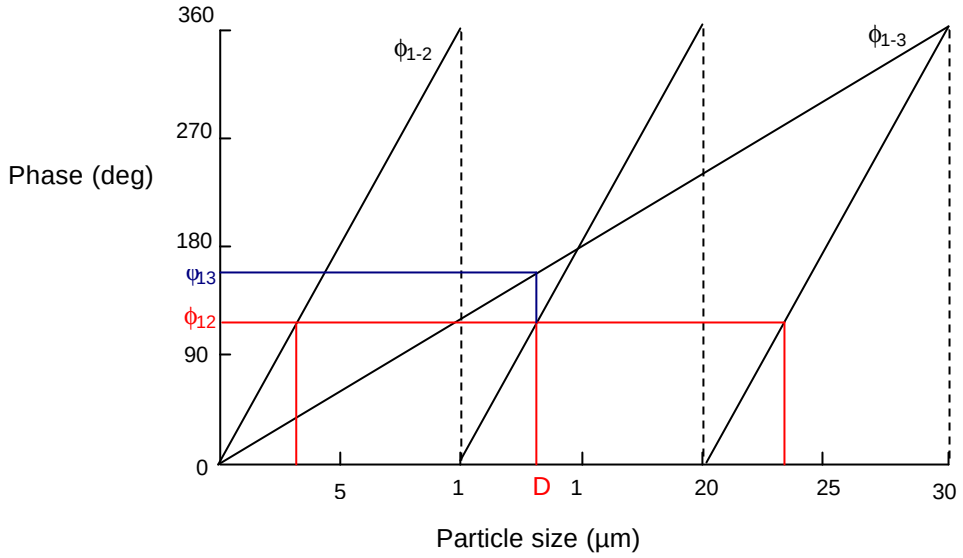

Figure 3-4: Phase Doppler anemometry calibration curve (from Bachalo and Houser, 1984).

- For reflection

$$F = \frac{2p\,d}{?}\,\frac{\sin? \sin?}{\sqrt{2(1-\cos? \cos? \cos f)}} \qquad (3.3)$$

- For 1st order refraction

$$F = \frac{-2p\,d}{?}\,\frac{n_{rel} \sin? \sin?}{\sqrt{2(1+\cos? \cos? \cos f)(1+n_{rel}^2 - n_{rel}\sqrt{2(1+\cos? \cos? \cos f)})}} \qquad (3.4)$$

where, d is the droplet diameter, θ is the beam intersection angle, ψ is the scattering angle, ϕ is polarisation angle and n_{rel} is the relative refractive index (ratio of the refractive indexes of Diesel and air). The scattering mode will be selected to ensure that light received by the optic is dominated by one single scattering phenomenon and that the signal-to-noise ratio is as high as possible. This will be discussed later in the text.

In some cases, a phase shift greater than 360° could occur and the calibration curve would no longer be valid; this phenomenon is known as the 2p ambiguity. A third detector is used to detect and remove such uncertainties. For instance, according to the diameter-phase diagram (Figure 3-4), a phase shift of 120º between detector 1 and 2 (ϕ_{12}) corresponds to 3 different particle diameters. The additional detector is used to select which diameter value is the correct

one. The third detector can also be used to eliminate sizing errors due to non-spherical particles. A spherical validation factor was used in the Burst Spectrum Analyser (BSA) Flow Software to define the maximum allowable deviation from sphericity.

The phase-diameter curve will be linear if only one scattering mode dominates from the two laser beams. Scattering may be composed of diffraction, absorption, reflection and refraction. The incident light ray on a sphere is illustrated in Figure 3-5. Three contributions are included in the representation; reflection from the surface of the particle, refraction through the particle (1st order refraction) and refraction with an internal reflection (2nd order refraction).

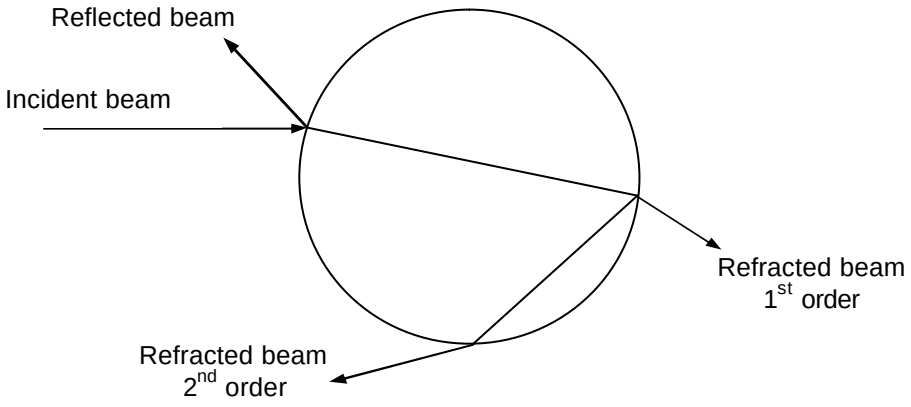

Figure 3-5: Illustration of three different scattering modes.

The light scattering component of either reflection or refraction will be measured to obtain the particle size. As the system estimates the particle size from the phase-diameter relationship of one of the scattering components, the system should be set-up so that only one mode of the scattering dominates the light received by the photomultipliers. If the light scattered by reflection and the light scattered by refraction have comparable intensities, a non-linearity in the phase-diameter relationship will occur resulting in particle sizing errors. The scattered light intensity from reflection and refraction varies with the scattering angle and the polarisation orientation of the incident light (Figure 3-6). Considering a parallel plane of polarisation, for angles close to the optical axis (? less than 30º), the scattered light is dominated by diffraction and contains no

useful phase information. For angle between 30º and 80º, the scattered light is dominated by refraction, while reflection is dominant in the range from 80º to about 110º. The green trace in Figure 3-6 represents the angular distribution of the relative intensity of scattered light according to the Lorenz-Mie theory.

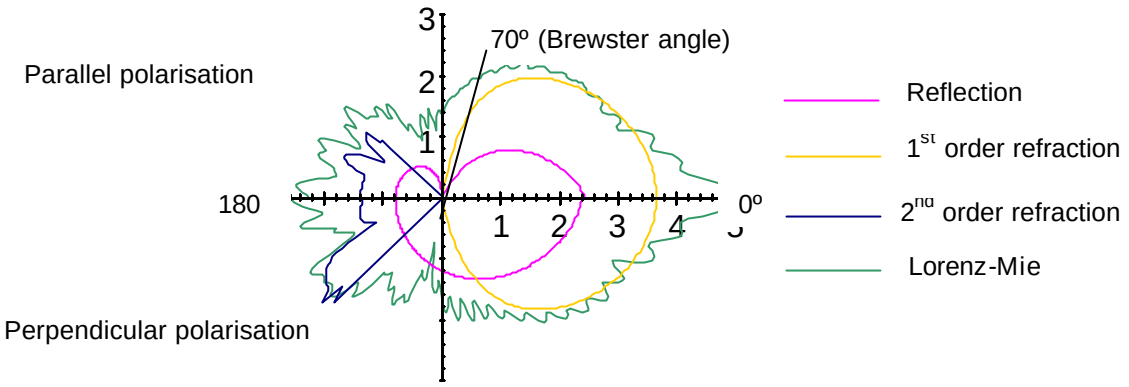

Figure 3-6: Angular dependence of the scattered light for a parallel and perpendicular plane of polarisation (from Dantec, 2002).

3.1.2 The fringe model

The velocity calculation can also be described using the fringe model. Laser light is monochromatic and coherent (all adjacent and successive waves are in phase). In the measurement volume, where the beams intersect, the wave fronts are approximately plane and consequently the interference produce parallel planes of light (light waves in phase) and darkness (light waves out of phase) (Figure 3-7).

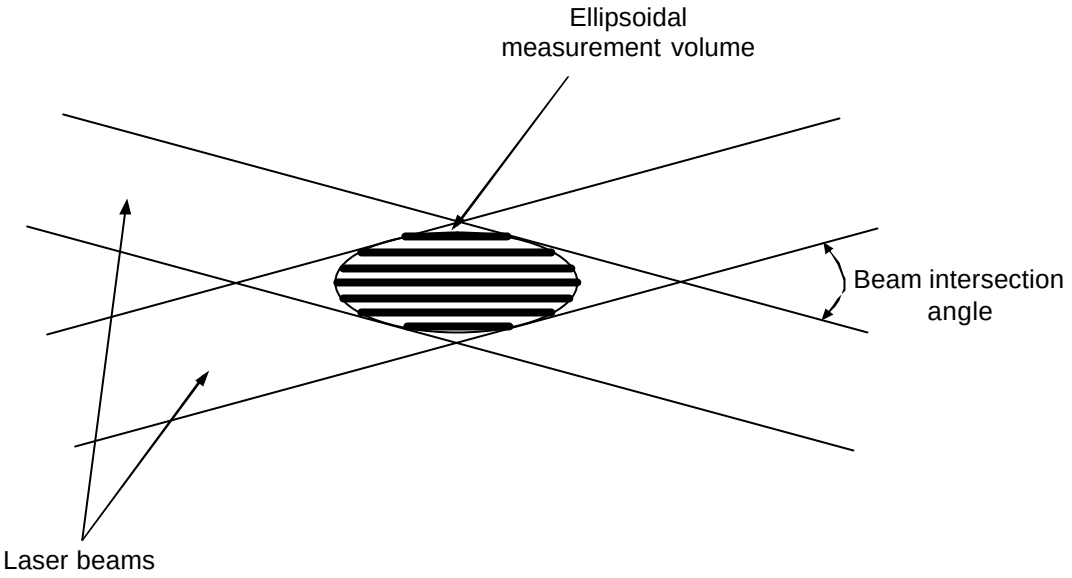

Figure 3-7: Detail of the measurement volume showing the formation of fringes.

The fringe distance s is defined by the wavelength ? of the laser light and the angle of intersection α.

$$s = \frac{?}{2\sin(a/2)} \qquad (3.5)$$

The relationship between the velocity of a particle and the frequency it generates can be determined. If the fringes are separated by a distance s and the velocity component of the particle normal to the fringes is U, then the particle will cross a total of U/s fringes per second. Thus the particle will generate a signal of frequency (Doppler frequency).

$$f = \frac{U}{s} = \frac{2U\sin(a/2)}{?} \qquad (3.6)$$

3.2 Consideration of the errors and accuracy within the present study

Phase Doppler Anemometers are among the most accurate flow measurement devices. However, they are susceptible to errors and, as with any other measurement technique, it is important to know the sources of error when making a PDA measurement.

3.2.1 Sources of error

3.2.1.1 Particle shape effects

The measurement of non-spherical particles with the phase Doppler method is often complex and sometimes unachievable. During a Diesel injection, the shape of the spray varies according to the in-cylinder conditions. Spherical droplets can be deformed into irregular-shaped particles or prolate and oblate ellipsoids. Irregular-shaped particles cannot produce reliable results, because the light reflected or refracted to the receiver optic from these particles will create uneven light scattering patterns.

When spherical particles are subjected to aerodynamic load or viscous stresses produced by turbulence or flow accelerations, the droplets may be converted into ellipsoids. In addition to the phenomena previously described, coalescence of droplets may occur in a dense spray, resulting in the formation of non-spherical particles. PDA responds to the radius of curvature of the particle entering the measurement volume, the results will vary according to the shape of the droplets and its orientation (Figure 3-8). Such deviations in sphericity can result in overestimation of droplet diameters up to 45% (Bachalo and Houser, 1984).

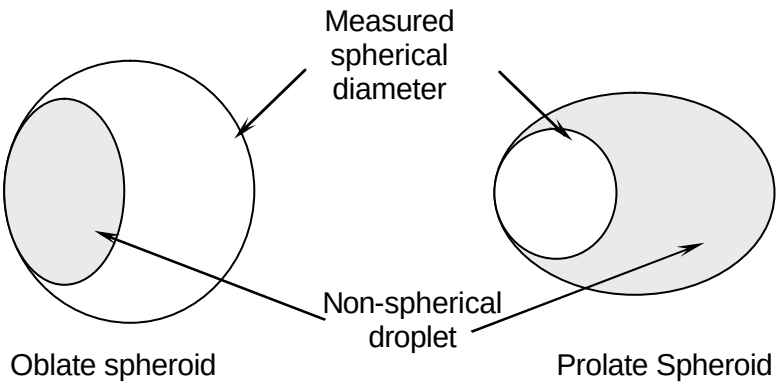

Figure 3-8: Response of the phase Doppler anemometer to non-spherical particles (Bachalo, 1994).

3.2.1.2 Burst validation

The burst signal sent to the photomultipliers will be triggered according to 3 different thresholds. Level 2 will trigger the beginning and the end of the

measurement (Figure 3-9). For a burst to be validated, its signal has to go beyond level 3 and beneath level 1.

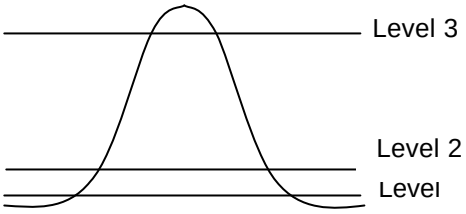

Figure 3-9: Burst detection trigger level (Dantec, 2002).

3.2.1.3 Particle averaging bias

A problem with PDA measurements is that they sense the velocity when a particle passes through the measurement volume. Unfortunately such a set of samples is biased, because if the flow velocity is high, more particles will pass through the measuring volume in a given time than if it is low. Thus by averaging the velocities of all the samples, the obtained estimation of the mean flow velocity will be over-estimated. The estimated velocity variance will also be in error. A solution is to weight each velocity sample by the amount of time it takes until the next particle arrives. Another solution is to break the data collection into a series of equal time intervals and then collect only the first sample in each interval.

3.2.1.4 Trajectory ambiguity effect

The trajectory ambiguity effect in phase Doppler anemometry, also known as the Gaussian beam problem, results from the Gaussian intensity distribution of the laser beams and becomes relevant for particles larger that the focused beam diameter. If a droplet is larger than the focused beam diameter, its trajectory through the beam can result in a non-uniform illumination and will lead to a significant mixing of the reflected and refracted light on the detectors. One of the two signals will dominate the light scattering but not both simultaneously (Figure 3-10). As the PDA signal analysis relies on the domination of one single scattering component, the measured size for larger particles can be erroneous (Hardalupas & Liu, 1997; Bachalo, 2000).

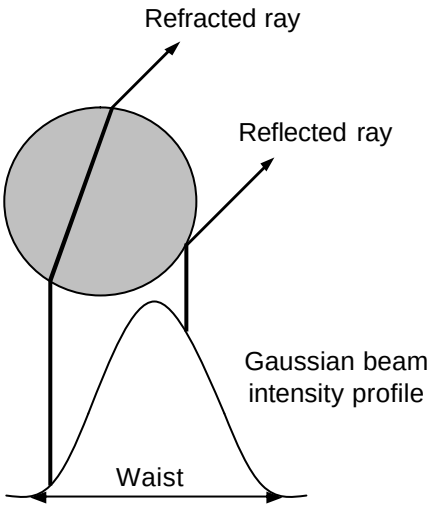

Figure 3-10: Source of the Gaussian beam trajectory effect for a particle larger than the focused beam diameter (Bachalo, 2000).

However, for the measurement of dense sprays, a small measurement volume is required to decrease the probability of having more than one particle in the control volume simultaneously. Hardalupas & Liu (1997) recommended an angular orientation for the receiving optic close to Brewster's scattering angle (usually ~ 70º) to reduce the effect of light scattered by reflection. According to Sankar et al. (1991), a proper configuration and alignment of the optics should allow the sizing of small particles with a resolution of ± 0.3µm. Bachalo (1995) showed that errors could be reduced by using a wide beam intersection angle. For example, the sizing error of a 45µm droplet decreased from 50% to 10% by changing the beam intersection angle from 1.8º to 5.4º.

3.2.1.5 The slit effect

The limiting effects of the slit aperture in receiving optical probes are in certain cases responsible for the complete suppression of the light scattering component selected for calculating the particle diameter from the measured phase difference. The consequences on the calculation of the particle diameter from the measured phase difference are the same as those described in the trajectory ambiguity effect section, because the presupposed scattering mechanism (1^{st} order refraction) is suppressed, the equipment records the wrong droplet size. The slit effect is illustrated in Figure 3-11.

In the case of refracted light, this effect occurs when the particle crosses the measurement volume, in the positive region of the z co-ordinate axis close to the edge of the projected slit aperture. For instance here, the refracted light is totally suppressed; leaving only reflectively scattered light to be detected by the photo detectors. As with the trajectory effect, such signals will result in incorrect size measurements.

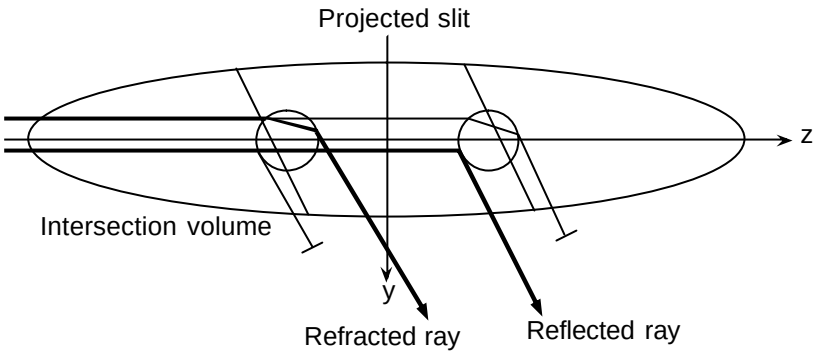

Figure 3-11: Suppression of scattered light due to the slit aperture (Dantec, 2002).

In an ensemble of several thousand droplets, a handful of improperly measured diameters can lead to significant errors in the mass flux due to its third power dependency on diameter.

3.2.2 Dense spray measuring difficulties

The concentration of particles can be such that there is a possibility that several droplets may occupy the measuring volume at the same time, leading to unprocessable overlapping signals, making measurements very difficult, with associated low validation rate. One possible solution is to reduce the control volume to avoid “multiple occupancies”; however there are problems related to small control volumes. Decreasing the size of the measuring volume will reduce the number of fringes; therefore the amount of light scattered by each droplet will be reduced, resulting in a weaker burst signal. As a consequence the PDA processor will have difficulties to process the signal and to determine the Doppler frequency.

However, despite the small control volume, coincidental events could still occur (Bachalo, 1994). For example, if a large and a small droplet are simultaneously present in the measuring volume, the signal from the large one will be dominant and may be successfully measured negating the smaller one. Another possible scenario, which may arise, is when two particles of almost identical sizes and velocities are present at the same moment in the measuring volume, only one will be validated.

Moreover, if one of the beams is intercepted by a particle before the probe volume that measurement will be rejected. If the light scattered from a single particle passing through the probe volume is intercepted by other particles or ligaments behind the probe volume (between the measuring volume and the receiver) the measurement may be distorted. The light scattered from a particle crossing the laser beam near the measurement volume could interfere with a droplet present in the control volume and will distort the signal sent to the receiver.

3.2.3 Optical alignment sensitivity

The slightest movement of any optical component will almost certainly result in the PDA set-up becoming misaligned, causing reduction or total loss of data rate. As a result, the Dantec benches, on which transmitting and receiving optics were mounted, were screwed onto a pneumatic table to avoid ground transmitted vibrations. The optical system maintained alignment through temperature and pressure changes.

The refractive index of air in the combustion chamber may be affected during the test by turbulence, pressure or thermal gradient effects. For instance, increasing the in-cylinder conditions (pressure and temperature) has a substantial effect on the laser beam alignment, due to the change in the index of refraction of the air, n. n increases from 1.00026 at 0.1 MPa to 1.00256 at 1 MPa and from 1.00026 at 20° C to 1.00021 at 100°C.

These variations of refractive index have three primary effects: they change the effective path lengths of the beams and the angle between the laser beams, and they increase the focal lengths of the lenses. The effects of a change in

refractive index on the intersection angle of the two laser beams and the location of the measuring volume is shown in Figure 3-12.

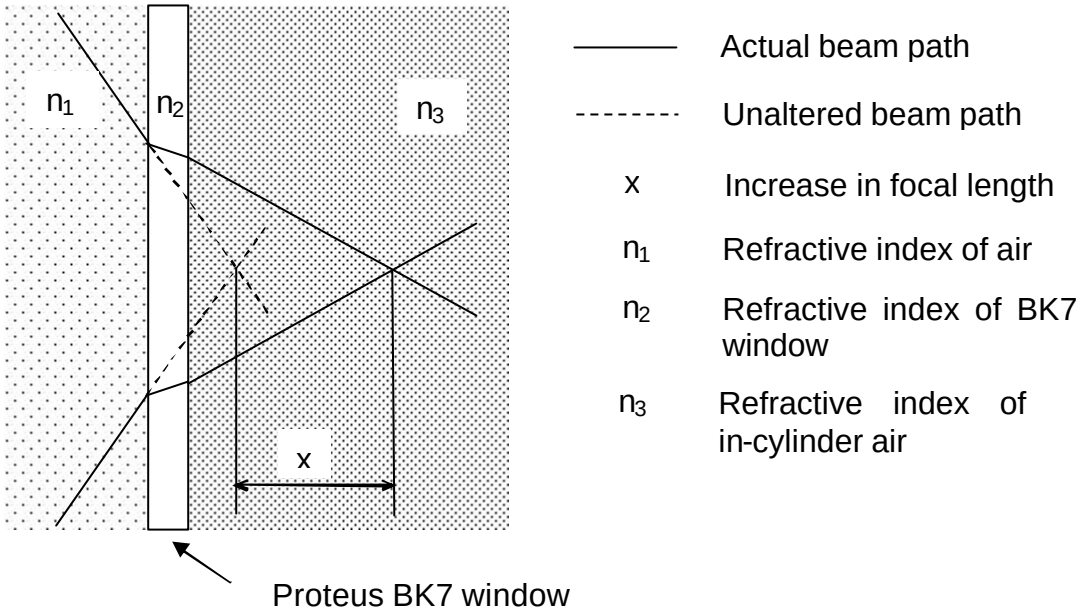

Figure 3-12: Variation of the position of the measuring volume due to changes in air refractive index.

The consequences of these changes in the laser beam path may be determined using trigonometry and Snell's law:

$$n_1 \sin\theta_2 = n_2 \sin\theta_1, \quad (3.7)$$

where $n_{1,2}$ is the index of refraction of the medium 1 or 2, θ_1 is the angle of the incident laser beam and θ_2 is the angle of the refracted laser beam. When calculating the new location of the measuring volume, the effect of the cylinder head window, which was made of sapphire, was taken into account.

The effects of in-cylinder conditions are repeatable, so it is possible to preset the position of the optics to make the beams crossing point coincide with the desired spray measurement point for each operating conditions.

For instance at 6 MPa, considering the effects of the window and change in air refractive index on the beam path, the increase of focal length was found to be approximately 6.8mm.

3.2.4 Effect of fuel refractive index on phase-drop size relationship

When droplet size measurements are undertaken in an engine, consideration must be given to the dependence of Diesel fuel properties on local pressure and temperature. Variations of these factors affect the liquid density and consequently the Diesel droplets' index of refraction and causes changes in signal phase and intensity. In this case, the temperature variation has a strong effect on the liquid refractive index. Indexes of refraction were calculated for fuel temperature varying between 293 K and 726 K (critical temperature) and obtained using Eykman relationship, which is derived empirically and specifically for hydrocarbons as given below:

$$\frac{n^2-1}{n+0.4} = ?.\text{const.}\,, \qquad (3.8)$$

where n is the index of refraction and ρ is the Diesel fuel density. Results are summarised in Table 3-1.

As the calibration curves are usually established for constant refractive index (Sankar & Bachalo, 1991), the air and fuel indexes of refraction have to be calculated prior to each test to minimise the measurement errors. The refractive index of Diesel fuel was measured at 20°C using an Abbe refractometer and was found to be 1.459 for a density of 831 kg.m^{-3}. The effects of a decrease in air and fuel refractive indexes on the phase-diameter relationship (given in Equation 3.8) were analysed for the PDA optical scattering geometry used in this study.

Temperature (K)	Density (kg m^{-3})	Refractive index n
293	831	1.459
393	738	1.405
493	667	1.364
536 (boiling)	640	1.348
726 (critical)	545	1.294

Table 3-1: Index of refraction for different fuel temperature.

The consequences of a change in the fuel refractive index will be analysed for two different cases:

- Variation of the refractive index during one injection

During the injection of fuel into a hot environment, the temperature throughout the spray may vary by several degrees; therefore the index of refraction will also vary. In the combustion chamber the droplets encounter a hot environment of hot gas and experience simultaneously heating and evaporation. For instance, when injecting in a hot environment, the fuel temperature at the start of injection can be estimated to be 423 K and 726 K (critical temperature) towards the end of the injection stage. This will lead to refractive index gradients within the droplet caused by internal temperature or concentration gradients.

The phase-diameter relationship for η_{rel} from 1.371 to 1.275, corresponding to in-cylinder condition of 573 K and 7 MPa and fuel temperature of 423 K and 726 K respectively, is shown in Figure 3-13. It can be seen, that a decrease in refractive index does not significantly affect the phase-drop size relationship. In fact, the sizing error between a refractive index of 1.371 and 1.275 for a phase of 200° is about 1%. Therefore, the consequence of an alteration of the refractive index during an injection can be considered negligible. As only a fixed calibration curve can be used in the practical application of the PDA, a sensible approach for a forward scattering optical configuration (angle varying between 30º and 80º) would be to select a phase-drop size relationship corresponding to the initial refractive index of the droplets in the combustion chamber (Schneider and Hirleman, 1994).

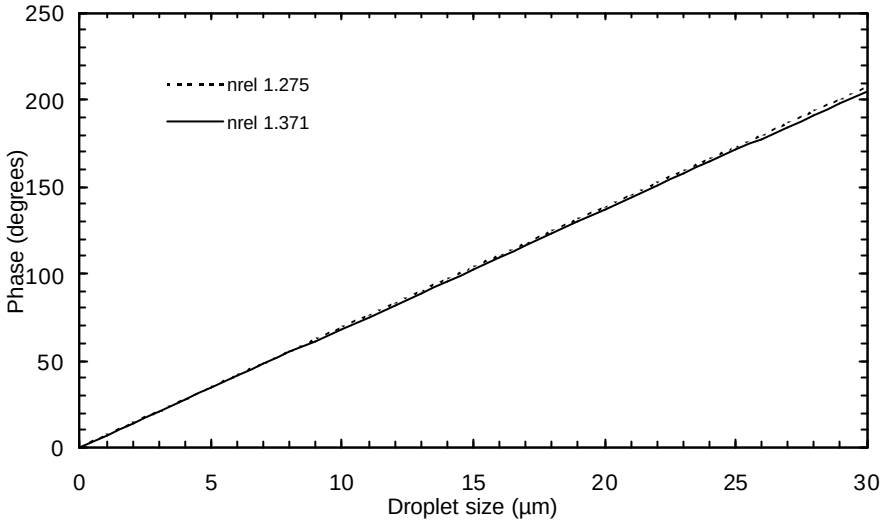

Figure 3-13: Phase-drop size relationship.

- Variation of the refractive index between two sprays

Even if the variation of the refractive index seems to have a small effect on phase-drop relationship, the index of refraction will still have to be reset before each test, according to the in-cylinder condition.

3.3 PDA measurements of Diesel sprays

In this section, a review of the literature on the application of PDA to Diesel spray is presented. The main findings of these investigations are summarised in Table 3-2.

In the past ten years, the development of laser and Phase Doppler anemometry has allowed the velocity and size droplets in Diesel spray to be measured. Using a 1-D PDA system, Koo and Martin (1990) found that the peak droplet size and velocity occurred on the spray axis, and that the peak droplet velocity decreased with distance downstream of the injector due to aerodynamic deceleration.

Hardalupas et al. (1992) analysed a 5-hole Bosch nozzle injecting into the atmospheric conditions at 10 Hz. Each hole of the nozzle had a diameter of 0.18 mm and an L/D ratio of 3.9. The injections had an area-averaged spray velocity of 132 m s^{-1}, corresponding to an injection pressure of approximately 20 MPa. A significant error analysis was presented in their work, possibly to quell the frequent objections to the application of PDA measurements at such conditions. For example, they noted that in the dense region of the spray, it could take up to 45 minutes to gather 5000 samples. In fact, during certain portions of the injection, data acquisition was not possible due to obscuration and high droplet velocity. Validation rates were noted to be as low as 25%. The authors offered reasonable uncertainty tolerances of less than 10%, but they did not have an answer to the fact that their measurements could be biased due to measurement inaccuracies from any signal-to-noise ratio decrease as the core region was approached. The authors reduced the problem of taking measurement in dense region by only looking at the far downstream regions. Measurements were taken at distances of 20, 40, 60, 80, 100 and 140 mm from the tip of the injector. Hardalupas et al. found that the spray was better atomised on the edge of the spray. During the injection, the SMD near the nozzle decreased from 80 µm to 28 µm, while on the periphery, the SMD dropped from 60 µm to 20 µm. This decrease in SMD was attributed by the authors to droplet break-up caused by large velocity differences between the droplets and the entrained air. However, far from the nozzle, the decrease in SMD is less with a drop from 38 µm to 30 µm on the spray axis and 30 µm to 25 µm on the edge.

The authors also observed in the downstream region that the larger droplets were faster than the smaller ones and that they tended to concentrate on the periphery of the spray. This was attributed to the fact that the smaller droplets lose momentum faster (larger droplets were less affected by aerodynamic drag due to their high ratios of volume to surface area) and were then overtaken.

Pitcher and Wigley (1990 and 1991) extended Diesel spray measurements by sizing sprays not only under ambient conditions, but also under real engine conditions. For instance in their 1991 study, the authors used a Bosch in-line fuel injector pump supplying fuel to a 0.2 mm hole diameter nozzle at an

injection pressure up to 40 MPa. PDA measurements were taken in a 3 litre, single cylinder, 2 stroke engine running at 500 rpm. Measurements were also performed at ambient conditions to allow comparison. Ethanol, a non-combusting fuel, was used for ambient and in-cylinder measurements to avoid spray ignition. Axial velocities and droplet sizes were measured at different locations on the spray axis and on a radial plane at 25 mm from the nozzle. Measurements were performed at 5, 15 and 25 mm from the nozzle in the engine case and at 5, 25 and 45 mm in the ambient case (in the last case, the engine was not optically restricted). The radial distance from the spray axis was varied from 0 to 1.2 mm at each location with an increment of 0.2 mm. In examining the spray under ambient conditions, the authors found that a dense region of the spray along the axis near the nozzle was not measurable and left about a 2 crank angle degree gap in the data set. The spray was partially atomised as a distance as close as 5 mm from the injector tip, while the periphery was completely atomised. At an axial distance of 25 mm, the spray core was found to be limited to a radius of 1 mm while the edges of the spray extended to a radius of 3 mm. The droplets within the spray were found to be uniformly distributed in time and space. There were four distinct periods of concentrated droplets, indicating a coherent wave structure longitudinal to the spray axis.

Under engine conditions, Pitcher and Wigley found no atomisation along the spray axis near the nozzle, but only partial atomisation on the periphery of the spray near the nozzle. Atomisation did not occur along the spray axis until 15 mm downstream of the nozzle. The spray radius was slightly larger with the spray edge at axial distance of 25 mm being at the radius of 4 mm. The spray core remained constant with a radius of 1 mm. Indications of the coherent longitudinal wave structures found in the ambient case remained but with a much reduced amplitude and coherence, probably due to increased air density and turbulent fluctuations. Drop sizes were smaller in the engine case. The majority of the droplets in the ambient case were less than 25 μm in diameter, while in the engine case droplets usually had diameter around 15 μm. In both cases, the largest droplets were found in the tail of the spray near the nozzle.

In the PDA studies mentioned above, there are some similar trends. PDA measurements tend to have rather low validation rates but appear consistent and repeatable. Secondly, except at very far axial distances from the nozzle, the measurements showed a lack of, or at least a decrease in, data acquisition in the main head of the spray body. This drop in measurement appears to be due primarily to the sheer number density of the spray. However, according to Yule and Salters (1995), the spray break-up length was of the order of 100 nozzle diameters, which represents in the above case an average length of 20 mm. Therefore, it could be concluded that the lack of measurement near the nozzle region could be caused by a non-atomised spray.

The measurement of Diesel sprays in a high density chamber was also investigated by Payri et al. (1996) by the use of high speed photography and PDA. The experimental set-up allowed the use of a two spring injector with injection pressures up to 20 MPa with maximum gas densities of the order of 30 kg m^{-3}. Three spray sections were analysed at 10, 20 and 30 mm from the injector tip with several radial measurement positions. Validation rates between 20 % and 60 % were obtained for different injection conditions and biasing towards large droplet sizes was expected by the authors. Payri et al. observed small droplet at the leading edge of the spray and large particles at the trailing edge of the spray. This behaviour was attributed to coalescence and weaker aerodynamic interaction between the droplets.

Ficarella et al. (1997) studied the sprays produced by a five-hole VCO nozzle. A common-rail electronically controlled injection system produced a dense spray into an atmospheric chamber with injection pressure up to 120 MPa. A photographic investigation was also conducted to analyse the penetration, the outlet diameter, the inclination and the angle of the spray. The researchers equally faced difficulties in validating their PDA measurements. The receiving optic of the PDA system was positioned at a known distance from the injector and the time delay between the injection pulse and the electrical signal coming from the first particle crossing the measuring volume was recorded on a digital oscilloscope. The velocity of the fastest particle at that location was then

calculated from the oscilloscope output and compared with a PDA measurement at the same position. For instance, the measurement at 120 MPa injection pressure from the time delay gave a velocity of approximately 220 m s^{-1}, whilst the PDA system was about 70 m s^{-1}. Several attempts were made at different injection pressure by the authors who found that they had to reduce the injection pressure down to 15 MPa, in order to obtain matching measurements. The rejection rate was around 30% in the LDA mode (velocity measurements only) and about 70% in the PDA mode (velocity and diameter measurements). This difference was probably due to the sphericity check on the droplets performed by the PDA mode. PDA measurements were taken at axial distances from 5 mm up to 30 mm from the nozzle and at all the radial positions with an interval of 1 mm. The authors observed a SMD increase with radial distance from the spray axis. However, the validity of this observation is dubious, because the AMD was found to be the precise opposite. This could have been be caused by a highly dispersed distribution of diameters. The limitations of the Phase Doppler anemometry technique to investigate dense sprays are viewed by Ficarella et al. as the main explanations for their lack of accurate results. But as previously mentioned their lack of measurement in the region close to the injector tip could be caused by spray that has not achieved a high degree of breakup.

Wigley and Pitcher (1997) compared Diesel fuel sprays produced by an electronically controlled high pressure common rail fuel injection system with a single-hole type injector of diameter 1.8 mm. The engine used was identical to the one used in their 1991 study and it was also motored at 500 rpm. The injection pressure varied between 30 MPa and 80 MPa and the injection duration time between 0.5 and 1.5 ms. Set of measurements were conducted in a horizontal plane 20 mm downstream of the nozzle at injection pressure of 30, 50 and 80 MPa. In all 3 cases, a broad range of velocities were observed with the lower and upper limits being representative of the local air velocity and the spray tip penetration respectively. At the highest injection pressure 471 injections were needed to gather sufficient data for analysis.

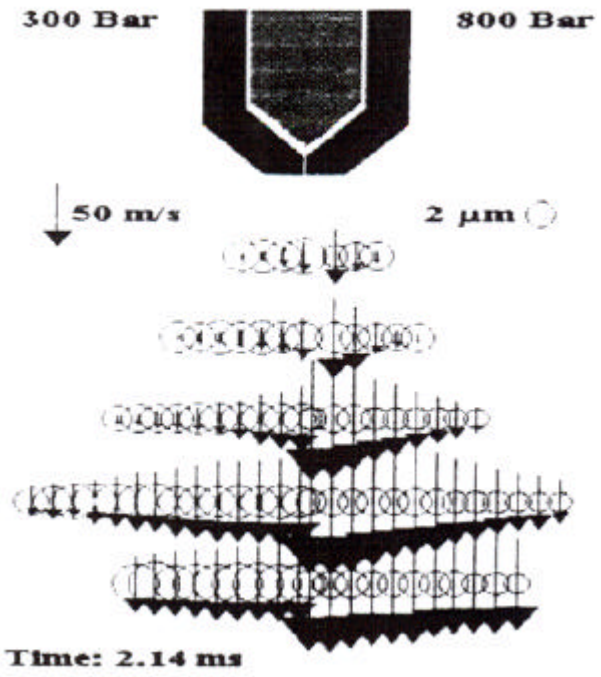

Figure 3-14: Velocity vector and drop size field frame at 2.14 ms after start of injection (Wigley and Pitcher 1997).

The second sets of measurements were undertaken and the results were mapped out to show the spatial and temporal distributions of velocity and size of the fuel droplets (Figure 3-14). The control volume of the PDA was moved axially (5, 10, 15, 20 and 25 mm from the nozzle) and radially (every 0.2 mm from the spray axis up to 1.8 mm). An increase in the droplet velocity and a decrease the size throughout the spray was observed with an increase in injection pressure.

Araneo and Tropea (2001) investigated sprays produced by a common rail system with a PDA technique. They investigated the optimisation of the optical system over a six-month period. A laser of 488 nm wavelength was found to provide a higher validation rate than the conventional 514.5 nm one. In this work an unrealistic sphericity factor (30%) was used to obtain data. Droplets would no longer be spherical at these velocities and the results would become skewed towards smaller drops, biasing distribution.

3.4 Conclusion

Previous PDA research in fuel sprays using a common rail injection system tends to suggest that the technique cannot easily be applied to measurements of dense sprays. It may be argued that examples of PDA measurements are available in the literature. Careful examination of the experimental conditions reveals that in many of these cases both injection pressures and in-cylinder conditions were reduced substantially to obtain a reasonable data rate. These conditions then become unrealistic of those in a real engine. For instance, Wigley and Pitcher (1997) used a bespoke optical system with a large beam separation and thick beams, which allowed the measurement of high injection pressure sprays, something that Ficarella et al. could not achieve. By using this configuration, a small control volume could be obtained, reducing multiple droplet interference in the measurement process. However, with the progress made in the past few years with PDA signal processing and with the ability to be able to more closely control PDA system parameters, the chances of success in sizing Diesel fuel droplets are much improved.

Various PDA applications have been described, with reference to injectors used in internal combustion engine. Most of the publications dealt with the injection of fuel or other suitable liquids into experimental bombs, rather than the injection into engine cylinder. The conclusion that can be drawn from all these previous literature is that PDA measurements in the motored or fired engine are difficult. However, with reference to previous work and the use of modern PDA processing and careful selection of optics, improvements over previous works can be achieved.

Table 3-2: Summary of PDA investigations on Diesel spray characteristics.

Author and year	Technique used	Main results
Arcoumanis et al. (1990)	Spray from a five-hole injector. Use of nozzle adaptor to study only one spray. Laser beam deflection used for velocity spray tip measurements. Dual beam LDA and laser diffraction used to measure droplet velocity.	Spray tip penetration and velocity depend on injection velocity rather than injected volume. Uneven distribution of the radial velocity, suggesting that the axisymmetric spray may not be realistic in multi-hole Diesel sprays. Observation of three parts in the spray structure.
Koo and Martin (1990)	Atmospheric spray. Measurement of particle size and velocity with a PDA system.	Largest velocity and diameter occur on the axis of the spray. SMD is larger near the nozzle. Correlation between droplet sizes and velocities at each crank angle.
Koo and Martin (1991)	Constant-volume chamber (four different pressures). Sizes and velocities of droplets measured by PDA.	Comparison of the experimental results with the stability criteria based on Weber number. At 10 mm from the nozzle, most of the droplets are subject to aerodynamic break-up. Distributions of droplet diameters at 60 mm from the nozzle are likely to be a result of collision processes.
Pitcher and Wigley (1991)	Spray measurements under ambient conditions and in a 3 litre single-cylinder two-stroke Diesel engine. . Single hole fuel injector, non-combusting fuel. PDA used to measure particles size and velocity.	Under ambient conditions: complete atomisation of the liquid on the spray periphery, uniform droplet distribution in time and space within the spray. Under engine conditions: partial atomisation of the liquid on the spray periphery in the near nozzle region, un-atomised spray on the centre line in the near nozzle region, wave structure of the spray.
Hardalupas et al (1992)	Five-hole injector. Atmospheric spray. PDA system used to measure droplet sizes and velocities.	Larger droplets tend to concentrate at the leading edge. Spray becomes smaller as far as the distance from the injector increases and tends to be better atomised on the periphery. Larger droplets move faster than the smaller droplets. Unable to measure in spray tip due to high droplet velocity and obscuration.

Author and year	Technique used	Main results
Hosoya and Obokata (1993)	Atmospheric spray from four different types of nozzle (measurement restricted to one hole). Droplet velocity and size measured using LDA and PDA.	Difficulties to measure the spray (unsteady under conditions of high temperature and pressure). Different spray characteristics between single-hole nozzle and multi-hole nozzles. The number and the position of the holes do not affect multi-hole basic spray characteristics.
Payri et al. (1996)	Low injection pressure (up to about 20 MPa). High density chamber. High speed photography and PDA technique used to measure the spray cone angle, the penetration length and the velocity and size of the droplets.	Lowest drop size measured at the leading edge of the spray. Largest droplet size measured at the trailing edge of the spray (coalescence and weaker aerodynamic interaction are probably responsible for this behaviour). Drop size is not significantly dependent on the radial distance to the spray axis. Radial velocity distributions at fixed distance from the nozzle tip are similar along time.
Ficarella et al. (1997)	High injection and vessel pressure Five-hole VCO nozzle (analysis of the spray produced by each hole). Sizes and velocities of the spray measured by Malvern method and PDA. Photographic technique used to analyse the spray from every hole.	Spray cone angle decreases with time. Increasing the feeding pressure decreases SMD. No effect of the injected quantity on SMD. Variation of the shape of the spray from hole-to-hole but size distribution remains constant. Limitation of the PDA technique to analyse dense Diesel spray.
Koo et al. (1997)	Computer simulation used to calculate the velocity and the turbulence intensity at various L/d ratios. Internal flow velocity of scaled-up nozzle measured with LDA. PDA and laser sheet photography used for velocity and particle size measurements of actual-scale nozzle.	Longer break-up length at low injection pressure for sharp inlet nozzles. Larger SMD with sharp inlet nozzle. Wider angle spray with sharp entrance nozzle. Cavitation of the actual scale Diesel injector (whitening of the fuel jet emerging from the nozzle).

Author and year	Technique used	Main results
Levy et al. (1997)	Low injection pressure and high pressure chamber. Sizes and axial velocities measured with PDA. KIVA-II code for numerical simulations.	Increase of SMD with distance from the nozzle (because of the coalescence of droplets at low temperature and evaporation of the small ones at higher temperature). Increase of axial velocity with the distance from the nozzle exit. Fastest velocity at highest temperature.
Wigley and Pitcher (1997)	1-D PDA used to measure drop size at 5 axial positions. Single hole sac injector. Engine running at 500 rpm.	Increasing the injection pressure increases the droplet velocity and reduces the particle size. Better penetration velocity of the spray tip at high injection pressure. Plot of velocity vector and drop size field frames.
Araneo and Tropea 2000	Dual PDA. Atmospheric spray (injection period: 8 ms). Common rail injection system.	Effects of the laser power, PM voltage and SNR validation level on the data rate. Optimisation of the PDA system. Velocity oscillations throughout the injection period.
Jimenez et al (2000)	Single hole Diesel injector. Spray into a low speed air cross flow at atmospheric pressure. PDA and CCD camera used for the measurements.	Correlation for spray penetration under atmospheric ambient conditions. Observation of two stages in the temporal evolution of the spray tip. SMD increases with air temperature, during the early stage of the injection.
Zhou et al. (2000)	Pressurised bomb. Different nozzle diameters and injection pressures. 1-D PDA. Mathematical regression of droplet SMD, droplets size distribution and their time-dependent properties.	Development of correlations for spatial Sauter mean diameter (SSMD) and temporal Sauter mean diameter (TSMD). Decreasing nozzle diameter decreases SSMD. Increasing injection pressure reduces SSMD. SSMD increases with an increase in injection quantity. Developed correlations produce results very close to the experimental values.

Table 3-3: Summary of testing conditions, set-up and material found in the literature.

Author	Year	IP (MPa)	ICP (MPa)	Nozzle	Emitting lens	Receiving lens	Scattering angle	λ (nm)	Validated samples	System	Miscellaneous
Araneo and Tropea	2000	30	Static	Sack single hole (0.19mm)	310 mm	160 mm	30°	514.5 488	20000	Dual PDA Dantec	U: 0 to 240 m s^{-1} V: -30 to 30 m s^{-1} ϕ: 0 to 50 µm Beam diameter: 1.35 mm Expander ratio: 1.98 Sphericity factor: 30 %
Arcoumanis et al.	1990		Static	5-hole			15°	514.5	2048		Ar+ laser with 0.6W power output
Ficarella et al.	1997	2.5 to 12	Static	5-hole VCO	250 mm	250 mm	30°	514.5 488	4000	2-D Aerometrics	U: -3 to 100 m s^{-1} V: -15 to 15 m s^{-1} ϕ: 2 to 103 µm Spatial filter (50µm)
Hardapulas et al.	1992		Static	5-hole	600 mm	300 mm	30°	514.5	5000	PDA	Laser power: 0.5 W
Hosoya and Obokata	1993	9.8	Static	Single and multi-hole			30°			LDA Dantec PDA Aerometrics	Data rate up to 100 kHz at the centre line of the spray.
Jimenez et al.	2000	40	Static	Single-hole	310 mm	600 mm	70°	514.5 488	3000	2-D Spectra Physic	Fringe spacing: 6.9393 and 6.308 µm. Data rate less than 1 Hz.
Koo et al.	1997	2.5 to 10	6	Single-hole	250 mm		72.5°		3000	Aerometrics	
Sanchez et al.	2000	30 to 45	Static	5-holes but 4 blocked			70°	514.5 488		Dantec 2-D PDA	Cross angle of 2.86° Velocity up to 300 m s^{-1} and size up to 200 µm
Wigley and Pitcher	1997	30 50 80	Engine running at 500 rpm	Single hole sac	450 mm	310 mm	70°	514.5		Dantec 1D PDA	Beam separation: 50 mm Beam diameter: 5 mm Fringe spacing: 4.64 µm U: -40 to 170 m s^{-1} ϕ: 0 to 88 µm
Zhou et al.	2000	15 to 21	4.5 to 5	3-hole nozzles			70°	514.5		Dantec 1D PDA	

4 CHARACTERISATION OF HIGH INJECTION PRESSURE DIESEL SPRAY

The objective of this study is to analyse the effects of injection pressure, in-cylinder pressure and nozzle configuration on high injection pressure Diesel spray. To capture the in-cylinder fuel sprays, a high-speed photographic technique was used, as a short exposure time was needed to freeze the fast moving spray; it also allowed the use of a fast framing rate that was required to record the characteristics of Diesel sprays with such short injection duration. The following sections present the instruments used and the results obtained in this study.

4.1 Experimental apparatus

4.1.1 Spray rig

The spray rig consists of a high-pressure Proteus engine and common rail injection system. The Proteus is a single cylinder two stroke operated engine, with ported intake that allows clean air to be added at each cycle. The engine is fitted with an optical chamber in place of the cylinder head to enable the visualisation of the fuel spray in quiescent air at high pressures and high temperatures. The engine specification are summarised in Table 4-1.

Bore	135 mm
Stroke	150 mm
Displacement	2.2 litres
Compression ratio	9:1
Combustion chamber flow	Quiescent

Table 4-1: Engine specifications.

Ambient temperatures and pressures representative of a modern Diesel engine at start of injection can be reached by boosting the charge up to 0.6 MPa. In-

cylinder pressure and temperatures up to 12 MPa and 750 K respectively can be achieved at start of injection. In-cylinder pressures were monitored using a 6121 Kistler pressure transducer. A dynamo connected to 6:1 ratio gearbox drove the Proteus at an engine speed of 500 rev/min. This was the operating engine speed for the test that were carried out in this study.

The optical cylinder head chamber has a diameter of 50 mm and a length of about 90 mm. Four 55 mm $\times$ 25 mm sapphire windows are fitted on each side of the chamber. A three-window optical cylinder head was specially designed for forward scatter PDA experimentations.

4.1.2 Injection system

A second generation Bosch common rail, electronically controlled injector system was used to generate and introduce the high injection pressure sprays into the chamber.

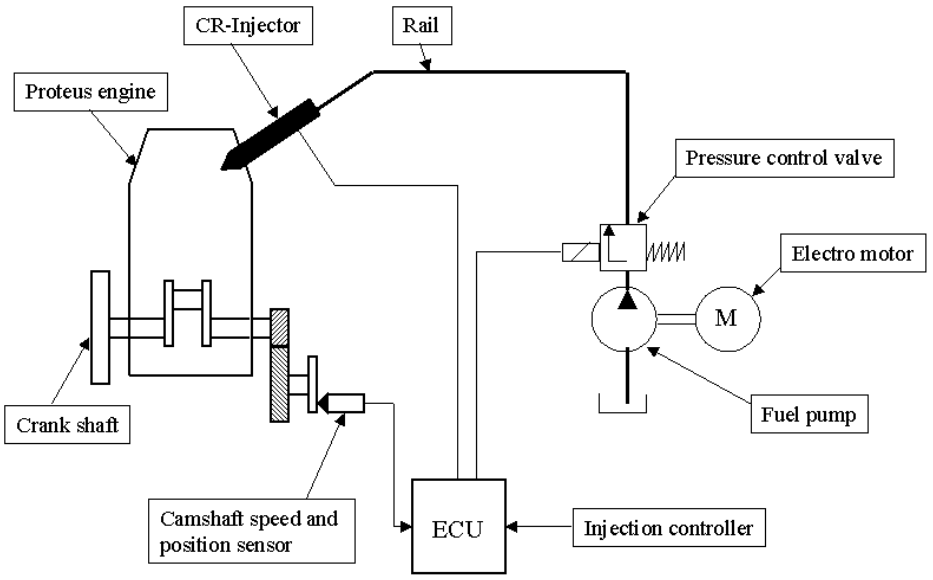

Figure 4-1: Schematic diagram of the fuel injection system (Kennaird et al., 2000).

This injection system gives flexibility in controlling the injection timing, injection duration and rail pressure. The FIE (fuel injection equipment) included a fuel pump, a common rail, an injector, a delivery pipe (kept short to be representative of a passenger car), an electric motor and an electronic control unit. Figure 4-1 shows the schematic of connections between these components. The fuel pump powered by an electric motor was running at 1400 rev/min ensuring a stable rail pressure with minimal fluctuation. A 4067 Kistler pressure transducer connected to an oscilloscope monitored and the delivery pipe pressure.

The fuel pump pressurises the fuel inside the common rail to pressures up to 160 MPa. The pressure regulator located at the exit of the high pressure fuel pump is controlled by the ECU and sets the correct pressure in the rail and maintains it at its level. The ECU regulates the fuel pressure to a set pressure ranging from 60 MPa to 160 MPa. An electronically controlled injector is used to convert the high-pressure fuel into Diesel sprays. Figure 4-2 shows a typical Bosch injector.

Figure 4-2: Bosch common rail Diesel injector

Various nozzles (Figure 4-3) can be fitted on the injector allowing the study of the effects of nozzle shapes, hole diameters and number of orifices on the spray characteristics. The nozzle holes are formed by electrical discharge machining methods.

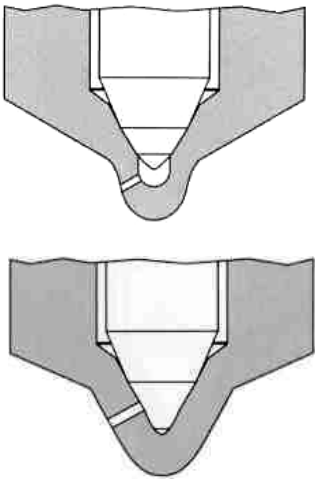

a

b

The holes of the mini-sac nozzle are located in the sac. Consequently, when the needle is closed, fuel is remaining in the sac and large fuel droplets might leave the nozzle after the end of the injection.

To achieve low HC emissions, the volume filled with fuel below the needle must be kept as short as possible. Therefore, the hole is located in the seat taper and is completely covered by the needle in the closed position.

Figure 4-3: Mini-sac (a) and valve covered orifice (VCO (b) nozzle (Bosch, 1999).

Type	Orifice diameter (mm)	Length to diameter ratio	Number of holes
VCO & mini-sac	0.10	10.0	Single
VCO & mini-sac	0.15	6.8	Single and five holes (VCO)
VCO & mini-sac	0.20	5.0	Single and five holes (VCO)

Table 4-2: Nozzle details.

The injection system is controlled by a custom electronic control unit and an injector controller, controlling the rail pressure (PID control), the injection duration, the injection angle, the number of skipped injections and the camera trigger angle. The custom controller has built in time trigger outputs to allow the synchronisation of external equipment. The rail pressure is set in load percentage of the high pressure pump, the injection angle in crank angle and the injection timing in milliseconds with a resolution of 0.05 %, 0.5º and 0.01 ms respectively. The injection controller can be operated in a test mode and simulation mode for static tests.

4.1.3 Image acquisition system

An optical system was arranged to visualise the fuel spray. The systems consist of Kodak Ektapro high-speed image analyser (Model 4540), two flood lights and two light diffusers. Figure 4-4 and Figure 4-5 show the optical set-ups used for the study of the spray characteristics.

The high-speed CCD video camera was capable of recording from 30 to 4500 frames per second at full resolution (256 pixels $\times$ 256 pixels $\times$ 256 grey levels). For faster recording rates (from 9000 to 40500 frames per second), the image resolution is reduced inversely proportional to the recording rate. In this study the majority of the pictures are captured at 27000 fps (128 pixels $\times$ 64 pixels), corresponding to an exposure of 37μs. The resolution is determined to be approximately 0.4 mm per pixel. Images were downloaded from the processor memory using interface software and converted into TIFF format to be compatible with other image manipulation software. The "full view" of the development of a single spray was achieved by mounting the injector in the cylinder head (Figure 4-4). However, to facilitate the observation of the development of the spray during the early stage of injection and multi-hole injector nozzles, modifications were made to the existing rig. The injector was mounted on the side of the optical chamber (Figure 4-5).

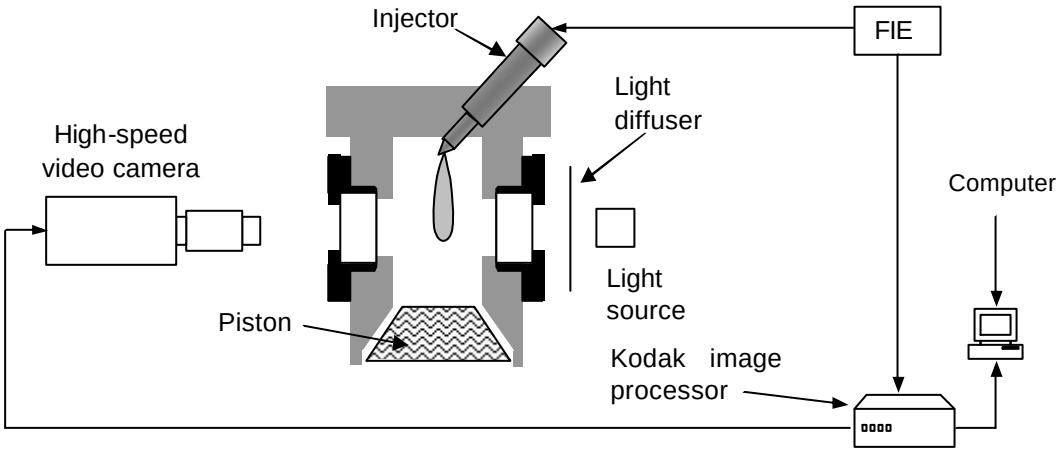

Figure 4-4: Schematic diagram of the optical set-up for single spray visualisation.

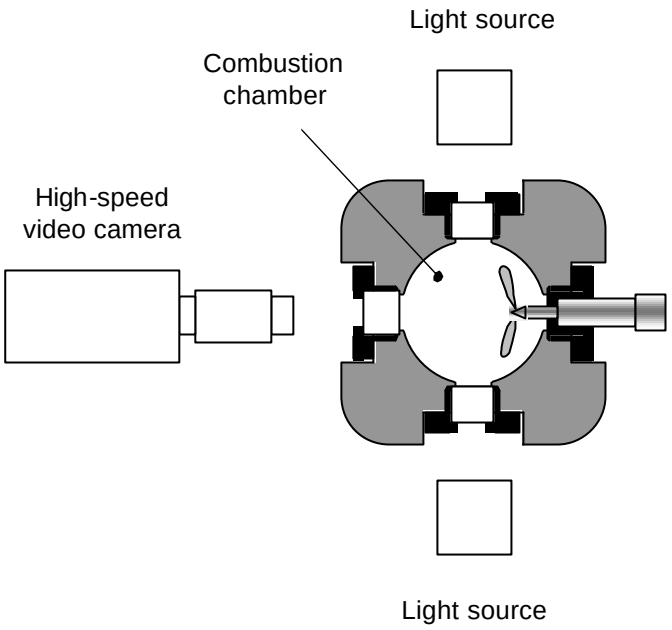

Figure 4-5: Schematic diagram of the optical set-up for multi-hole spray visualisation.

The camera was externally triggered with the injector driving pulse taken from the injector control box.

4.2 Results and discussion

4.2.1 Time delay

Assessment of the delay between the injection signal and the first sight of fuel leaving the nozzle was studied using the high speed video for different injection pressures and nozzle types (Figure 4-6). This injection delay proved to be independent of the in-cylinder charge density and nozzle type but closely related to the injection pressure.

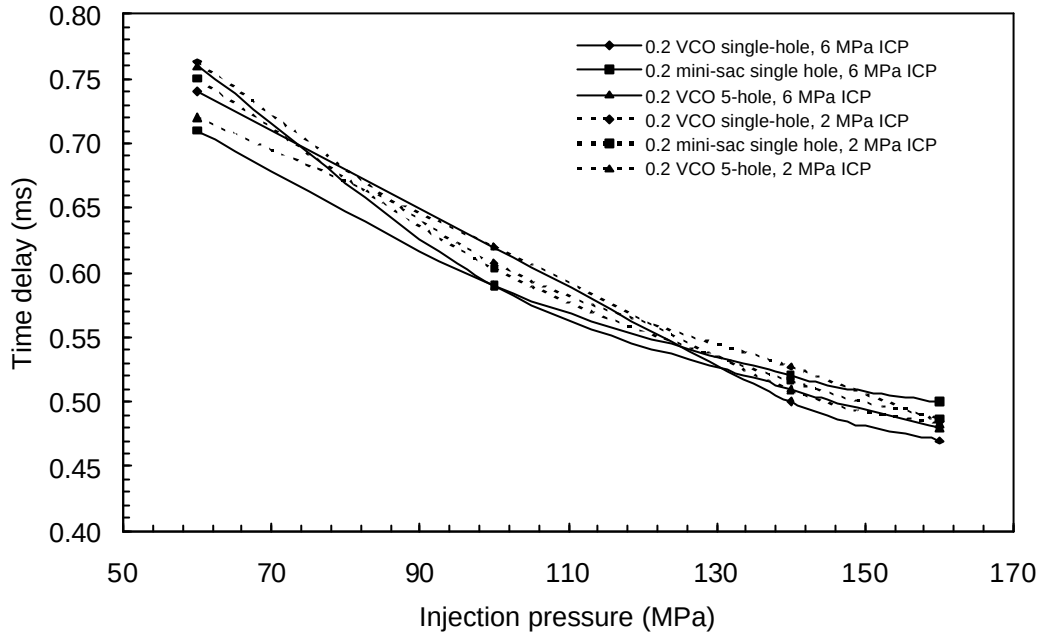

Figure 4-6: Time delay between injection signal and first sight of fuel for different injection pressure and nozzles at 2 and 6 MPa in-cylinder pressure, 10 mm^3 fuelling.

This indicates that downstream in-cylinder conditions have a negligible effect within the nozzle region during the opening phase and can be considered insignificant when considering injection delay.

4.2.2 Initial spray hesitation

Figure 4-7 shows an initial "hesitation" in penetration length at the beginning of the visible injection, despite the needle continuing rise.

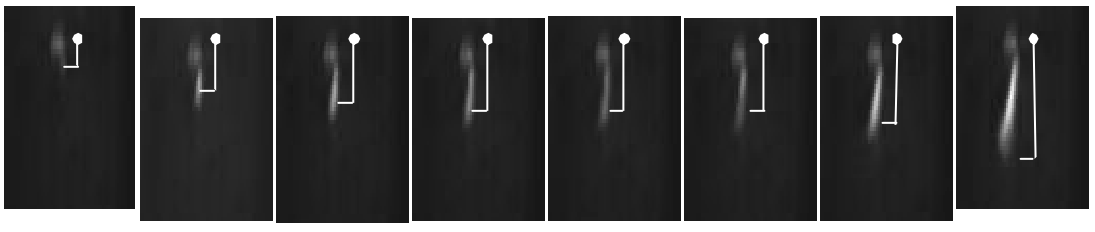

0.48 ms 0.52 ms 0.56 ms 0.59 ms 0.63 ms 0.67 ms 0.70 ms 0.74 ms

Figure 4-7: Single-guided single-hole 0.2 mm VCO nozzle, 160 MPa injection pressure and 4 MPa in-cylinder pressure.

Similar hesitations were also observed on the injection rate profile measured on the Lucas rate gauge, while associated fluctuations were observed in the videos at the end of the injection period; these however would not affect the spray penetration length (Figure 4-9).

Similar tests were conducted with an identical nozzle with a double-guided needle and a 0.15 mm single-hole VCO which both showed the same phenomenon to a lesser extent. This behaviour was not observed with the multi-hole VCO, the 0.10 mm single-hole VCO or the mini-sac nozzle tested (Figure 4-8).

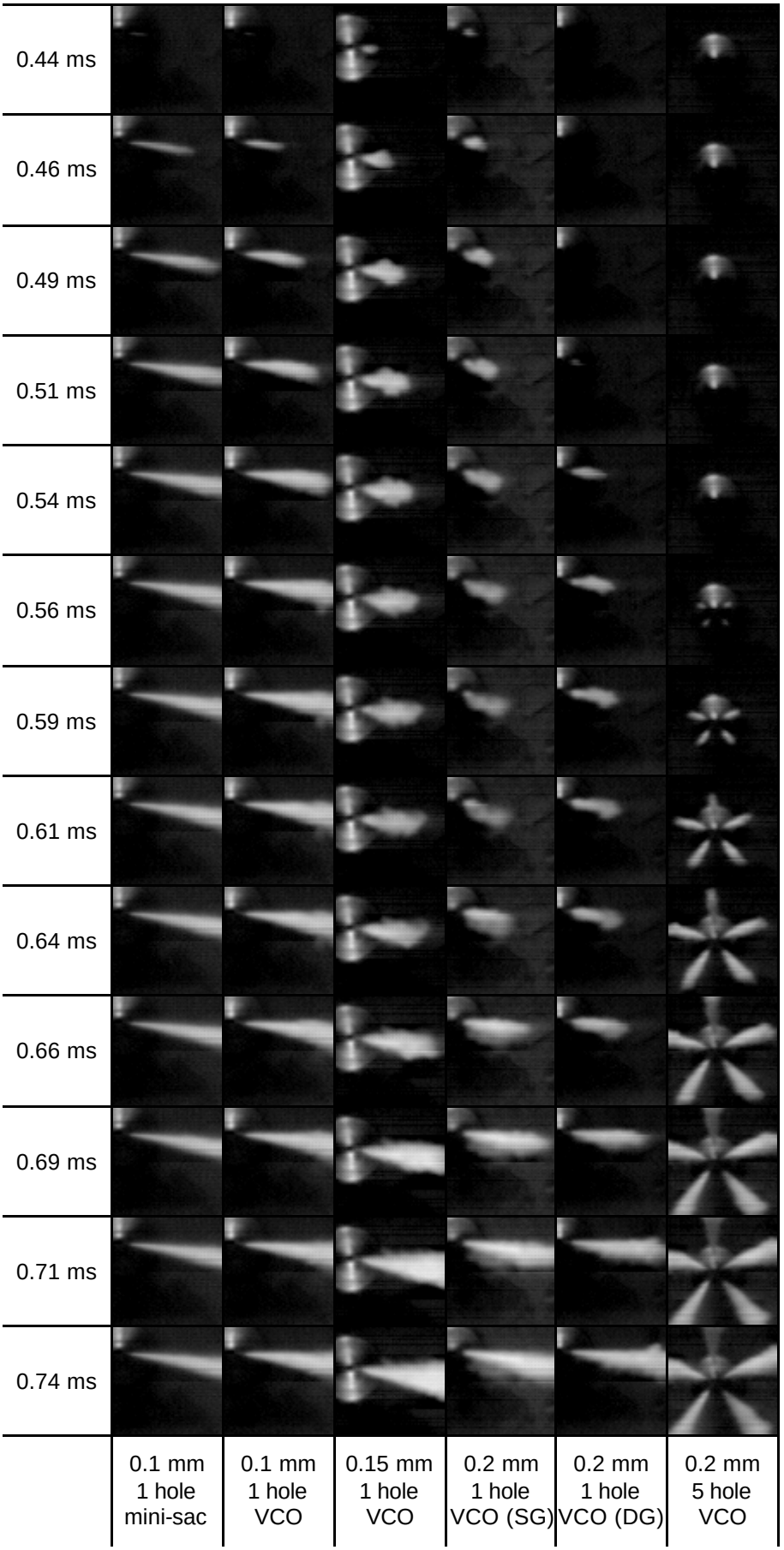
0.44 ms
0.46 ms
0.49 ms
0.51 ms
0.54 ms
0.56 ms
0.59 ms
0.61 ms
0.64 ms
0.66 ms
0.69 ms
0.71 ms
0.74 ms
0.1 mm 1 hole mini-sac
0.1 mm 1 hole VCO
0.15 mm 1 hole VCO
0.2 mm 1 hole VCO (SG)
0.2 mm 1 hole VCO (DG)
0.2 mm 5 hole VCO

Figure 4-8: Comparison between 0.1 mm single-hole mini-sac nozzle, 0.1 mm single-hole VCO nozzle, 0.15 mm single-hole VCO nozzle, 0.2 mm single-hole and single guided needle VCO nozzle, 0.2 mm single-hole and double guided needle VCO nozzle and 0.2 mm 5-hole VCO nozzle, for an injection pressure of 160 MPa and in-cylinder pressure of 6 MPa.

Spray structure and hole-to-hole variations have previously been observed in multi-hole VCO nozzle injections by Gupta et al. (2000) and were linked to the needle oscillations and cavitation. Prior to lifting, pressures around the needle are balanced, however once the lift starts, pressure can become temporarily unbalanced, especially if the holes are not uniformly spaced around the nozzle (single hole case). The unbalanced pressures around the nozzle lead to needle deflection and pulse closure of the orifice. This is not possible with a sac volume nozzle design due to the internal geometry. Figure 4-9 shows a graphical representation and video image capture of the effect of the closure on the flow (the negative measurement are caused by the pressure wave). Decreasing the nozzle hole section reduced this pressure balance effect to a point where the hesitation stops, reinforcing the hypothesis.

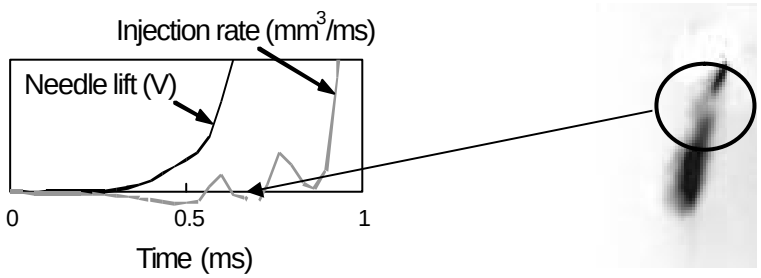

Figure 4-9: Injection needle lift trace and injection rate trace for a 0.2 mm VCO single guided, single hole nozzle, at an injection pressure of 160 MPa.

Single and multi-hole nozzles, of similar design, were shown to have comparable stable penetration rates (Crua, 2002). This implies that through the application of a time offset to adjust for the hesitation period, it is acceptable to compare single-hole nozzle data with penetration correlations in the literature. A time offset based on Figure 4-6 is equally acceptable to compare the effect of injection pressure since this can be implemented in an engine controller. This

positions the penetration rate as the most important feature of the penetration curve.

4.2.3 Spray characteristics at end of injection

In the close-up visualisation, liquid ligament are observed at the end of the injection. Figure 4-10 shows the end of injection of a single guided 0.2 mm VCO nozzle at an injection pressure of 160 MPa and in-cylinder pressure of 6 MPa. Significant liquid ligament sustaining for a long period of time, approximately 0.8 ms, is observed at the end of injection. Both the size of the trailing ligament its duration are reduced as the nozzle hole diameter is reduced (Figure 4-11). This phenomenon could also be explained by the bouncing of the needle. As described earlier, the pressure around the needle is unbalanced leading to needle deflection and pulse closure of the nozzle hole. This is confirmed by Figure 4-12, for the double guided 0.2 mm VCO nozzle, where no liquid ligaments trailing ligaments are observed towards the end of the injection. Because of the fuel remaining in the sac hole after the nozzle closure, a cluster of droplet was expected, unpredictably, no liquid ligament is observed in the mini-sac nozzle case (Figure 4-13).

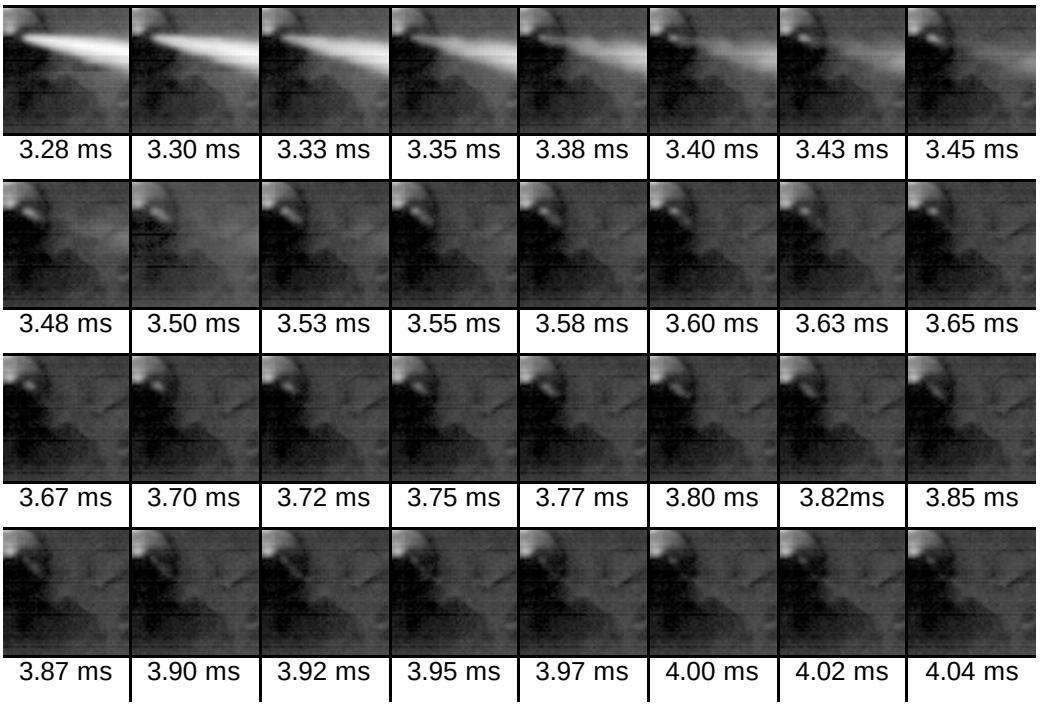

Figure 4-10: End of injection of a single guided 0.2 mm VCO nozzle, 160 MPa injection pressure and 4 MPa in-cylinder pressure

This remaining liquid ligament after the needle closure will result in higher HC emissions, as this injection end product will not atomise and is unlikely combust.

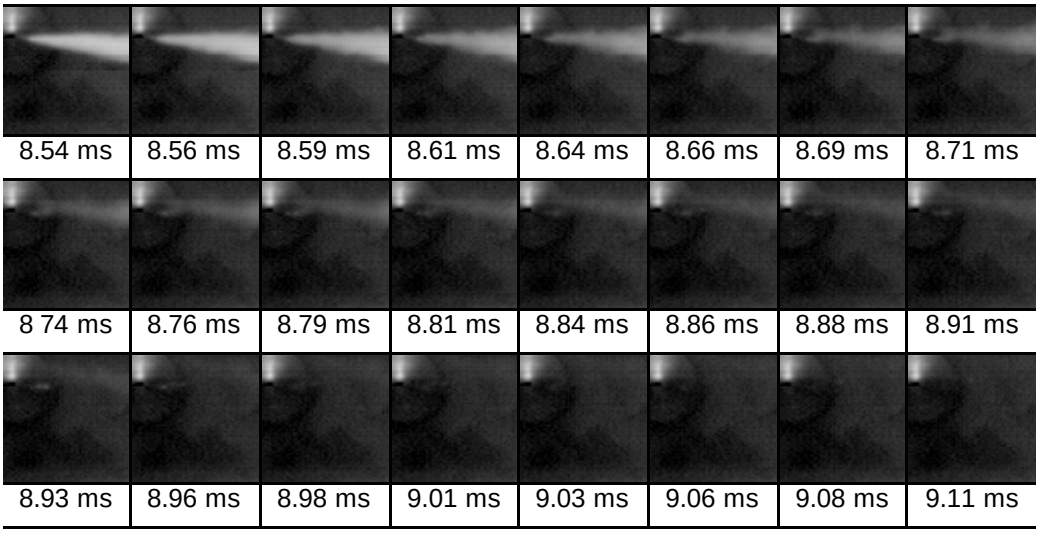

Figure 4-11: End of injection of a single guided 0.1 mm VCO nozzle, 160 MPa injection pressure and 4 MPa in-cylinder pressure

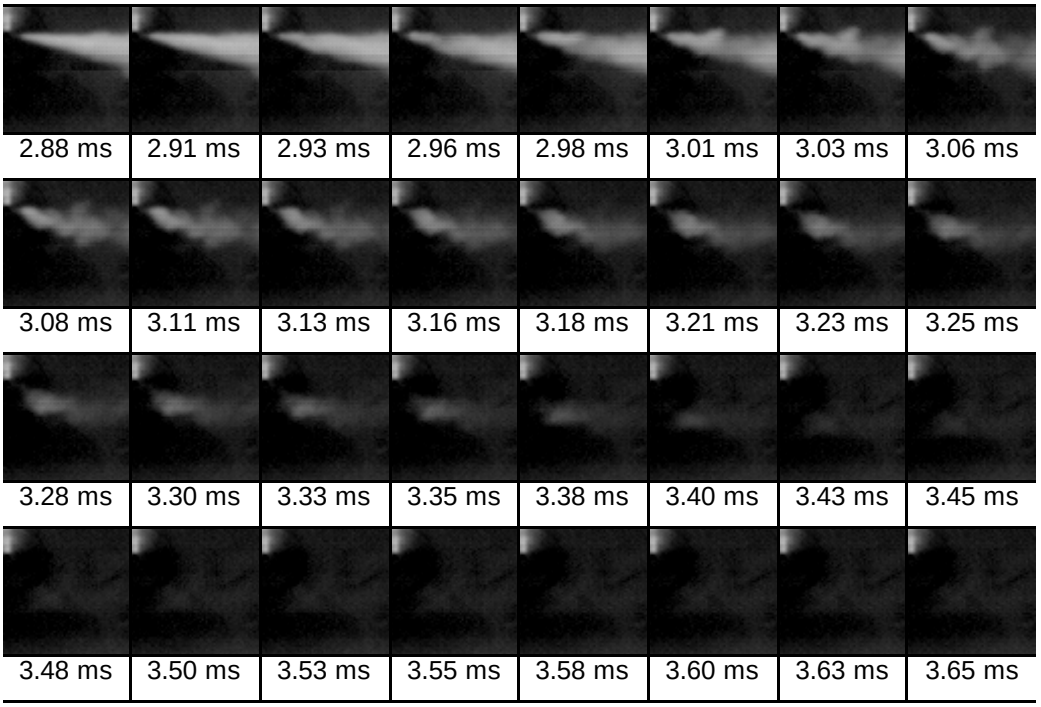

Figure 4-12: End of injection of a double guided 0.2 mm VCO nozzle, 160 MPa injection pressure and 4 MPa in-cylinder pressure

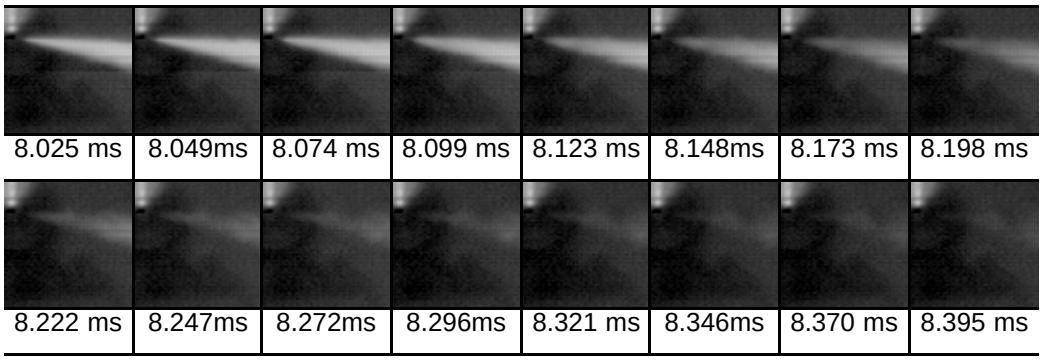

Figure 4-13:End of injection of a double guided 0.1 mm mini-sac nozzle, 160 MPa injection pressure and 4 MPa in-cylinder pressure

4.2.4 Hole-to-hole variability

Figure 4-15 to Figure 4-18 show the penetration for the sprays of three different nozzles operating at two in-cylinder and injection pressures. The spray tip penetration length is measured directly from the spray images, using the technique described by Crua (2002). The processing of the video was undertaken by specially developed software that measures the spray penetration length at each video frame after appropriate pixel thresholding. The maximum spray length was calculated by finding the spray pixel furthest from the nozzle. The software measured the spray penetration for each image and the results were saved on an excel file.

The hole-to-hole variability was studied using a 5-hole 0.2 mm VCO nozzle (K factor 0), a 6-hole 0.2mm factor K1 nozzle and a 6-hole 0.2mm factor K2 nozzle. The K factor 0 nozzle is also referred as a cylindrical nozzle, and the K factor 1 and 2 as a convergent nozzle.

A K factor nozzle possesses a tapered hole instead of a straight hole and was defined by Bosch as follows:

$$K = \frac{F_{entrance} - F_{exit}}{10} \quad (\mu m) \qquad (4.1)$$

Table 4-3 summarises the characteristics of each VCO nozzle used in this study.

K	Entrance diameter (µm)	Exit diameter (µm)	Number of holes
0	0.2	0.2	5
1	0.185	0.175	6
2	0.185	0.165	6

Table 4-3: Specifications of injector nozzle

Significant hole to hole variation in penetration of the sprays of a VCO nozzle is observed, especially in the early stage of the injection (Figure 4-15 and Figure 4-16). For both the low and high injection pressure case, the fastest spray of the VCO nozzle appears in the hole 2 direction, while the slowest one is almost on the opposite side in the hole 5 direction. In addition, puffy structure along the edges of the sprays is also observed (Figure 4-8).

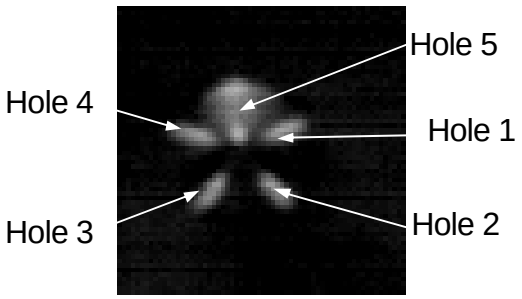

Figure 4-14: VCO nozzle hole description

There are mainly two reasons for the hole-to-hole variability:

- Needle eccentricity leading to difference in spray penetration. Evidence of needle eccentricity can be observed on Figure 4-8, where the hole heading in the “12 o’clock” direction (hole 5) remained covered by the needle in the early stage of the injection.
- Different hydrodynamic behaviour of each orifice

The spray retardation was not altered by the injection pressure as hole 5 was always the last one to inject.

In Figure 4-15 and Figure 4-16, an increase in the variation of the penetration can be observed with an increase in the injection pressure. The effects of these variations will be described later.

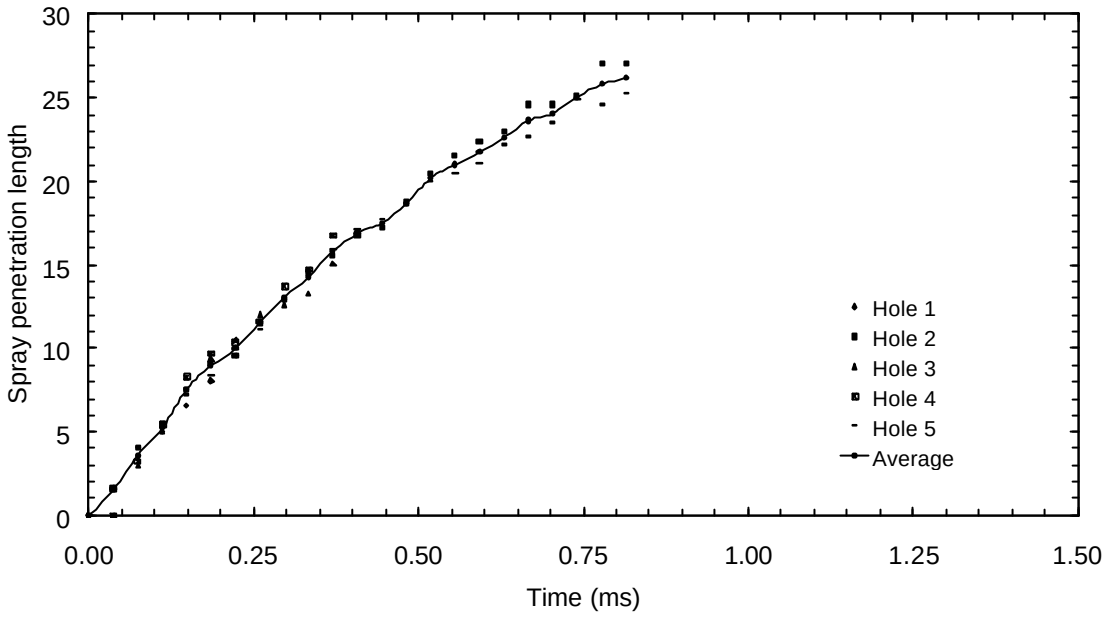

Figure 4-15: Hole-to-hole spray penetration length variation; 5-hole 0.2 mm VCO nozzle, 60 MPa injection pressure and 4 MPa in-cylinder pressure.

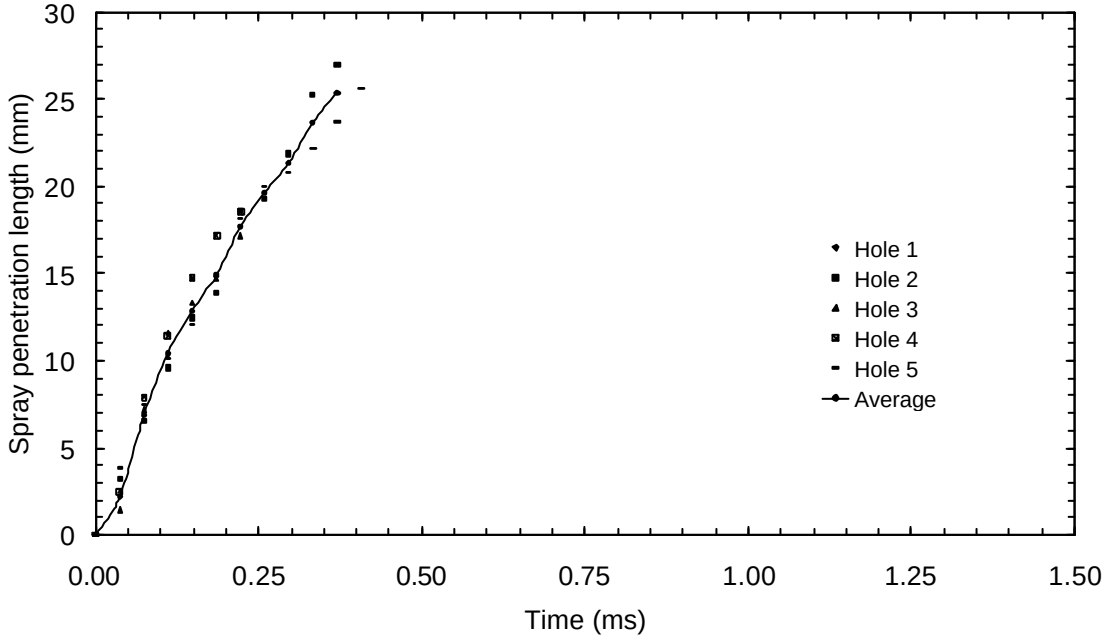

Figure 4-16: Hole-to-hole spray penetration length variation; 5-hole 0.2 mm VCO nozzle, 160 MPa injection pressure and 4 MPa in-cylinder pressure.

Figure 4-17 represents the spray penetration length variation of a 6-hole factor K2 0.2 mm VCO nozzle at 160 MPa injection pressure and 4 MPa in-cylinder pressure.

As summarised in Table 4-4**,** the variation of spray penetration length depends mainly on the injection pressure and nozzle shape. In general, observations show that the injector equipped with a k1 factor nozzle has the best performance in terms of variation in penetration length. These variations may have some effects on combustion controllability and pollutants emissions. Considering a Diesel engine running at 3000 rpm, at 160 MPa injection pressure for a K2 factor nozzle, the time variation between the slowest and the fastest spray is 0.148 ms, which is equal to 2.66 crank-angles. This time lag could result in significant variation in possible mixing and air utilisation and combustion variation among each of the sprays from a single injector.

The comparison between the spray penetration of a convergent VCO nozzle and a cylindrical nozzle was unfortunately not possible in this study, as the internal holes had different diameter.

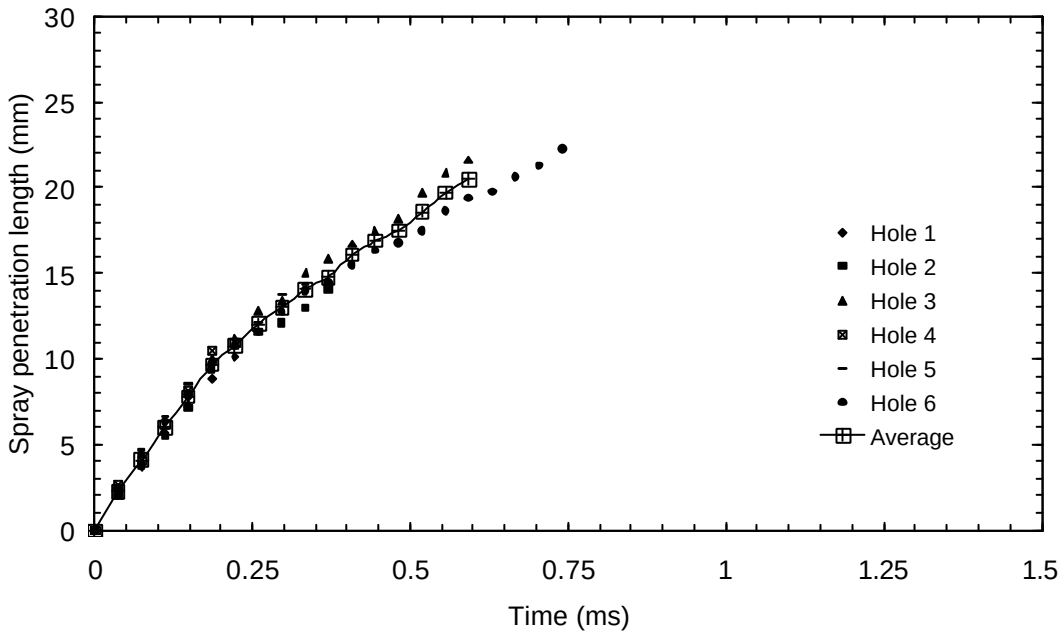

Figure 4-17: Hole-to-hole spray penetration length variation; 6-hole 0.2 mm factor K2 VCO nozzle, injection pressure of 60 MPa and in-cylinder pressure of 4 MPa.

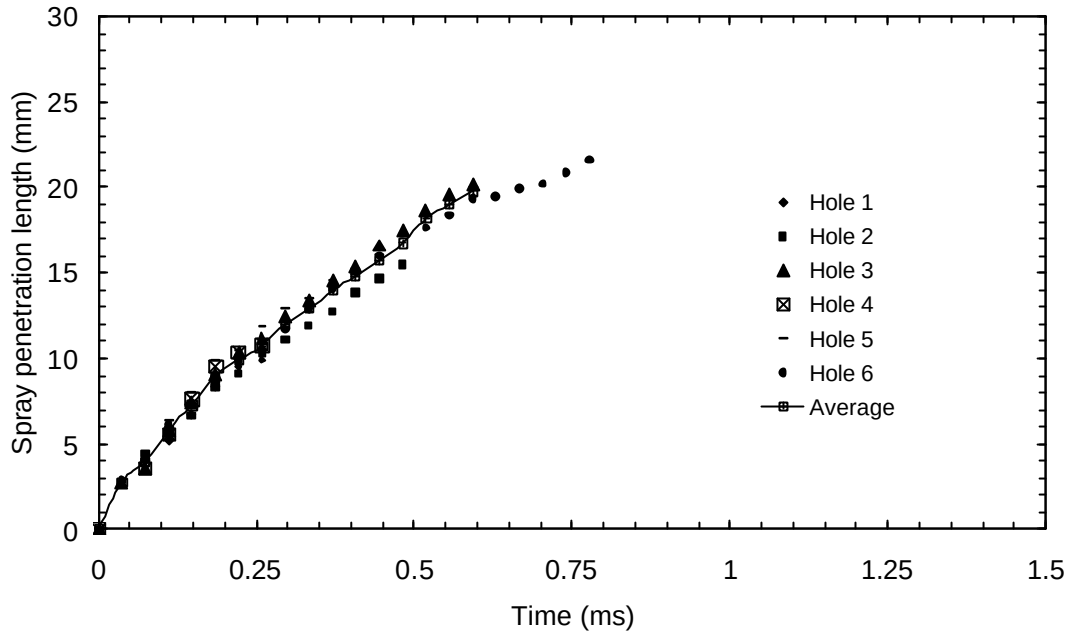

Figure 4-18: Hole-to-hole spray penetration length variation; 6-hole 0.2 mm factor K1 VCO nozzle, injection pressure of 60 MPa and in-cylinder pressure of 4 MPa.

Nozzle	Injection pressure (MPa)	Variation of penetration (mm)
Factor K1	60	1.92
	160	2.35
Factor K2	60	2.19
	160	3.13

Table 4-4: Comparison of hole-to-hole spray penetration length variation for 4 nozzles at 60 and 160 MPa injection pressure and 4 MPa in-cylinder pressure.

4.2.5 Spray structure of a K factor nozzle

The spray structure of a 6-hole K1 factor VCO nozzle was undertaken by measuring the penetration of 1 of the 6 spray plumes, instead of the value of the six independent sprays.

Figure 4-19 shows the effect of injection pressure and ambient condition on the penetration of the spray tip. As shown in Figure 4-19, for example, at 0.3 ms after start of injection with 4 MPa in-cylinder pressure, the penetration increased

from 12.3 to 20 mm corresponding to increase of injection pressure from 60 MPa to 160 MPa. Similarly, with a fixed injection pressure of 160 MPa, at 0.3 ms after start of injection pulse, the penetration decreased from 20 to 14.6 mm corresponding to the increase of the in-cylinder pressure from 4 to 8 MPa. The results show that both ambient and injection pressure have significant effect on spray tip penetration. The effect of injection and in-cylinder pressures on spray penetration profiles were found to follow the trends observed by Crua (2002), although the author's tests were undertaken with 0.2 VCO single hole nozzle only.

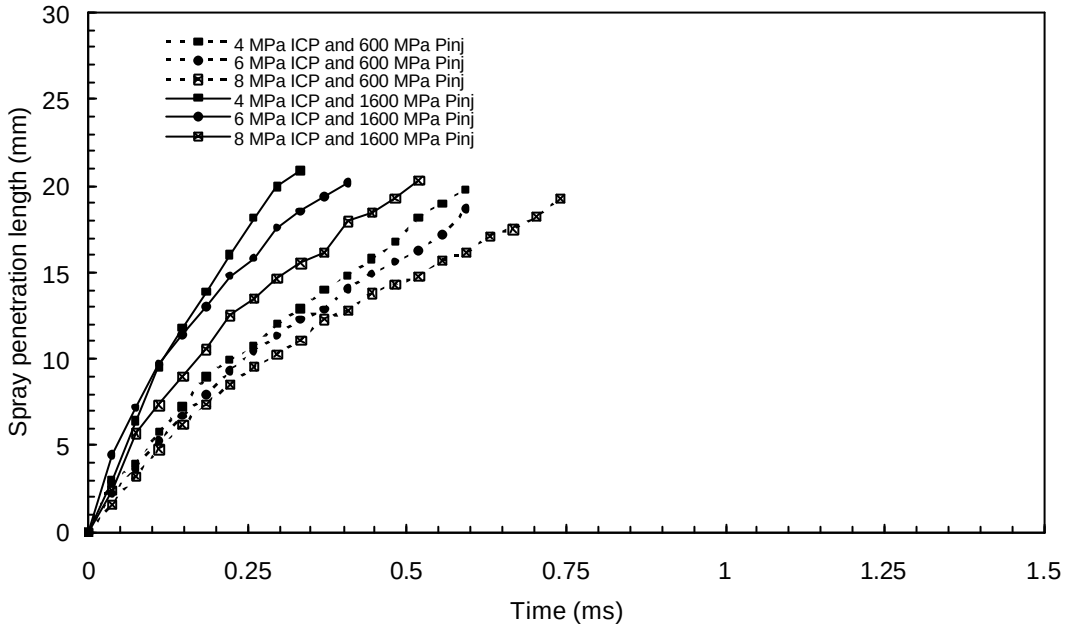

Figure 4-19: Effect of injection and in-cylinder pressures on the spray penetration length; 6-hole 0.2 mm factor K1 VCO nozzle, injection pressure 60 and 160 MP, in-cylinder pressure ranging from 4 MPa to 8 MPa and 566K TDC gas temperature.

The previous studies on the effects of ambient density and injection pressure (Crua, 2002 and Kennaird et al. 2002) were focused on the aerodynamic effects on spray behaviour. In this section, the effects of the nozzle hole inlet configuration on spray characteristics are analysed by using two convergent K factor nozzles of different configurations, a K factor 1 and a K factor 2. The VCO nozzles investigated in this study had an identical inclination angle and spray

cone angle of 150°. Table 4-5 displays the injection conditions for the experiment.

In-cylinder pressure (MPa)	4, 6, 8
Injection quantity (mm^3)	30
Injection pressure (MPa)	60, 160
Injection pulse width (ms)	2.4, 1.2
Intake temperature (K)	283
Estimated TDC temperature (K)	566
Injection angle	TDC

Table 4-5: Experimental in-cylinder and injection conditions.

Figure 4-20 and Figure 4-21 present the effects of the taper ratio, K factor, in VCO nozzle hole on the spray tip penetration length. In the first part of the injection (before 0.25 ms), the spray tip penetration length of the spray from the nozzle with a K factor of 1 is similar to that of the spray from the nozzle with a K factor of 2. The figures also show that there is a large difference in penetration length between the sprays from a K factor 1 and the sprays from K factor 2. The faster spray penetration rates, for the lower K factor, are observed at each in-cylinder and injection pressures.

Sprays from the nozzle with high K factor were expected to have longer penetration due to a more concentrated momentum flux with higher injection velocity. However, spray from a K factor 2 nozzle had a slower penetration rate than the spray from a K factor 1 nozzle. This discrepancy may be explained by decreased cavitation in the nozzle hole leading to a more important axial velocity decay. This smaller axial velocity results in a shorter spray tip penetration. This means that increasing the K factor of a convergent VCO nozzle leads to a slower mixing process that could deteriorate the combustion.

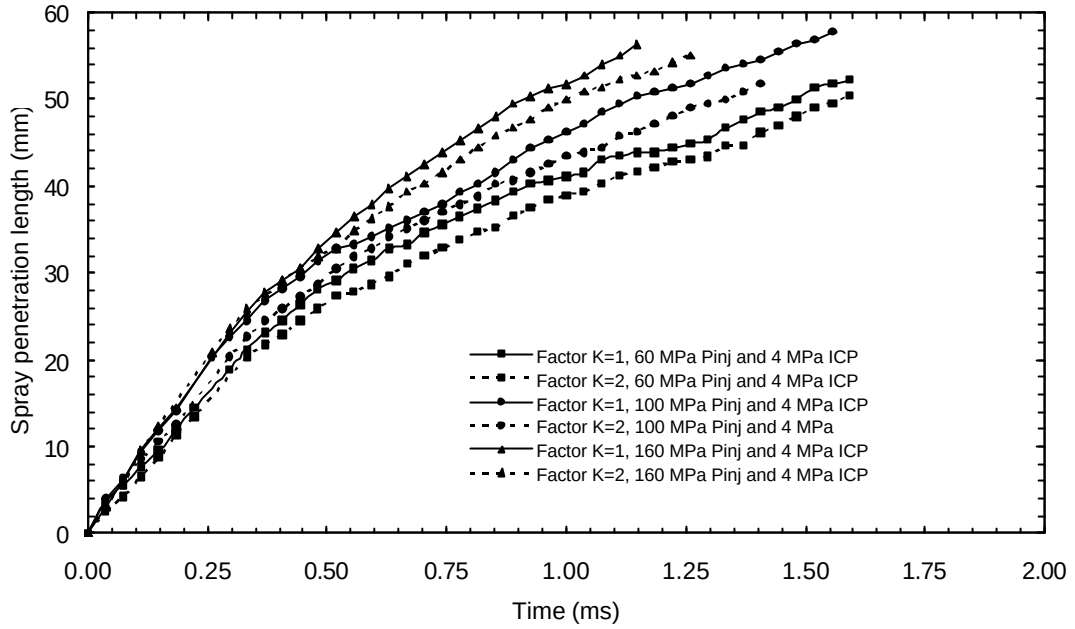

Figure 4-20: Effect of K factor on spray tip penetration length, injection pressure of 60 MPa and 160 MPa, in-cylinder pressure of 4 MPa and in-cylinder temperature of 572K

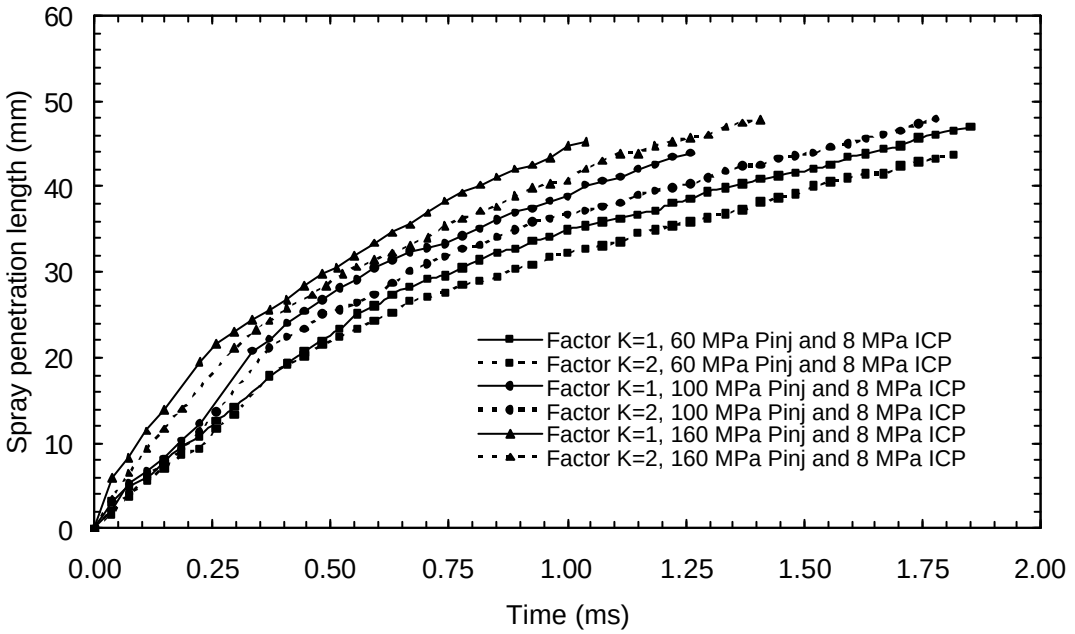

Figure 4-21: Effect of K factor on spray tip penetration length, injection pressure of 60 MPa and 160 MPa, in-cylinder pressure of 8 MPa and in-cylinder temperature of 572K.

4.3 Errors in the measurements

Repeatability tests were performed to assess the variability in penetration for a various range of in-cylinder conditions. The accuracy of measurements of spray tip penetration was estimated to be ±0.4 mm (Figure 4-22).

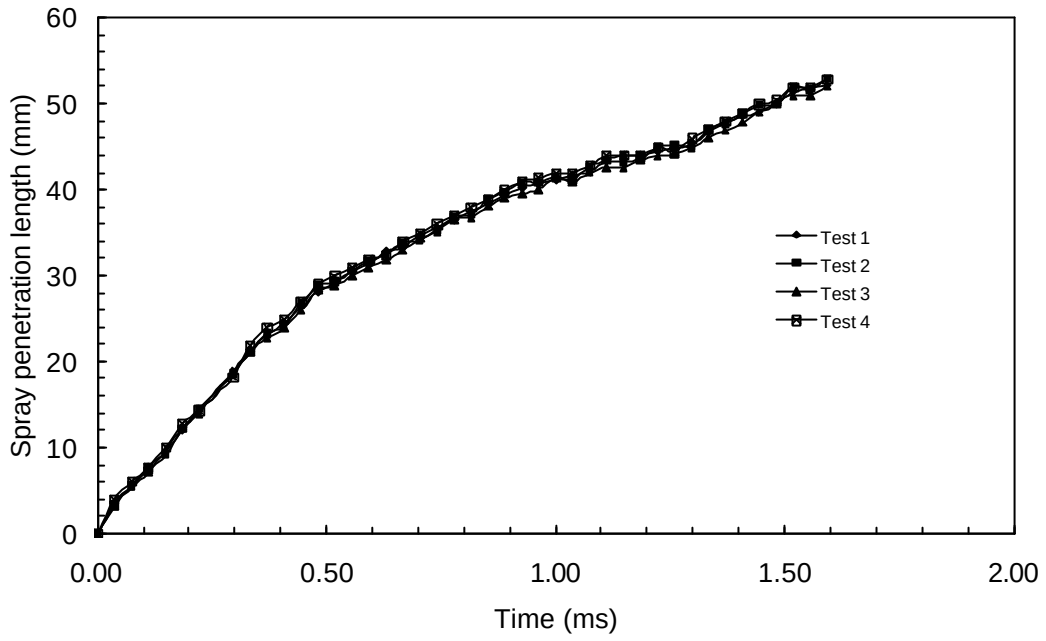

Figure 4-22: Repeatability test of a K1 factor VCO nozzle, at 60 MPa injection pressure and 4 MPa in-cylinder pressure

4.4 Conclusion

A complete methodology to characterise Diesel sprays has been presented. Specific findings obtained from those spray visualisations can be summarised as follows:

- Injection delay proved to be closely related to the injection pressure but independent of the in-cylinder charge density and nozzle type.
- Both injection pressure and in-cylinder pressure affect the spray tip penetration significantly. The penetration increase corresponding to an increase of injection pressure or decrease of ambient pressure.

- The spray characteristics at the end of the injection are shown to be strongly dependent upon the nozzle hole dimensions and geometry (VCO or mini-sac nozzle).
- The hole-to-hole variations appear to be strongly linked to the nozzle hole geometry and diameter.
- The variations in spray penetration are mainly caused by needle eccentricity and variation in hydrodynamic behaviour between each hole.

5 PDA EXPERIMENTAL SET-UP AND METHODOLOGY

5.1 PDA optimisation for optimal measurement

Phase Doppler anemometry has become reported as a technique that requires minimal optimisation. However this is not generally true, when very high accuracy is required (Tropea, 1995). The measurement of a Diesel spray remains difficult due to the density of the spray, and is affected by uncertainties introduced by bias effects. Some of these errors can only be minimised. Therefore, a thorough study and careful selection of the operating parameters of the system must be utilised to significantly improve the statistical significance of the data collected.

Tests carried out for the calibration of the PDA were performed at 45 mm from the nozzle and for 60 MPa injection pressure and 1.6 Mpa in-cylinder pressures.

5.1.1 Photomultiplier effect

The sensitivity and the relative balance of the photomultipliers (PMT) were determined to ensure reliable and repeatable measurements that were not affected by the PMTs' voltage. This voltage was controlled via computer software. The PMTs' voltage were varied between 900 V and 1700 V. Below 900 V the processor calibration procedure calibration cannot be successfully completed because of the weakness of the signal, and above 1700 V the signal is saturated and may influence the reliability of the data obtained. It should be noticed that saturation of signals from the larger droplets can also occur.

The balance of the photomultipliers connected to channels U1, U2 and U3, used to measure droplet axial velocity and diameter, is checked by using the "system monitor" in the BSA Flow Software. To ensure, a perfect balance between all photomultipliers, the voltages need to be adjusted to obtain equal Doppler burst amplitude on each channel (Figure 5-1).

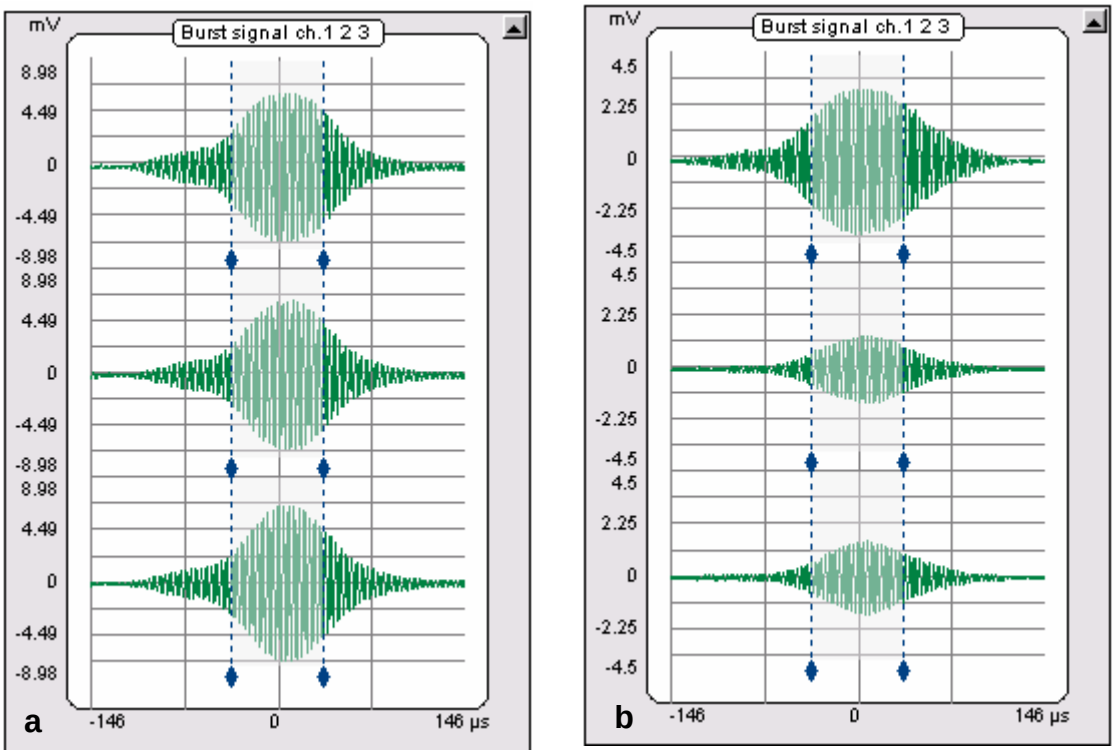

Figure 5-1: (a) Balanced photomultiplier voltage. (b) Unbalanced photomultiplier voltage.

Arithmetic mean diameter (AMD) and Sauter mean diameter (SMD) can be used to determine an optimum photomultiplier voltage. However SMD is more erratic due to the influence that a few additional large droplets may have upon the mean value. Figure 5-2 shows how the measured arithmetic mean diameter varied with the PMT voltage. When the voltage is low, small droplets with relatively weak signals are less readily detected. As fewer small droplets are detected, the mean diameter increases and the greatest spread in droplet diameter distribution are observed. The data rate is also affected by the voltage; an increase in voltage will increase the data rate. However, the velocity measurements were not affected by an increase in voltage. The AMD increases slowly at low PM voltage, indicating that small particles are no longer detected.

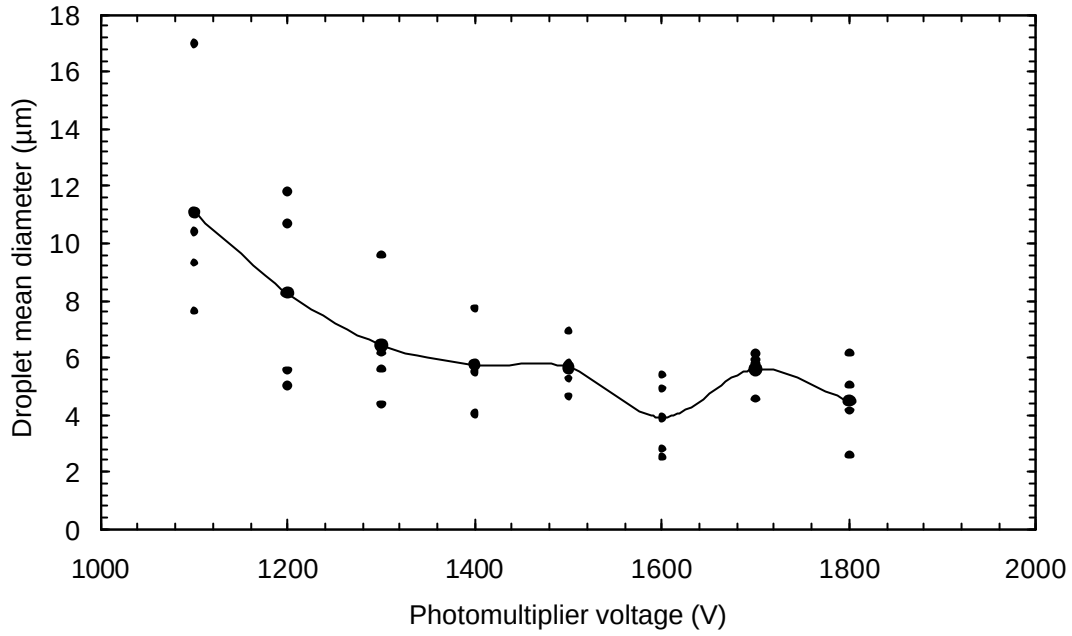

Figure 5-2: Droplet mean diameter as a function of the photomultiplier voltage under standard test conditions.

The photomultiplier voltage was chosen to maximise the acquisition of small particles and to avoid signal saturation. The appropriate voltage was selected by picking a value that ensured that the mean diameter drops to a "plateau" (Figure 5-2). The voltage saturation can be observed after 1500V, where the curve does not follow the trend previously taken. At this point PMT's are likely to be damaged and continued operation will quickly lead to their failure. Signal saturation is also accompanied by the generation of spurious velocity and droplet size data.

5.1.2 Laser power

The laser power effects should show the same trends as photomultiplier voltage (Figure 5-3). Increasing the laser power will decrease the AMD, because small droplets will be detected. However, the system noise is increased; the validation rate decreases and spurious data are generated.

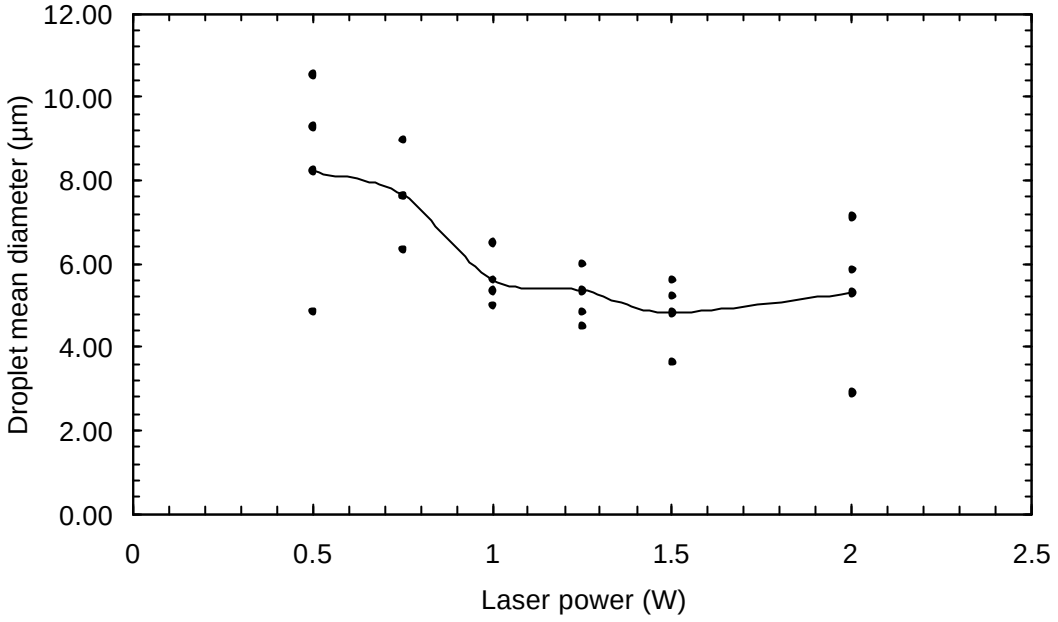

Figure 5-3: Droplet mean diameter as a function of laser power.

However, the effects of laser power on AMD are less pronounced than the photomultiplier voltage effects. As can be observed on Figure 5-3, a plateau is reached for a laser power at the laser head between 1 and 1.25 watt. This was equivalent to a measured laser power of 500 mW at the probe volume.

5.1.3 Measurement volume size

The phase Doppler anemometer measurement capabilities are determined by the components of the system. For example, the PDA transmitter will determine where the green laser beams will intersect and will also determine the range of droplet velocities and sizes that can be measured. However, by changing parameters such as the focal length, the expander ratio and the beam separation on the transmitting optic, the measurement range can be altered. In this study only one transmission optic was available with a 310mm focal length lens and beam expander ratio of 1.98. Therefore the only available variable parameter on the transmitting optic was the beam separation. The size of the measuring volume and the number of fringes were calculated from the beam diameter, the lens focal length, the laser wavelength, the expander ratio and the beam separation using the equations given below.

- Length

$$d_z = \frac{4F?}{p E_R B_d \sin(a/2)} \quad (5.1)$$

- Width

$$d_y = \frac{4F?}{p E_R B_d} \quad (5.2)$$

- Height

$$d_x = \frac{4F?}{p E_R B_d \cos(a/2)} \quad (5.3)$$

- Fringe separation

$$d_f = \frac{?}{2\sin(a/2)} \quad (5.4)$$

- Number of fringes

$$N_f = \frac{8F\tan(a/2)}{p E_R B_d}, \quad (5.5)$$

where F is the focal length, ? the wavelength, E_R the expander ratio, a the intersection angle of the laser beams and B_d the beam diameter. Results are summarised in Table 5-1. Note that as the beam intersection angles are small, the width and the length of the measuring volume are almost equal. The maximum measurable velocity bandwidth and diameter were determined from the BSA engine processor.

	Beam separation (mm)							
Before expander	5	10	15	20	25	30	35	40
After expander	9.9	19.8	29.7	39.6	49.5	59.4	69.3	79.2
Height d_x (mm)	2.92	1.46	0.97	0.73	0.59	0.49	0.42	0.37
Width d_y (mm)	0.047	0.047	0.047	0.047	0.047	0.047	0.047	0.047
Length d_z (mm)	0.047	0.047	0.047	0.047	0.047	0.047	0.047	0.047
Beam intersection half-angle (deg)	0.91	1.83	2.74	3.65	4.56	5.47	6.37	7.28
Number of fringes	3	6	9	12	14	17	20	23
Fringe spacing (µm)	16.11	8.06	5.38	4.04	3.23	2.70	2.32	2.03
Max measurable diameter (µm)	314	157	105	79	63	53	45	40
Max velocity bandwidth (m s^{-1})	1933	967	645	483	388	324	278	244

Table 5-1: Investigated PDA measurement capabilities for different beam separations (F=310 mm, ?=514.5 nm, E_R=1.98 and B_D=2.2 mm)

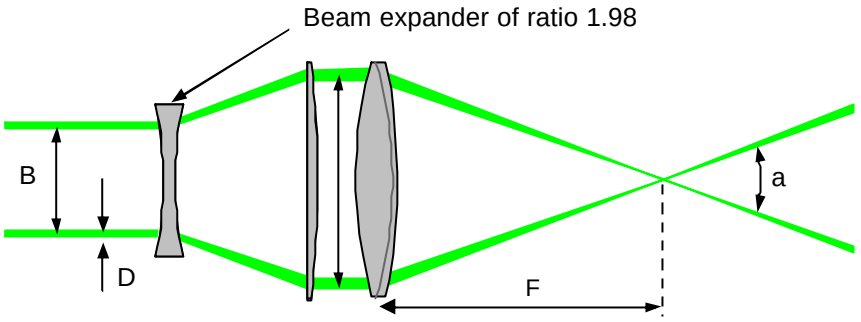

Figure 5-4: Transmitting optic (Dantec, 2002).

The physical size of the measurement volume is inversely proportional to the beam separation. A large beam separation on the transmitting optic will produce a small measurement volume. A large measurement volume allows larger diameter and high velocities particles to be measured. However, for a given laser power, the intensity of any scattered light will be reduced, and small droplets possessing weakened signals will not be detected. A larger measurement volume is also susceptible to multiple droplets at a single instance and will lead to the rejection of the signal by the processor (multiple scattering). Conversely, a smaller measurement volume will limit the maximum droplet velocity and diameter that can be measured although the light intensity is increased. This will allow measurement of small droplets as it will improve the intensity of the scattered light and will minimise the probability of having multiple droplets within the probe volume. Under these spray conditions, reducing the size of the measurement volume will also increase the droplet acquisition data rate (Figure 5-5). This is due to the reduced risk of having more than one particle in the measurement volume, but also because the burst signal sent to the processor is greater in magnitude and shows increased modulation.

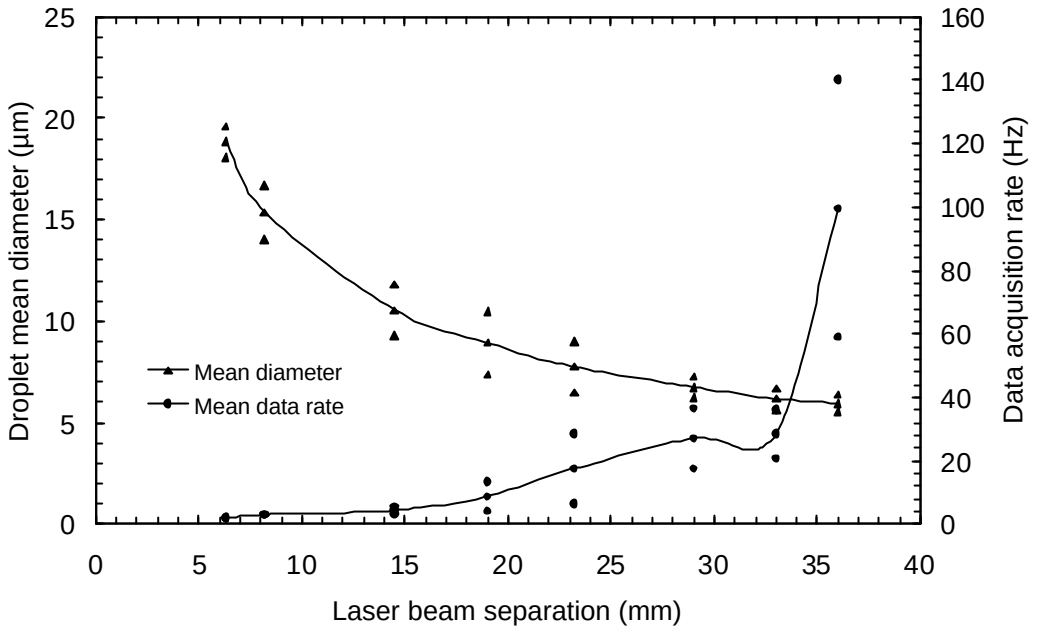

Figure 5-5: Droplet mean diameter and data acquisition rate as a function of beam separation.

A large beam separation will result in a wider beam intersection angle which will also reduce the trajectory ambiguity effect.

5.1.4 Receiver optic aperture

The optic used in this study was a Dantec “classic” receiver, where the aperture is set by a micrometer controlled knife edge. By varying the micrometer slit from 2 (maximum) to 0 (minimum) mm, the droplet sizing range can be increased by a factor of 2.6. For instance, if a 310 mm focal length lens is used on the transmitting and receiving optics with a beam separation set to 36 mm on the transmitting optic, the largest measurable diameter is 43.967 µm and 114.299 µm, for a micrometer set on 2 mm and 0 mm respectively. However, as the aperture is reduced, there is a reduction in light collection efficiency and the laser power or signal gain should be increased to compensate, a small droplet may be well below the detection threshold. As described above, an increase in laser power would decrease the validation rate and generate spurious data; therefore the micrometer controlled knife edge was set to 2 mm. One could argue that by choosing such a receiver optic aperture and its associated

measurable diameter, a portion of droplet population (above 44 µm) could be ignored.

Droplet distributions were plotted for each measurement gathered in the Diesel spray, to ensure the statistical reliability of the results (Figure 5-6).

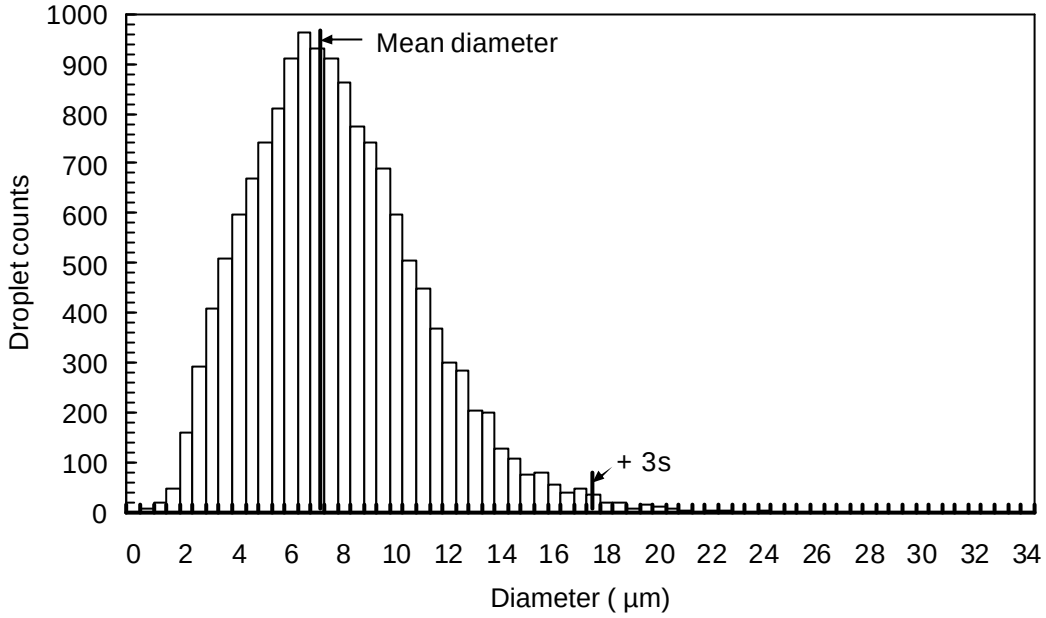

Figure 5-6: Typical droplet distribution at 45 mm from the nozzle along the spray axis at 4 Mpa ambient pressure and 60 Mpa injection pressure (Lacoste et al., 2003).

It is advantageous to maximise the number of droplets acquired during measurement. Following this viewpoint, other filtering parameters were also set to maximise data collection. High signal gain (26 dB) and low signal-to-noise ratio (-3 dB) were used.

As described in chapter three, droplet diameter measurement was performed by two different pairs of photodetectors. If the size determined from each of the photodetectors differs by more than a selected amount, that droplet will be considered as non-spherical and will not be validated. Koo and Martin (1991) demonstrated that little difference was observed in the data when the spherical validation band was increased from 3 to 9 %. The spherical validation band was set to 10 %. A higher setting would increase the validation rate, but the

measured droplets would no longer be spherical and the results would become skewed towards a large droplet bias.

5.2 Selection of the scattering angle

The choice of the scattering angle is also important when determining the overall performance of the PDA equipment. E.g.: for liquid Diesel droplets, two forward scattering angles are commonly used: 30º and 70º (Koo and Martin (1990), Wigley and Pitcher (1997), Hosoya and Obokata (1993)).

The main advantage of 30º configuration is the high signal to noise ratio. At 70º, which is close to the Brewster angle for Diesel fuel, the incident light is parallel polarised in the plane of scattering. In theory, no light should be reflected from the droplets towards the receiving optic; the only signal should come from the refracted light. A second advantage in using an angle of 70º is that the variation in the refractive index, which can occur if the fuel temperatures changes, has little effect on the slope of the calibration curve (Kneer et al., 1994).

Considering the above, a scattering angle of 70º was chosen as the most suitable scattering angle for these experiments, utilising a special Proteus cylinder head configuration (Figure 5-7).

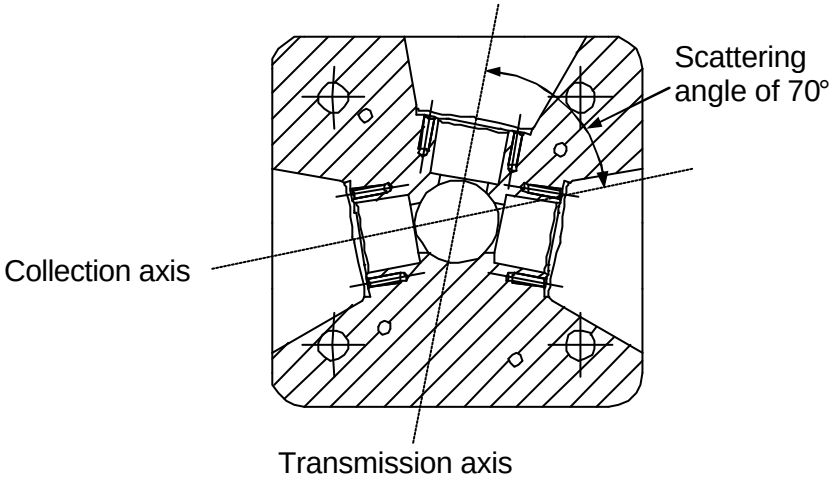

Figure 5-7: Cross-section view of the PDA Proteus cylinder head

5.3 Optical set-up

The optical experimental set-up, shown below, consists of nine components. Firstly, the fuel injection system is mounted on top of the spray rig chamber. The fuel is injected into the chamber through a 0.2 mm VCO single-hole injector.

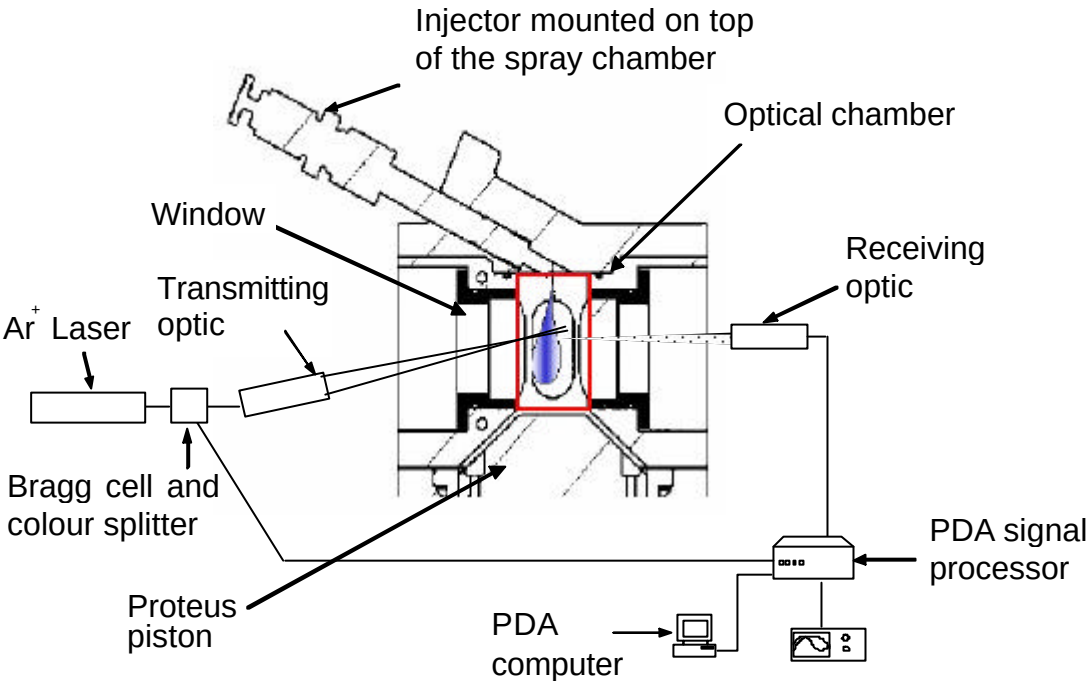

Figure 5-8: Experimental set-up.

The light source is a Spectra Physics Argon-ion laser operating in “all lines” modes. The beam passes through a Bragg cell and colour separator, which splits the incoming beam into four beams and shifts the frequency of each pair by 40 MHz. The beams then travel to the transmitting optic through an optical fibre. A lens mounted on the transmitting optic focuses the two beams to form the measurement volume at a focal length of 310 mm. The receiving optic is positioned at 310 mm from the measurement volume, at an angle of 70°. The collection optic consists of a 310 mm focal length lens of telescope and four photomultipliers. The lens focuses the scattered light from particles crossing the measurement volume onto these four detectors. These convert the fluctuations of light intensity into fluctuations in a voltage signal that can be interpreted by

the Doppler signal processor (Dantec BSA P70). Power and control of the Bragg cell and PMT (shutter and calibration signal) are provided by the Dantec processor.

Control of the phase Doppler system is via a computer linked to the processor. Sizeware Dantec PDA software sets the operational parameters such as PMT voltage, velocity bandwidth and the relative refractive indexes. The computer is also used as a storage devive and post-processing centre.

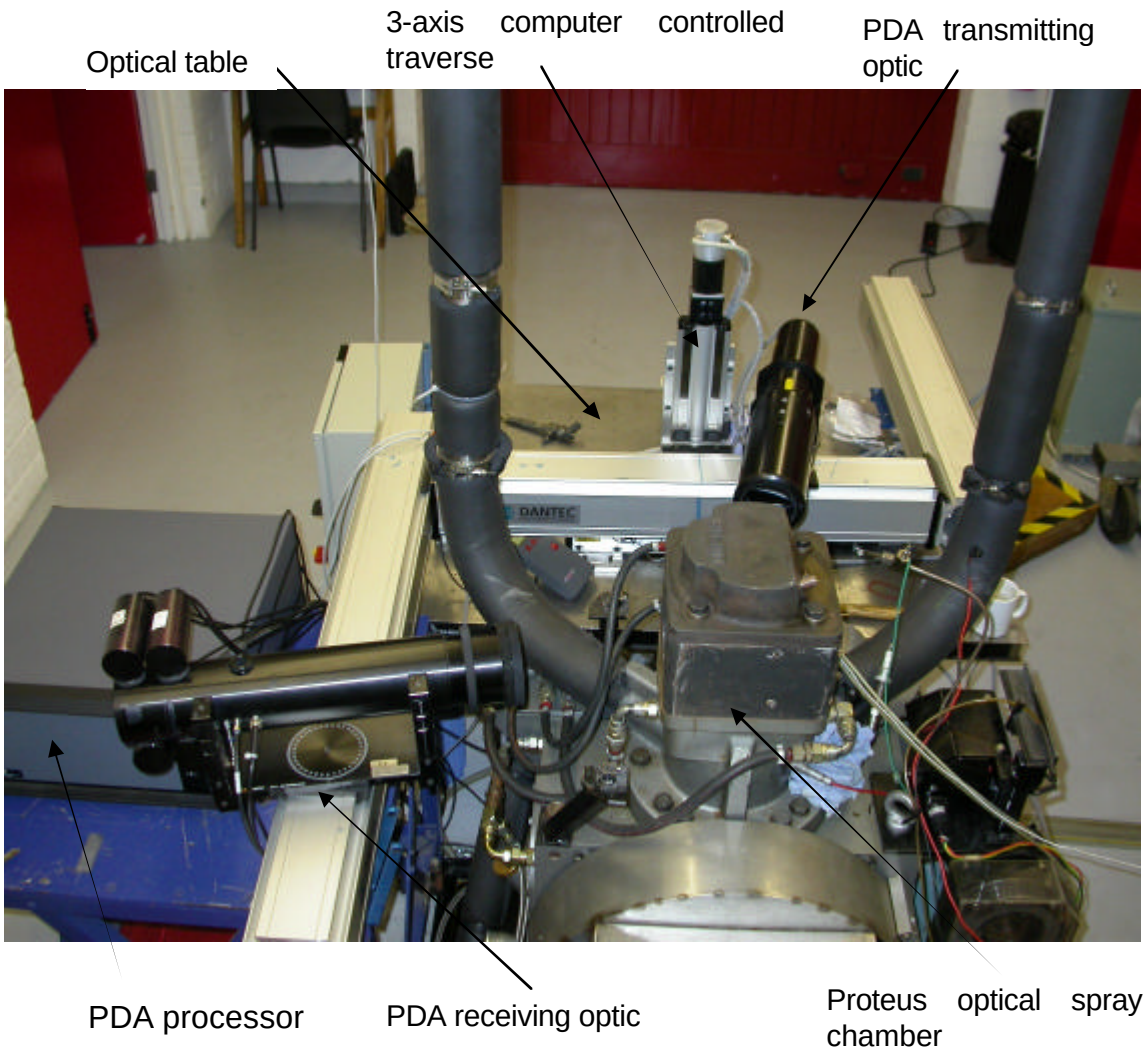

Figure 5-9: Phase Doppler Anemometry rig around the Proteus Engine.

Figure 5-9 shows a photograph of the actual experimental set-up with the spray chamber in place, the injection system and the traverse. It can be seen that the

PDA transmitting and receiving optics are mounted on a 3-axis traverse secured onto an optical air table to avoid ground transmitted vibrations.

Tests were undertaken with a Dantec Phase Doppler Anemometer. The total input power to the Bragg cell was approximately 1 watt and the laser wavelength was 514.5 nm. The characteristics of the PDA system are summarised in Table 5-2.

Laser	
Wavelength (green beam)	514.5 nm
Beam diameter	2.2 mm
Focal length of lenses	
Transmitting optic	310 mm
Receiving optic	310 mm
Beam separation (before expander)	36 mm
Scattering angle	70°
Scattering mode	First order refraction
Beam intersection angle	13.116°
Fringe spacing	2.252 µm
Number of fringes	20
Fringe direction	Positive
Probe volume	9.01×10^{-4} mm^3
d_x	0.047 mm
d_y	0.047 mm
d_z	0.408 mm
Velocity bandwidth	202.71 m s^{-1}
Centre frequency	45.05 m s^{-1}
Maximum measurable diameter	45 µm
High voltage level on PMT 1	1400 V
High voltage level on PMT 2	1250 V
High voltage level on PMT 3	1250V
Signal gain	26 dB
Burst detector SNR level	-3 dB
Spherical validation band	10%
Particle refractive index (non-evaporating spray)	1.45
Particle refractive index (evaporating spray)	1.34
Medium refractive index(non-evaporating spray)	1.005
Medium refractive index (evaporating spray)	1.004

Table 5-2: Optical parameters of the PDA system used to analyse Diesel spray.

Before the PDA system was applied to Diesel sprays in the Proteus engine, some measurements were undertaken with a pharmaceutical nebuliser at a

data rate between 1.5 and 2 kHz. When the intersection of the beams was visible and aligned with the cross in the receiving optic, the system was correctly focused. The cross was also used for angle and height adjustement. The data rate was periodically used as one of the main parameters to check the quality of the optics alignment.

Commercially available BP white Diesel fuel was used for all the tests.

5.4 Measurement under motored engine conditions

5.4.1 Experimental procedure

At each in-cylinder position the velocity and the diameter of individual droplets were recorded over consecutive injections. For each test, validated data were acquired for a period of 500 s or until 10,000 samples were collected. This ensured good phase plot linearity and a Gaussian droplet distribution. This required between 40 and 270 injections depending upon the location of the measurement within the spray. Each sample consisted of the axial velocity component, the droplet diameter and the droplet arrival time relative to the injection trigger pulse. The injections were then compared graphically relative to a common injection trigger point. The velocity and the diameter profiles were ensemble-averaged over consecutive 0.25 ms time bins.

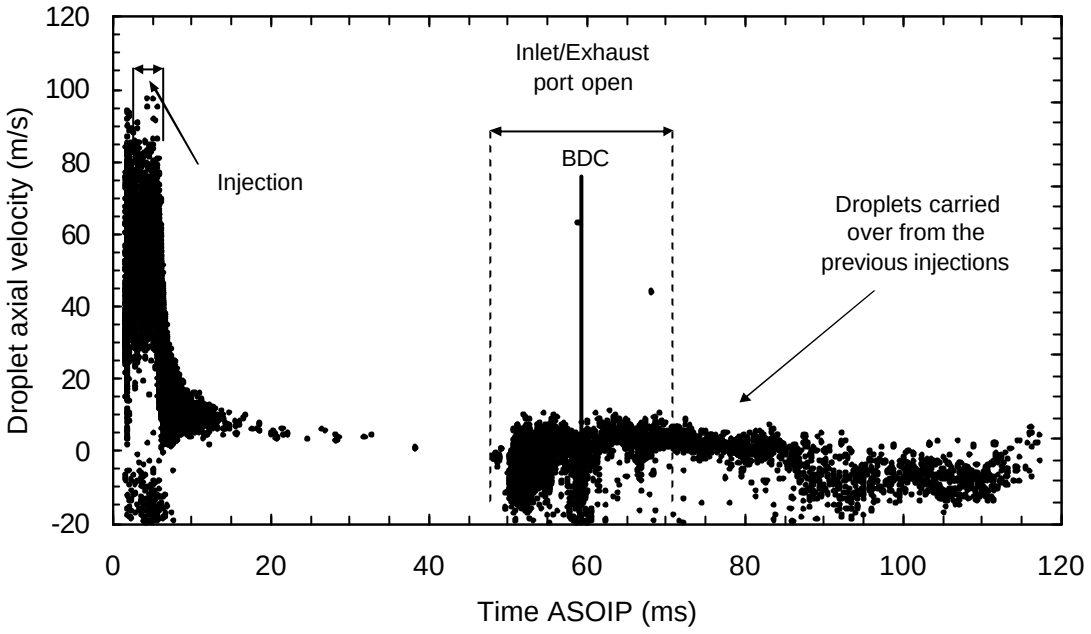

Figure 5-10: Instantaneous axial droplet spray velocity over consecutive engine cycle.

The instantaneous velocity data over several injections have been superimposed in Figure 5-10 over consecutive engine cycle (120 ms). Droplets are recorded during the injection, but also during and after the scavenging process. When the inlet ports are open, the droplets carried over from the previous injections are forced towards the measurement volume by the air entering the cylinder. Post-processing was therefore required to ensure that the velocities and particle diameters were averaged over the injection pulse period only `to avoid bias towards droplets carried over from previous injections that had diameters below 5 µm.

5.4.2 Measurement locations and operating conditions

Phase Doppler measurements were taken of high pressure Diesel sprays in several locations. These locations are noted in Table 5-3, where z is the distance along the spray axis from the nozzle and x is the radial distance from the spray axis.

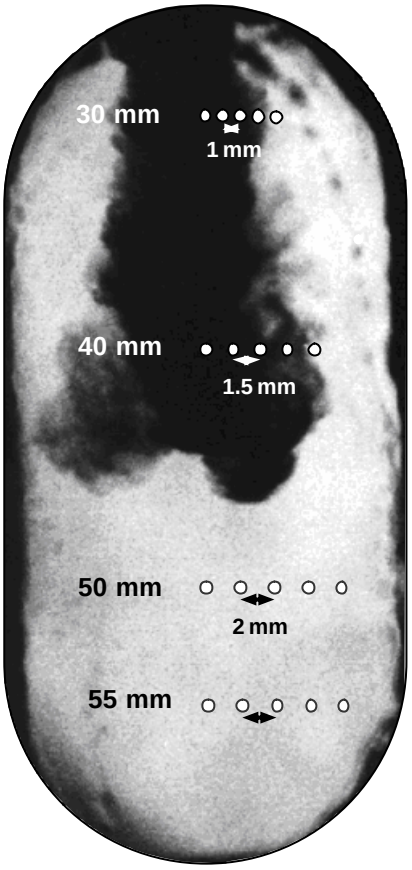

Figure 5-11: Position of the measurement locations.

z (mm) \ x (mm)	0	1	1.5	2	3	4	4.5	6	8
30	•	•		•	•	•			
40	•		•		•		•	•	
50	•			•		•		•	•
55	•			•		•		•	•

Table 5-3: Diagram of the measurement locations (note that the diagram is not to scale).

The experimental test conditions are given in Table 5-4. The operating conditions (injection pressure and in-cylinder pressure) were chosen in regards with the experimental conditions selected by Crua (2002) for its spray penetration and soot measurements. This would facilitate the comparison between spray penetration measurements and PDA measurements.

In-cylinder pressure (MPa)	2, 4, 6
Injection quantity (mm^3)	30
Injection pressure (MPa)	60, 160
Injection pulse width (ms)	4.2 (at 60 MPa), 2.4 (at 160 MPa)
Intake temperature (K)	283, 353
Estimated TDC temperature (K)	566, 682
Injection angle	TDC
Measurement locations from the spray axis (mm)	Each 1 (at 30 mm from the nozzle), each 1.5 (at 40 mm from the nozzle), each 2 (at 50 and 55 mm from the nozzle)

Table 5-4: Experimental in-cylinder and injection conditions.

5.4.3 Effect of window fouling

The fuel deposition on the surface of the Proteus chamber window may lead to sources of uncertainties. The window fouling can result in attenuation of the beam intensity forming the measuring volume or to defocusing of the receiving optic as a film of fuel is formed on the window surface. Several tests have been undertaken to study the effects of window fouling on the measurement accuracy. Five sets of measurements were carried out in a row without cleaning the window. Each test consisted of 210 injections at a 60 MPa injection pressure and a 2 MPa maximum chamber pressure. Table 5-5 shows the mean velocity, the mean diameter, the droplet counts and the data rate obtained for five different levels of windows obscuration. It is clear that the window fouling had a strong effect on the number of droplets measured. However, the window obscuration did not have a strong effect on the measurement accuracy.

	Test 1	**Test 2**	**Test 3**	**Test 4**	**Test 5**
Mean velocity ($m.s^{-1}$)	28.85	28.25	25.64	27.33	24.96
D_{10} (µm)	7.5	7.7	7.6	7.8	7.7
Counts	22752	22514	20048	13690	9352
Data rate (Hz)	10834	10720	9546	6519	4453

Table 5-5: Effect of window fouling on mean velocity, mean diameter, counts

and data rate.

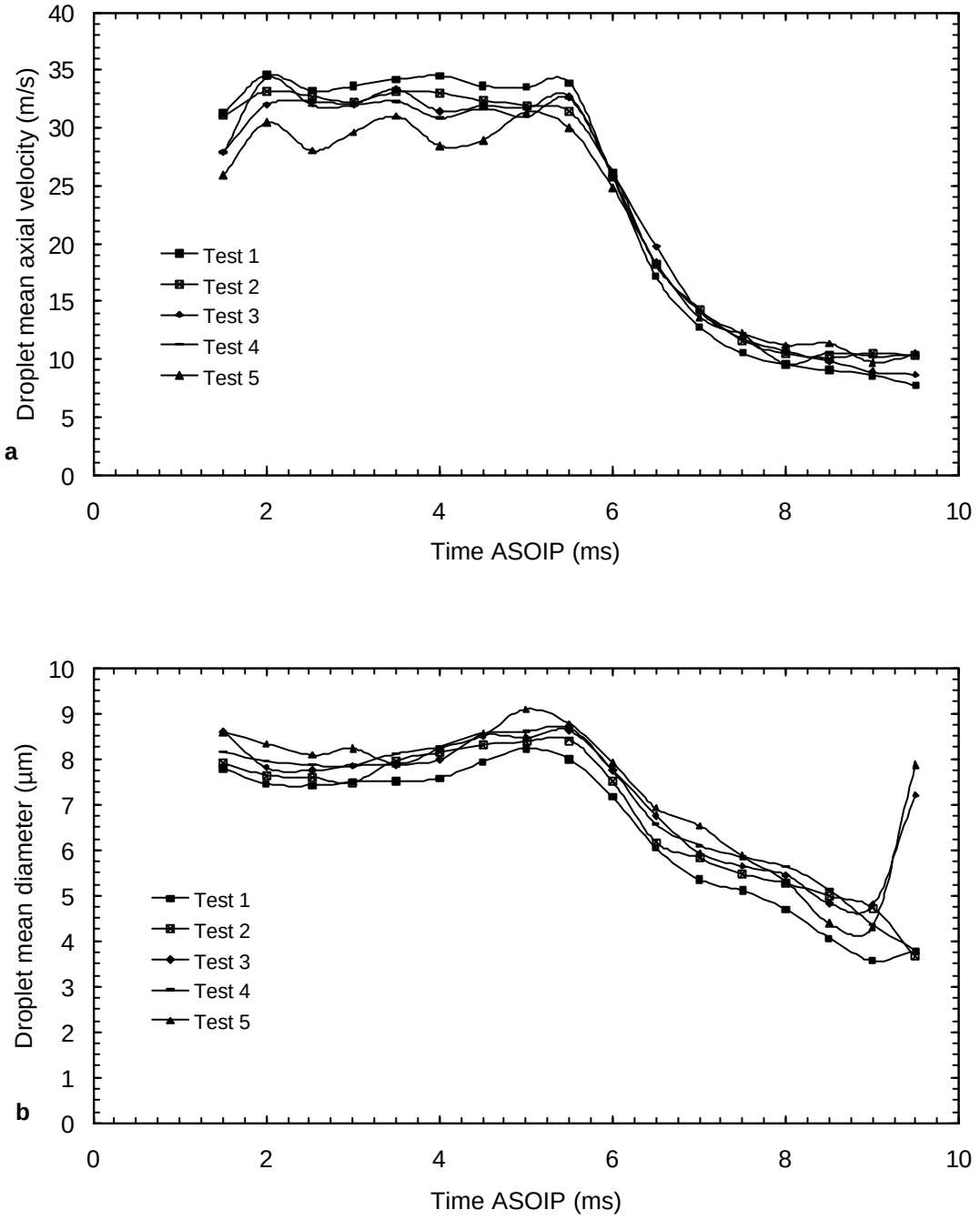

Figure 5-12: (a) Influence of window fouling on the axial velocity measurements. (b) Influence of window fouling on the diameter measurements. 60 MPa injection pressure and 2 MPa in-cylinder pressure, 40 mm from the nozzle on the spray axis.

Consequently, windows were cleaned every two tests to ensure maximum validation rates and avoid signal rejection.

5.4.4 Effect of the fuel remaining in the chamber

An issue raised during the experiments was that due to the data being affected by the droplets left over in the optical chamber from prior injections. As previously described, post-processing was undertaken to avoid bias towards residual droplets. However, during the spray injection, droplets located in the spray head can penetrate and coalesce with a cloud of particles remaining from the earlier injections. A few droplets are measured before the start of injection that can only be attributed to fuel or oil particles already present in the chamber. The question is to what extent these droplets affect the measurement of the spray and the droplet velocity and diameter averaging. As a check, measurements were carried out at a distance of 30 and 40 mm from the nozzle, outside of the spray envelope, to ensure that the spray was not penetrating a cloud of droplets left over from the previous injections. These tests were undertaken using the same conditions as the optimised PDA measurements. Only a few droplets were recorded on a 500 s period. The number of droplets measured prior to the start of injection was insufficient to affect the statistical reliability of the results.

5.5 Application of phase Doppler anemometry to dense Diesel sprays

As discussed in chapter 3, the physical nature of the Diesel spray presents some difficulties for phase Doppler systems. This includes high droplet number density, non-spherical droplets and the relationship between droplet velocity and the range of the instrument setting.

Dense fuel sprays have regions where these criteria are often not met. For example, Figure 5-13, 14 and 15 show the mean velocities, the mean diameters number and the data rate as a function of the radial and axial position through a plane in the spray. These tests were performed at 40 mm from the nozzle, for

an injection pressure of 60 MPa and in-cylinder pressure of 2 MPa. As can be seen from Figure 5-13, Figure 5-14 and Figure 5-15 data rate and average droplet velocities and diameters are strongly linked to the measurement position. At the point where the laser beams path and the scattered light path directed towards the receiving optics are shorter inside the spray, measurements are less altered by the presence of other drops. A very high data rate and a reliable size measurement can be achieved. When the beam path and the scattered light paths are disrupted by the presence of too many droplets, the data rate decreases. The scattered light absorption and the secondary light scattering will decrease the signal strength and increase the system noise and explain the low data rate measured before the spray axis.

As can be seen from Figure 5-15, low validation rates are achieved on the spray axis, indicating that a majority of the particles crossing the measurement volume violate the acceptance criteria for one reason or another. Thus it is possible that the droplets that do produce valid measurements represent a subset of data that is not representative of the actual spray behaviour. Such results could generate a misleading picture of the true spray characteristics. As the spray cannot be measured axis-symmetrically using the phase Doppler system, measurements were undertaken on the x-axis from the centre on the spray cone towards the spray periphery.

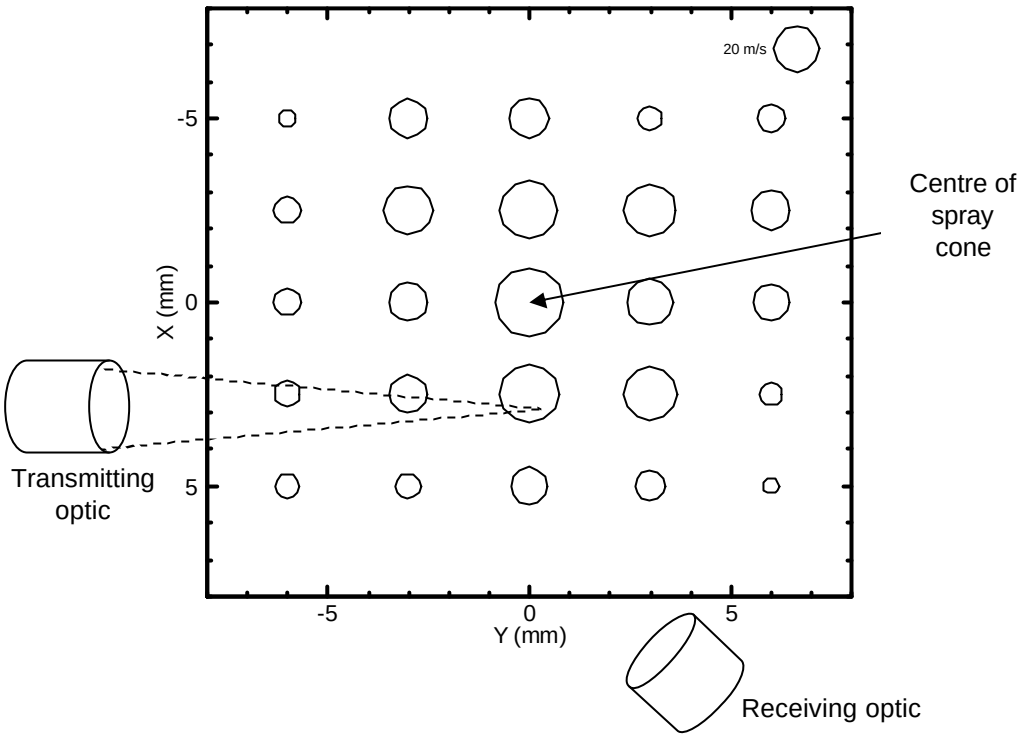

Figure 5-13: Mean velocity in the 25 points grid at 40 mm from the nozzle at 60 MPa injection pressure and 2 MPa ambient pressure.

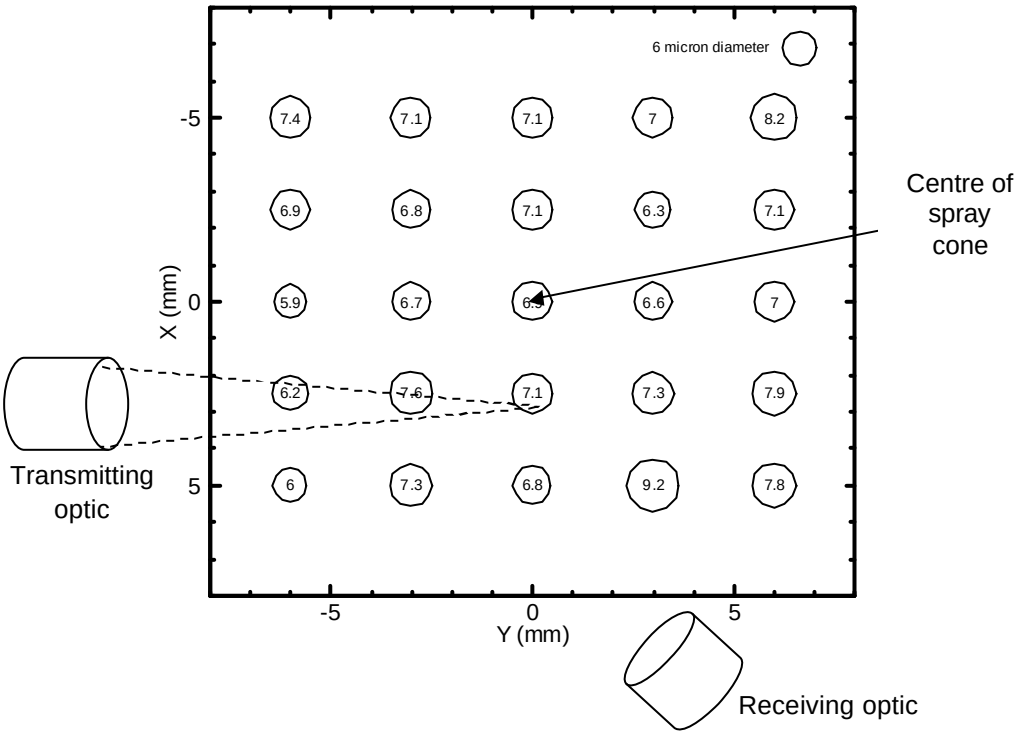

Figure 5-14: Mean diameter in the 25 points grid at 40 mm from the nozzle at 60 MPa injection pressure and 2 MPa ambient pressure.

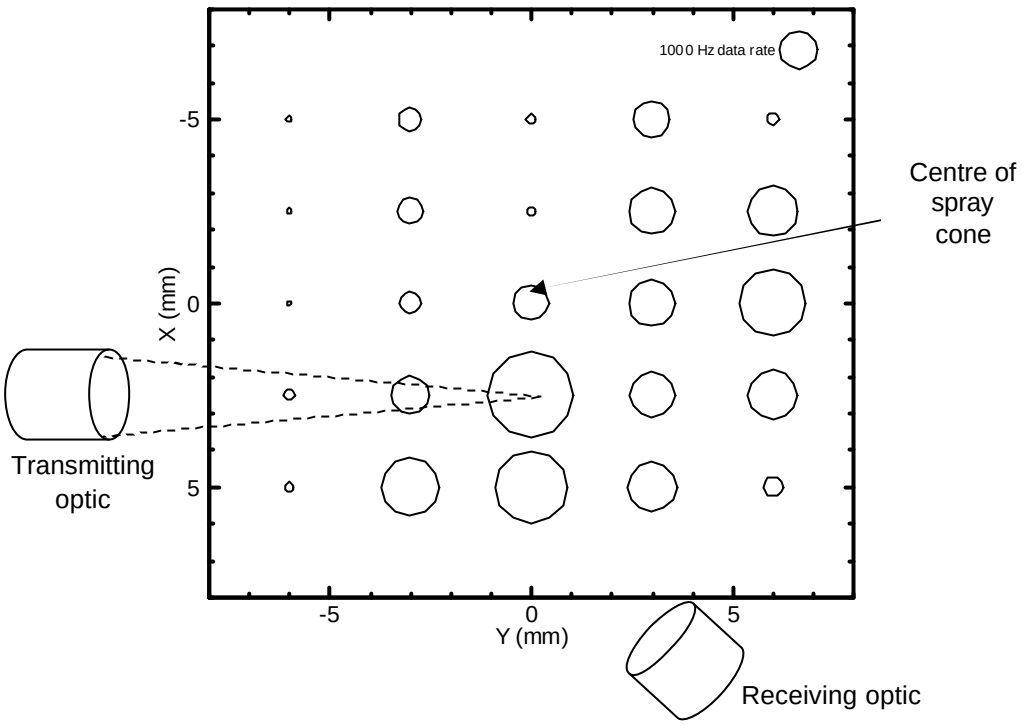

Figure 5-15: Data rate in the 25 points grid at 40 mm from the nozzle at 60 MPa injection pressure and 2 MPa ambient pressure.

A check to see if the results are biased to particular size classes was undertaken by comparing LDA measurements (velocity measurement only) and PDA data at the same conditions. This is effective because of the much higher validation rates achieved when making LDA measurements. As can be seen from Figure 5-16 the PDA results are simply a sub-set of those droplets passing the additional PDA spherical validation checks. The difference in mean velocities is interpreted as an indication that at this location in the spray the liquid ligaments (non-spherical contributors) are moving faster than the spherical droplets. However, as illustrated in Figure 5-17, the characteristics of the velocity plots are almost identical.

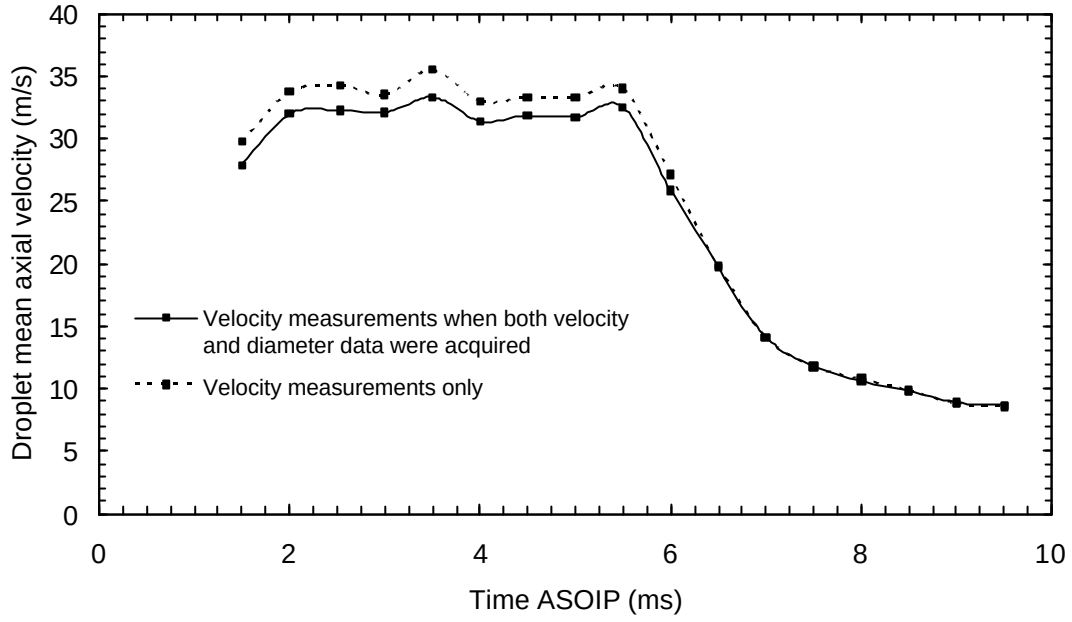

Figure 5-16: Mean droplet axial velocity at an injection pressure of 60 MPa and in-cylinder pressure of 2 MPa.

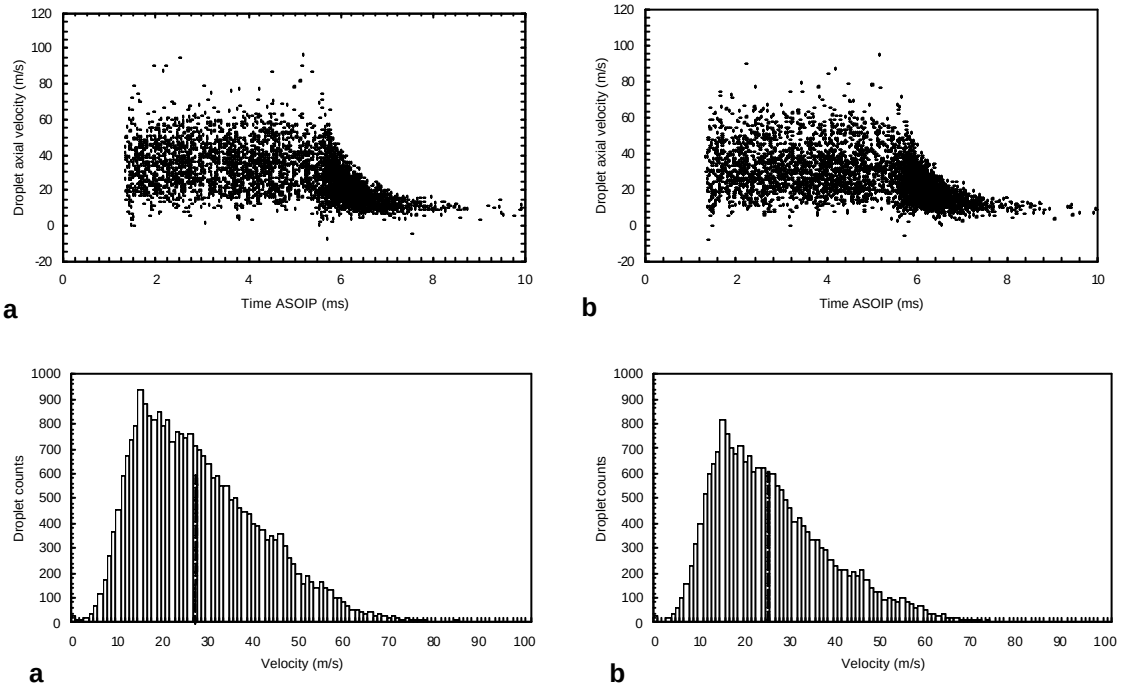

Figure 5-17: (a) Axial velocity measurements only (U_{mean}=27.58 m.s^{-1}), (b) Axial velocity measurements when both velocity and diameter data were acquired (U_{mean}=25.57 m.s^{-1}). Injection pressure of 60 MPa and in-cylinder pressure of 2 MPa.

In order to determine if the measurements represent the ensemble, several tests and comparisons were performed. Firstly, consistency checks were undertaken in a spray where 100% validation rates were achieved. For this purpose, a pharmaceutical nebuliser was used to validate the measurements by generating a cloud of water droplets of a known diameter range (3 to 6 µm) so as to compare them with the obtained PDA data. The mean water droplet diameters were around 4.5 µm. Then a comparison of the spray tip penetration, determined from high-speed video photography, with the tip penetration obtained from the PDA measurement was undertaken and showed similar trend. This illustrated in Figure 5-18.

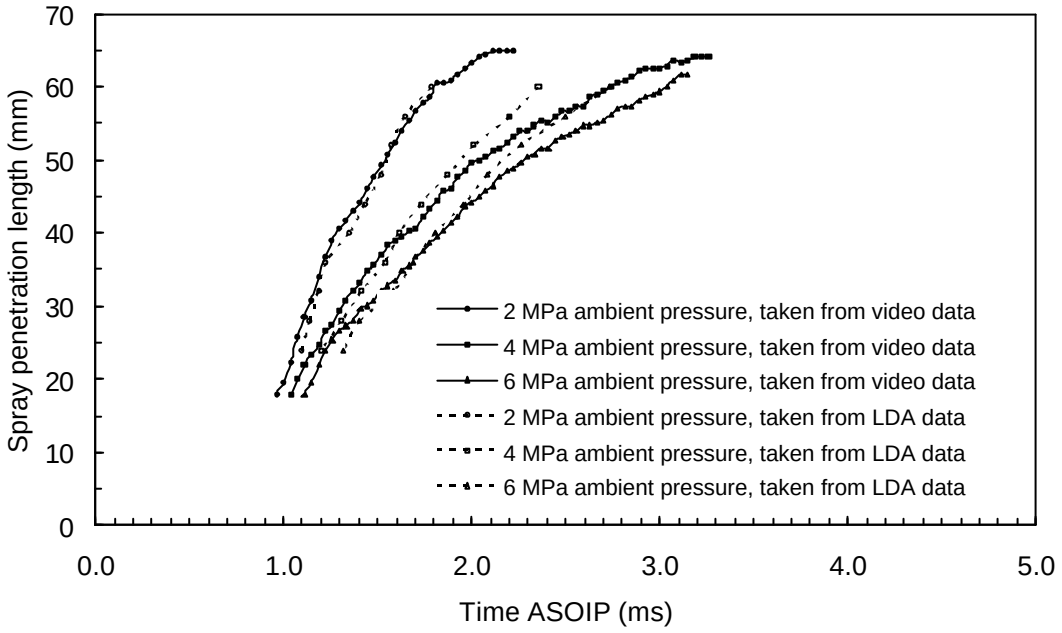

Figure 5-18: Spray penetration length for an injection pressure of 60 MPa at different ambient pressures determined by video and LDA measurements.

5.6 Conclusion

The effect of the set-up parameters on the velocity and size spray measurements was investigated. The photomultiplier voltage, the laser power, and the measurement volume size all show significant effects on the detected droplet diameters. A study of the PDA systems parameters has proved to be necessary to tailor the system to the measurement of dense sprays.

The number of droplets measured is generally less than the real number of droplets that are passing through the measurement volume. This can be observed by comparing the results obtained in the spray head to the results obtained in the spray tail, where measurements are “easier” to perform (Figure 5-19).

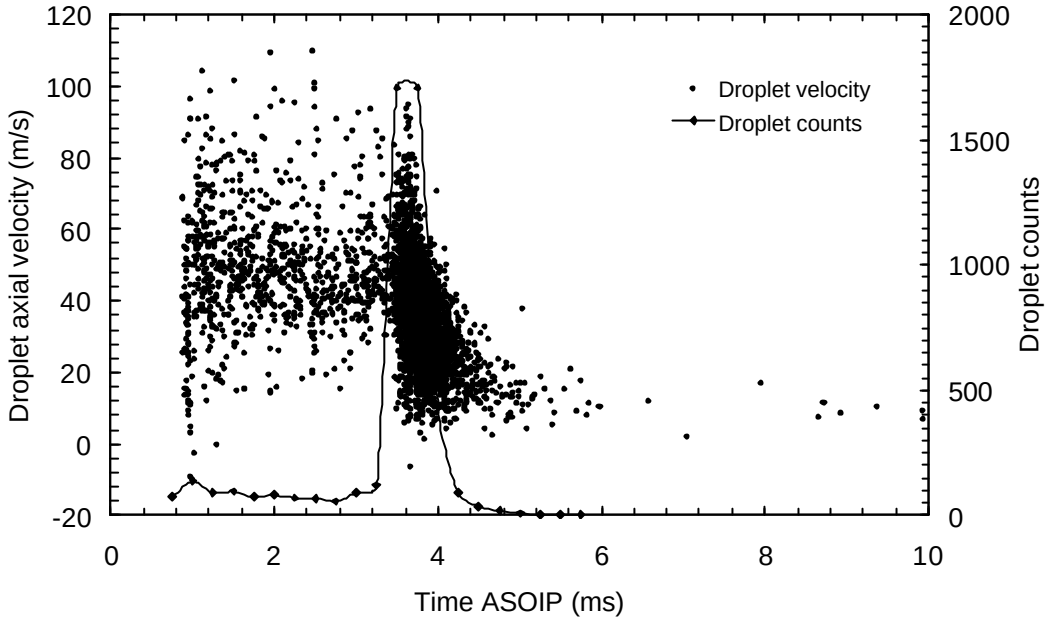

Figure 5-19: Axial droplet spray velocity and droplet counts at an injection pressure of 160 MPa and in-cylinder pressure of 4 MPa.

Therefore, it is hard to have direct verification that the obtained drop-size distributions are, in fact, the same as the actual size distributions in the spray. However, the abovementioned results tend to support the hypothesis that these results, for the size at which measurements were carried out, are similar to the actual spray characteristics. However, PDA results from a Diesel spray must be looked at in the context of knowledge of the uncertainties involved in the measurement and the values at certain locations and times must be treated with caution.

6 THE INFLUENCE OF INJECTION AND IN-CYLINDER PRESSURE UPON DROPLET BEHAVIOUR

6.1 Introduction

High-pressure injection seems to be one of the most efficient ways to tackle stringent emission standards of diesel engines. The use of high-pressure common rail systems in recent vehicles illustrates this efficiency. But although high-pressure injection will soon become a standard, the consequences of this new technology on spray formation have yet to be understood. To examine the effect of this strategy upon droplet behaviour, PDA measurements were carried out at two different injection pressures. The Proteus combustion chamber gas pressure was varied to investigate the effect of aerodynamic resistance on the spray while the air intake was altered from atmospheric temperature up to 373 K, in order to examine its effect on fuel evaporation.

6.2 Spray structure

The description of a high-pressure Diesel spray was divided into two parts. These are referred as the “spray head” and the “spray tail”. A typical injection period is shown in Figure 6-1. The temporal division between the head and the tail was selected at the point where the droplet velocities exhibited a steep negative gradient.

In Figure 6-1, the injection delay is the time between the pulse at the start of injection and the first droplets arriving at the measurement volume.

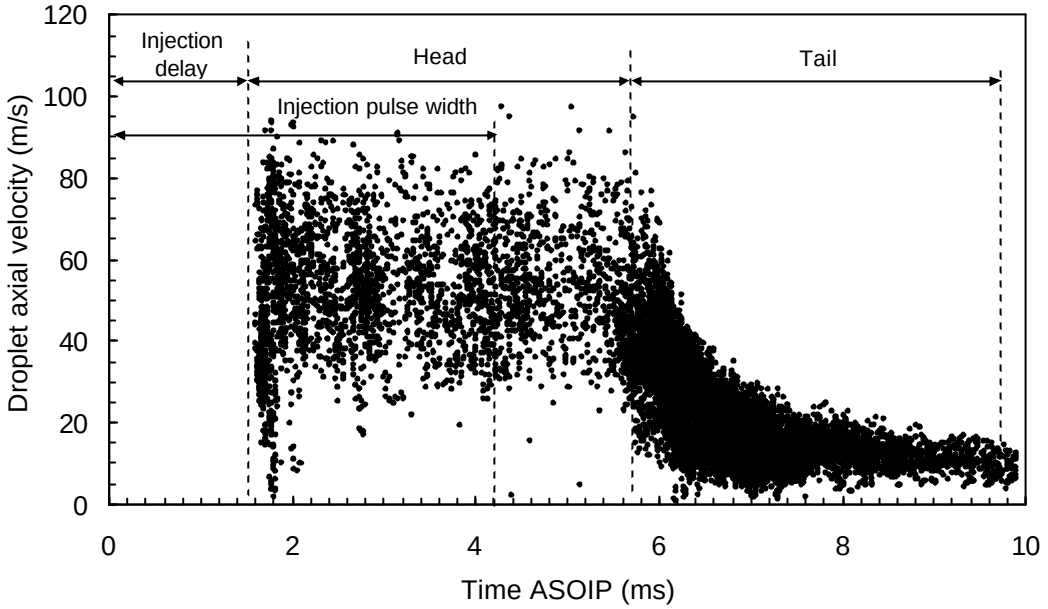

Figure 6-1: Injection delay, spray head and spray tail definition. Time resolved axial droplet velocities and sizes at 40 mm from the nozzle on the spray axis (r = 0 mm); 572 K TDC temperature, 160 MPa injection pressure and 4 MPa in-cylinder pressure.

In this descriptive case, the range of velocities observed in the spray head is between 0 and 80 $m.s^{-1}$ (Figure 6-1). This spread is attributed to aerodynamic effects occurring in the spray head. Droplets located in the spray tip will be affected by shear between the surrounding gas and the spray envelope. Early injected droplets that impart momentum to the gas are then quickly hit and overtaken by the droplets that follow them. Following those collisions, the particle trajectories are entrained towards the spray periphery. In the measurement volume, droplets with a true axial velocity are acquired but also those having a modified trajectory. The axial velocity component of those entrained droplets is then lower than those droplets with unmodified trajectories.

Phase Doppler velocity and diameter scatter plots measured on the spray axis did not represent a complete profile of the spray until the measurement volume was moved 30 mm from the injector nozzle. Spray head droplet measurements were not possible at a distance of 25 mm along the spray axis (Figure 6-2). Spray head droplets are quasi non existent, only 15 droplets being detected in 540 ms (i.e. within 270 injections), before droplets are once again detected in

the spray tail. The measurements performed closer to the nozzle showed a much lower data rate. Using a fast cinematographic technique Gülder (1994), showed that diesel sprays at lower injection pressure are completely atomised at 20 nozzle diameters, whereas Yule and Salters (1995), using a conductivity probe technique, found that the diesel spray breakup length was of the order of 100 nozzle diameters. A recent study by Bruneaux (2001) showed that the spray transit from a cavitating flow outside the nozzle to a fully atomised spray at 1 to 2 mm from the nozzle. It may be argued that at 25 mm from the nozzle (125 nozzle diameters), the lack of measurements and the poor data rate are not the consequences of a liquid jet, as it was first thought by Pitcher and Wigley (1991).

Figure 6-2 clearly shows the difference of measurements between the spray head (only 15 acquired droplets) and the spray tail (1594 acquired droplets). This tends to suggest, that we may be in presence of a high optical dense region. Those results agree with recent findings by Heimgärtner and Leipertz (2000), in which the conclusion was that, for comparable testing conditions, the spray shows a dense core of approximately 30 mm long.

Particles are also subjected to aerodynamic load and viscous stresses produced by gas density. Turbulence and local flow acceleration may shape the droplets into ellipsoids. In addition to these phenomena, coalescence of droplets may occur in the spray, resulting in the additional formation of non-spherical particles. If the particle is not spherical, a valid droplet measurement will not occur. The concentration of the particles is such that there is also a possibility that several droplets may occupy the measurement volume at the same time, leading to overlapping signals, with associated low validation rate. The reason for rejection of data outlined above would all be applicable in areas of the spray considered dense.

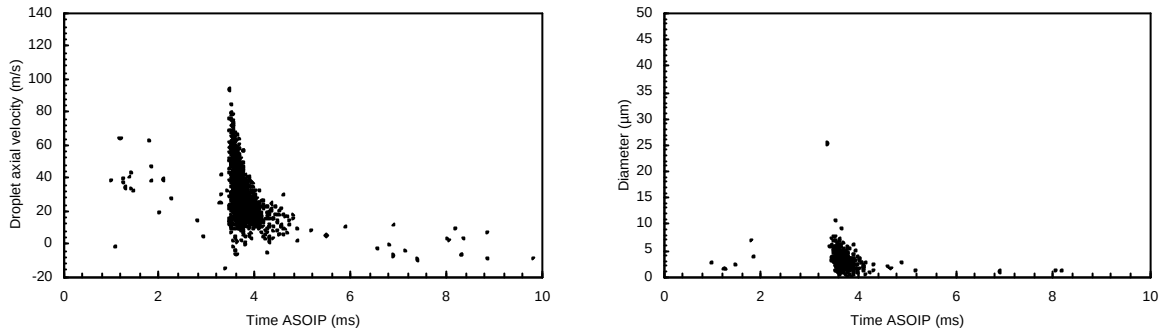

Figure 6-2: Time resolved axial droplet velocities and sizes at 25 mm from the nozzle at 160 MPa injection pressure and 4 MPa in-cylinder pressure.

6.2.1 Global spray characteristics

PDA measurements were performed on a 0.2 mm VCO single hole nozzle. The injection pressure was varied from 60 MPa to 160 MPa. The injection characteristics describe the performance of the injection system at specific injection setting. In Figure 6-3 , the needle lift profile is approximately rectangular in shape. The response in time of the needle to injection pulse is rapid, wit full opening condition being rapidly achieved.

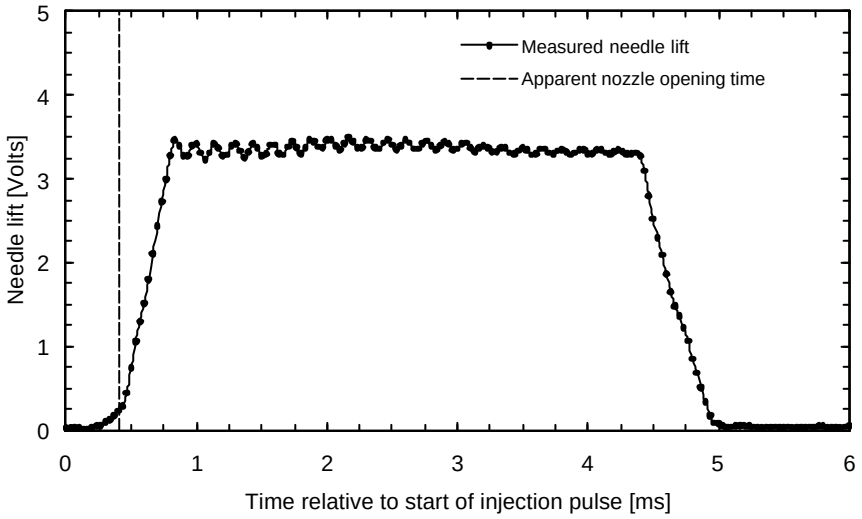

Figure 6-3: injection needle lift trace for a 0.2 mm VCO single hole nozzle for an injection pressure of 160 MPa.

Droplet measurements for the spray axis position at 30 mm from the nozzle are shown in Figure 6-4. The first droplets arrive approximately 1.4 ms after the signal for start of injection. These scatter plot of velocity and diameter reveal that the main body of the spray, the head, is travelling on average at 25 $m.s^{-1}$, with droplet ranging from -10 to 60 $m.s^{-1}$. The head consists of droplets with diameters spreading from 2 to 20 µm. Few large particles with diameter around 40 µm can also be observed. These particles may be ghost droplets (Koo and Martin, 1990), they are probably caused to multiple droplet occupancy in the measurement volume.

It is interesting to note that few droplets with negative velocities are present during the early stage of the injection (1.5 to 1.75 ms). Droplets entrained by spray head vortices are believed to cause those negative velocities. Experimental results reported by Morgan et al. (2001) showed similar phenomena.

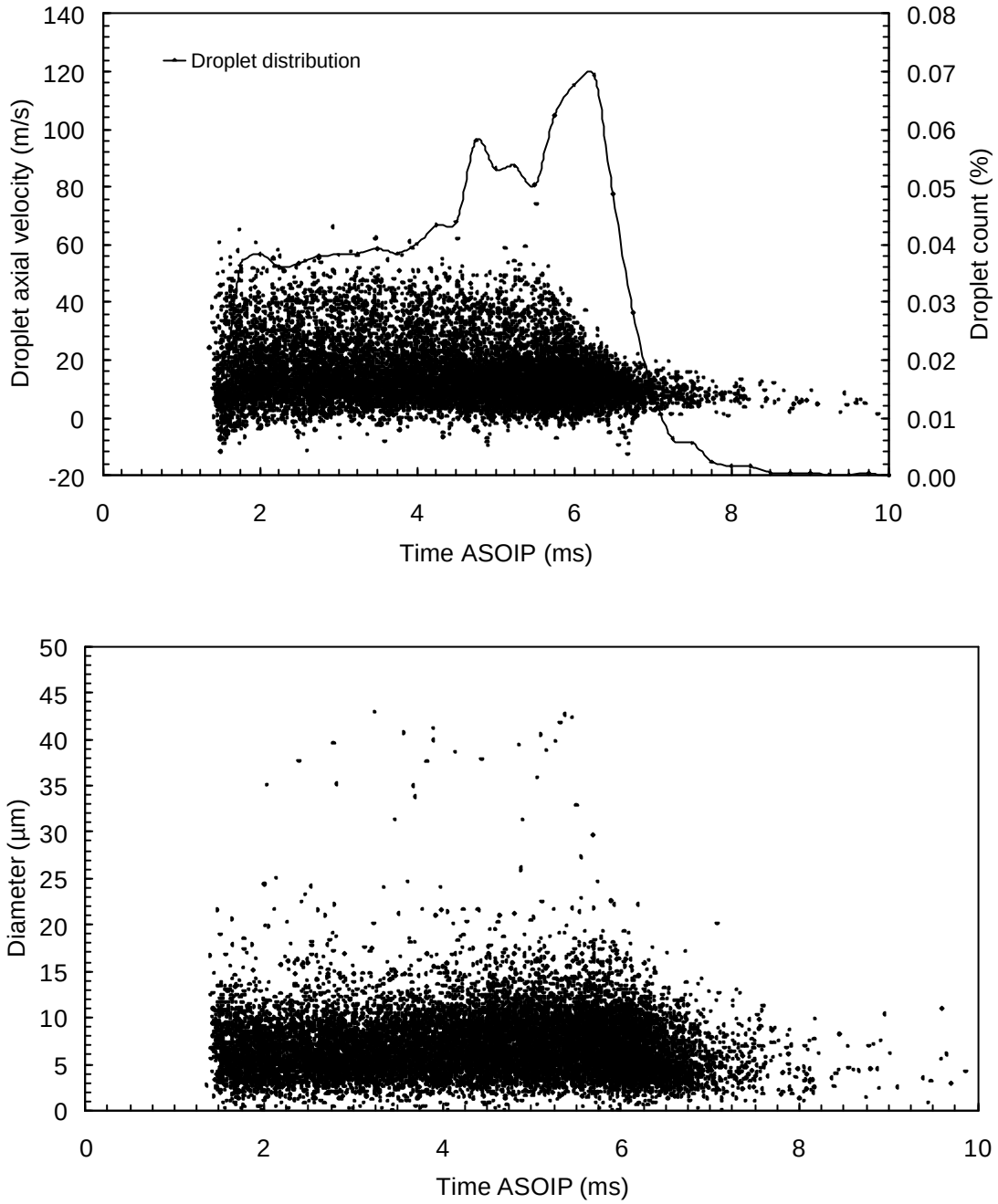

Figure 6-4: Time resolved axial droplet velocities and sizes at 30 mm from the nozzle on the spray axis (r = 0 mm); 572 K TDC temperature, 60 MPa injection pressure and 4 MPa in-cylinder pressure.

Figure 6-5 shows the scatter plot for the same locations but for a higher injection pressure spray. There are several similarities between the low injection pressure spray (60 MPa) data and the high injection pressure (160 MPa) spray. For instance, the profile is similar for both cases. Droplet velocities drop off rapidly at the transition point between the head and the tail.

By comparing both sets of data, it can be observed that the number of droplets gathered in the spray head is much higher in the high injection pressure case than in the low injection pressure case. This is better seen by looking at the droplet distribution in Figure 6-4 and Figure 6-5. These graphs show that the droplet count is higher at certain portions of the spray and very low in others. There is, however, no variation of the PDA operational parameters within the individual head and tail sections of the spray. The only factor affecting the data acquisition is the spray itself. The number of droplets measured in the spray head is twice and 20 times higher than the number of droplets in the spray tail at 60 MPa and 160 MPa respectively. The lack of measurements observed in the spray head for an injection pressure of 160 MPa could be due to incomplete spray atomisation. However, at such a distance from the nozzle this is unlikely to be the case. There are several explanations for the poor acquisition of droplets in the spray head, in terms of measurement rejections by the PDA. High injection pressures produced faster particles and made the droplets more susceptible to aerodynamic breakup; the spray atomisation will then be improved. Therefore, the number of small droplets present in the spray increased. This could lead to the violation of the single particle constraint due to the high droplet number density. Disturbance of the transmitter beams and obscuration of the scattered light could also have affected the droplet acquisition rate.

The presence of certain periods with diminished data acquisition means that one should consider how the data might be affected. A high droplet number density could bias the result. For instance, if multiple droplets within the measurement volume are a significant problem affecting the data acquisition and the droplet number density was sufficiently high, the valid measurements could be biased towards larger droplets. However, velocity only measurements, for the 160 MPa spray at 30 mm from the nozzle along the spray axis, show a very similar profile to the velocity profile obtained with diameter measurement capability on. It is therefore strongly believed, that high density region might interfere with droplet acquisition but not bias results.

For an injection pressure of 60 MPa, the spray velocity was steady for approximately 4 ms and for an injection pressure of 160 MPa, the spray was

steady for 2 ms. This is due to the fuel injected quantity being kept constant to 30 mm^3, corresponding to an injection timing of 4.2 ms and 2.4 ms at 60 MPa and 160 MPa injection pressure respectively.

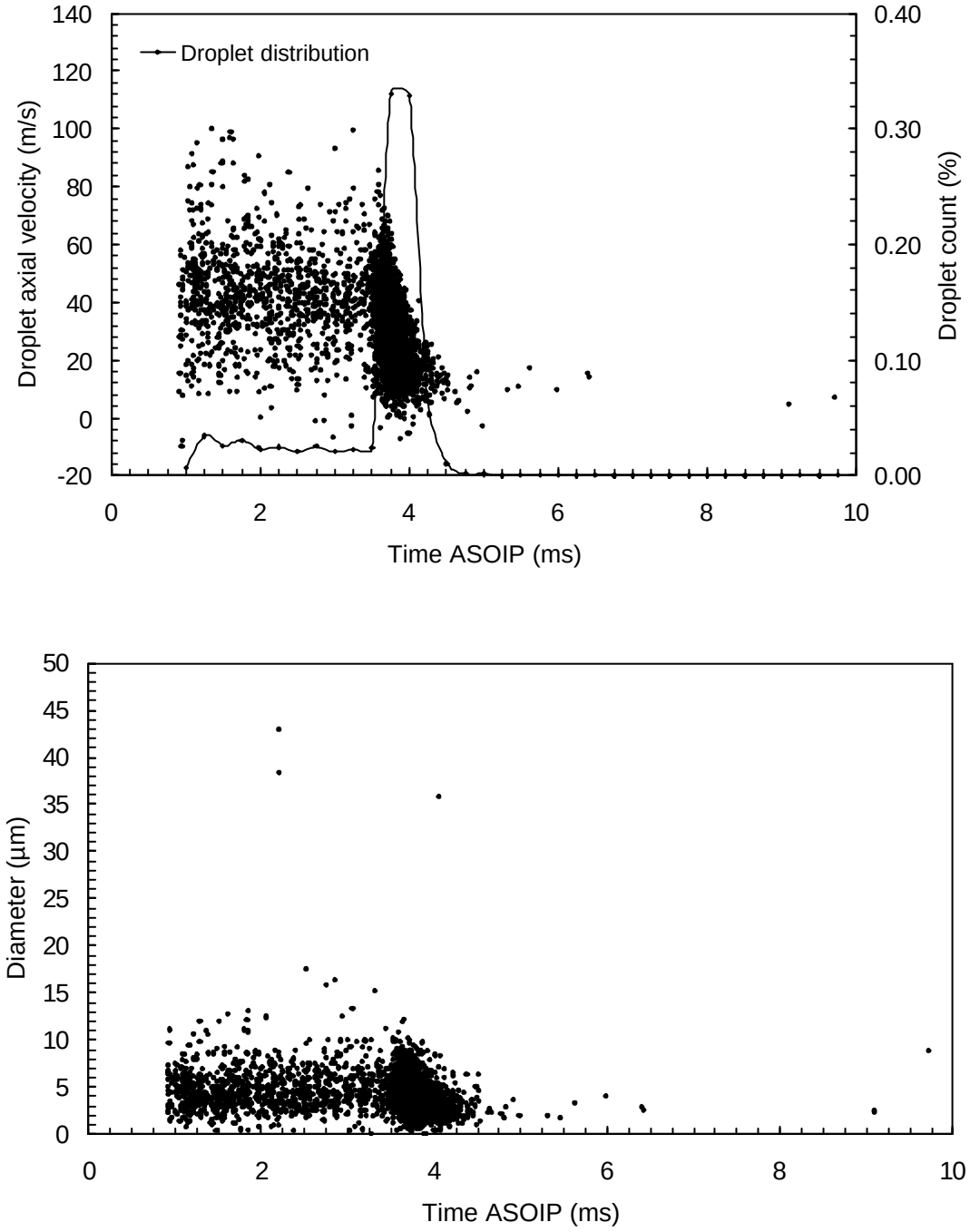

Figure 6-5: Time resolved axial droplet velocities and sizes at 30 mm from the nozzle on the spray axis (r = 0 mm); 572 K TDC temperature, 160 MPa injection pressure and 4 MPa in-cylinder pressure.

Figure 6-4 and Figure 6-5 show several clear differences. The expected velocity difference can be seen. At 160 MPa injection pressure, the spread of droplet velocities is from -15 to 100 $m.s^{-1}$ in the main body of the spray and the spray average velocity is 38 $m.s^{-1}$. At the lower injection pressure of 60 MPa, the average velocity is only 25 m.s-1 with a spread from -10 to 50 $m.s^{-1}$. i.e. the average velocity in the head of the spray at 160 MPa is 1.5 times the average velocity at 60 MPa. The expected decrease in droplet diameter is also observed, with droplets ranging from 2 to 10 µm. A few “ghosts” droplets around 40 µm, probably caused to multiple droplet occupancy in the measurement volume, are also noticeable. The trends observed are consistent with other publications reported in the literature (Minami et al. (1990), Ficarella et al. (1997), Zhou et al. (2000) & Jeong et al. (2003)). The rate at which the velocity dropped after the end of the injection reduced as the injection pressure increased.

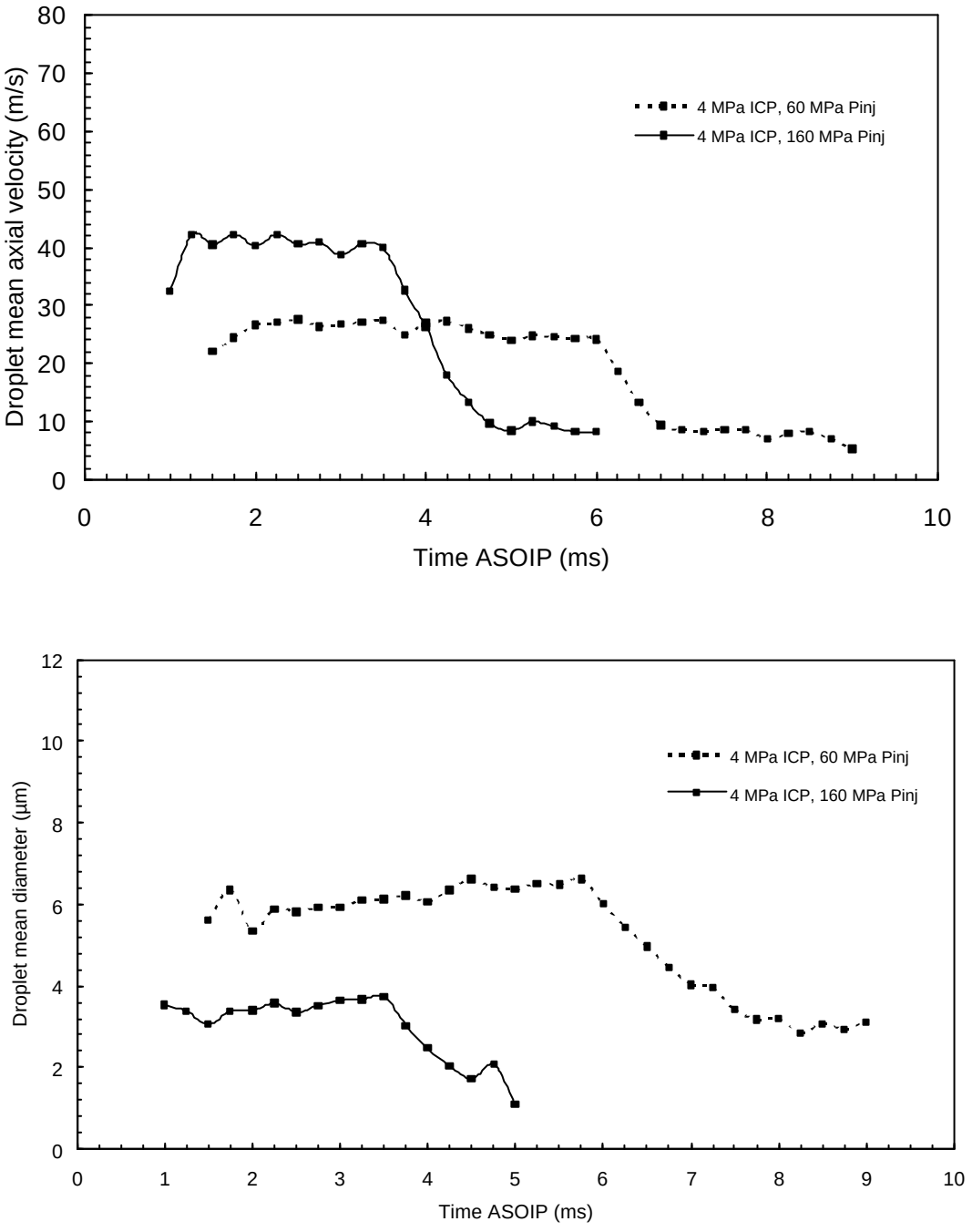

Figure 6-6: Mean droplet axial velocity and diameter profiles at 30 mm from the nozzle on the spray axis; 572 K TDC temperature, 60 MPa and 160 MPa injection pressure and 4 MPa in-cylinder pressure.

Figure 6-6 shows the variation of mean velocity and the mean diameter with time on the spray axis at 30 mm from the nozzle for two different injection pressures. The mean values were calculated in steps of 0.25 ms and at a minimum of 5 droplets was required in any time bin. In reference to Figure 6-6,

the mean velocity profile and the mean diameter are greatly affected by the injection pressure. A study of the droplet velocity profiles yields a further interesting and fundamental fact about diesel sprays. The velocity profile for the high injection pressure is of a square form with a steep velocity gradient of 57 $m.s^{-1}$/ms, while at the lower injection pressure, this plateau is attained much more slowly (velocity gradient of 9 $m.s^{-1}$/ms). This can be explained by assuming that the first droplets sprayed into the chamber, however fast they are travelling, are rapidly decelerated by the in-cylinder gas. Fuel sprayed after this initial stage will then be injected into a jet stream of air. The relative velocity between the air and the droplets will be reduced, and the droplets less retarded in velocity. These drops will then catch up those first injected drops and overtake, collide or coalesce with them. Once this happens, they will then enter relatively quiescent air and once again be decelerated rapidly. This explains the velocity fluctuation in the spray head with is a complex function that is temporally dependent upon the injection phases and their relationship to a fixed point measurement technique.

The diameter profiles displayed in Figure 6-6 are practically constant in the spray head, before a reduction in droplet size towards the end of injection (spray tail). As previously described, particles introduced in the spray chamber during the early stage of the injection rapidly loose their momentum. Those droplets will then breakup into smaller ones (secondary breakup) and will reach the measurement volume towards the end of injection. This explains the diameter decrease which is a complex function related to the spatially fixed measurement volume. Under certain circumstances, a droplet measured in the spray tail may have had an origin within the initial phase of injection. Data are consistent with other data sets reported in the literature (Araneo and Coghe, 2002; Whitelaw et al., 2001).

Comparison of droplet measurements gathered on the spray periphery proves interesting. Figure 6-7 and Figure 6-8 show the velocity and the diameter scatter plot for the low injection pressure case and high injection pressure case, respectively. Both sets of data are plotted on the same scale for easy comparison. The high injection pressure case exhibits droplets spanning a

larger range of velocities than the low pressure case. In the diameter plots, the low pressure case has a greater range.

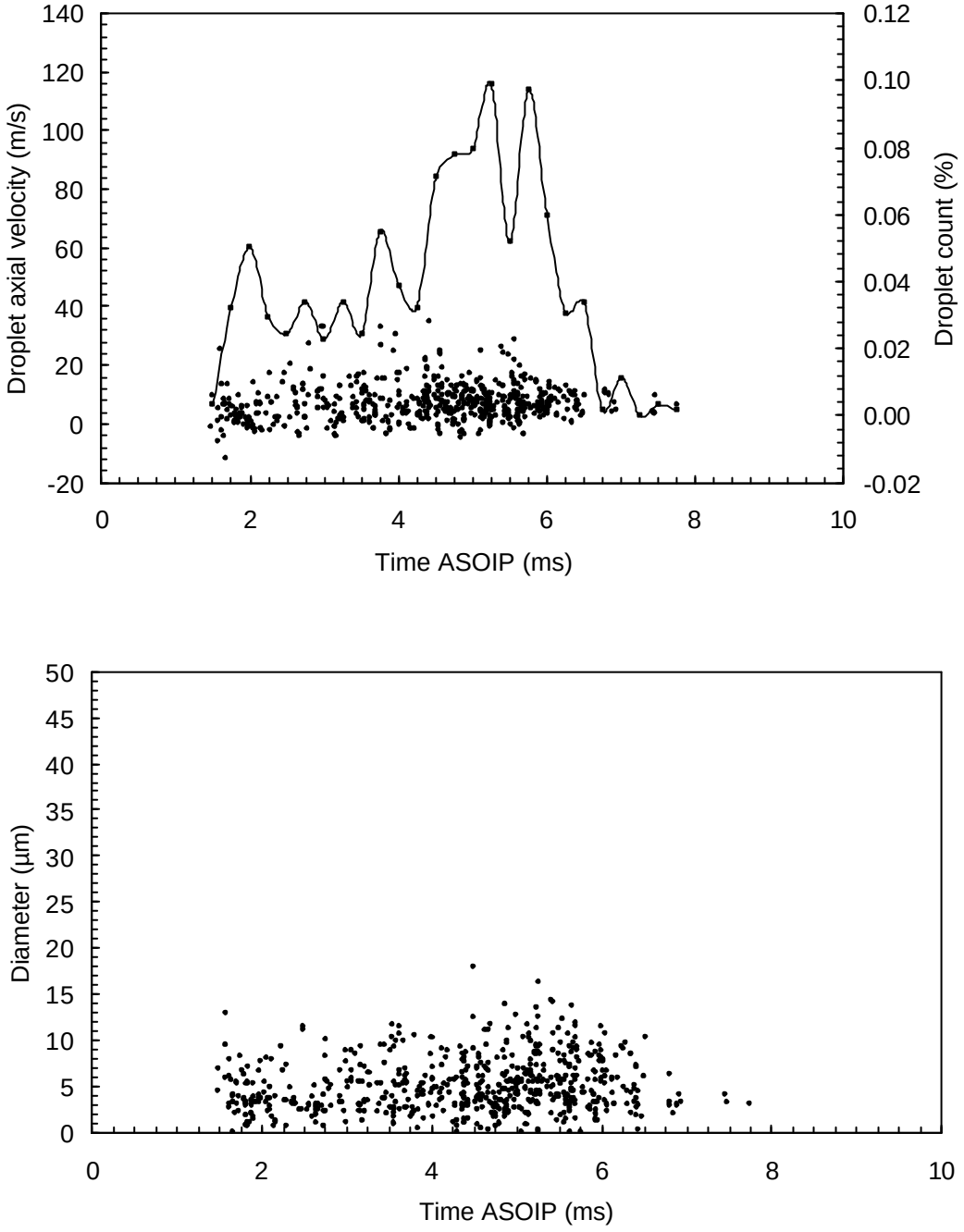

Figure 6-7: Time resolved axial droplet velocities and sizes at 30 mm from the nozzle on the spray periphery (r = 4 mm); 572 K TDC temperature, 60 MPa injection pressure and 4 MPa in-cylinder pressure.

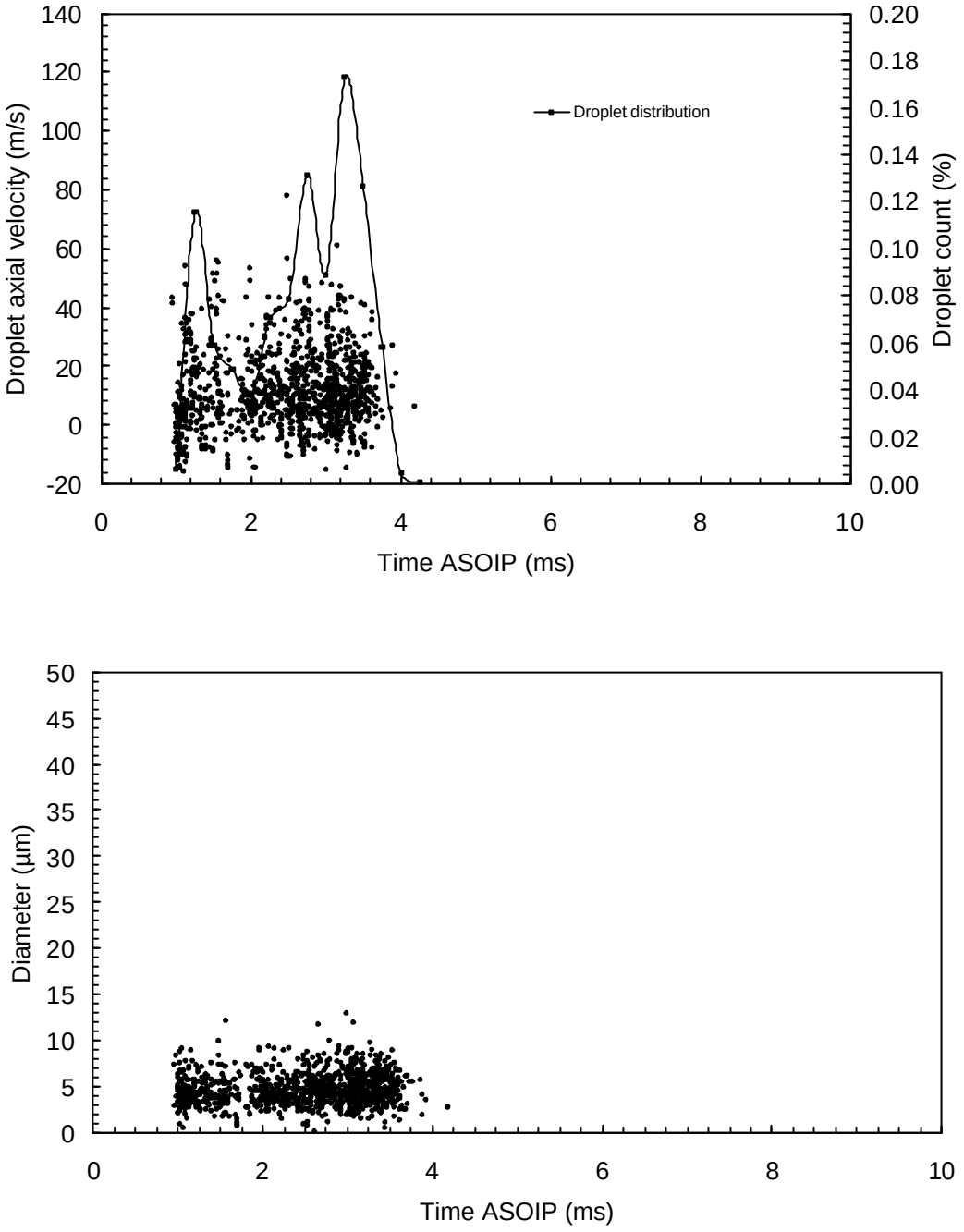

Figure 6-8: Time resolved axial droplet velocities and sizes at 30 mm from the nozzle on the spray periphery (r = 4 mm); 572K TDC temperature, 160 MPa injection pressure and 4 MPa in-cylinder pressure.

For both measurements undertaken at 60 MPa and 160 MPa on the spray periphery, “ghost” droplets are no longer detected. When the radial distance is increased the droplet density decreased, therefore the chance of having multiple occupancy is reduced. This tends to support the hypothesis that those

large measured diameter are probably caused by the presence of more than one particle in the measurement volume.

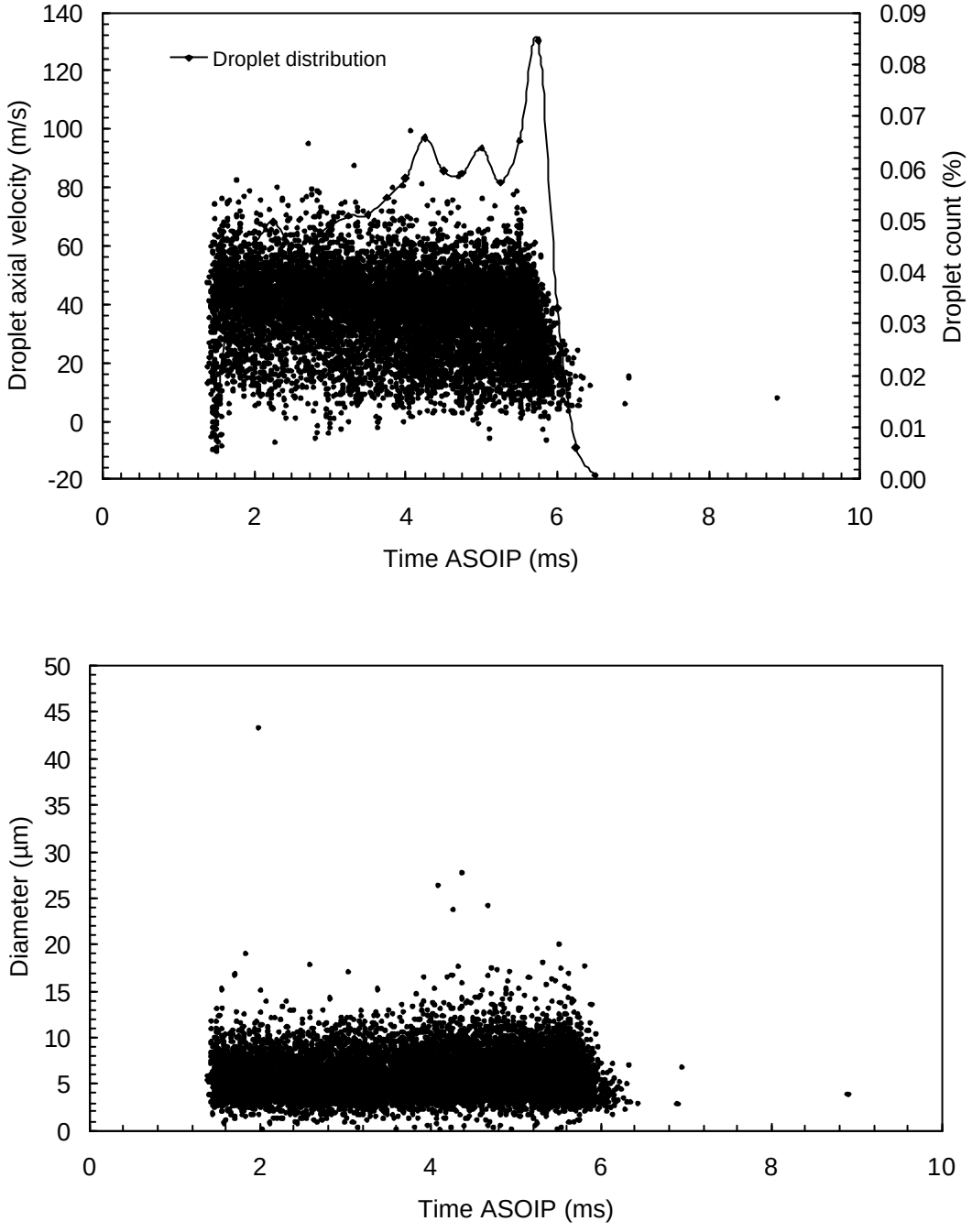

Figure 6-9: Time resolved axial droplet velocities and sizes at 30 mm from the nozzle on the spray axis (r = 0 mm); 684 K TDC temperature, 60 MPa injection pressure and 4 MPa in-cylinder pressure.

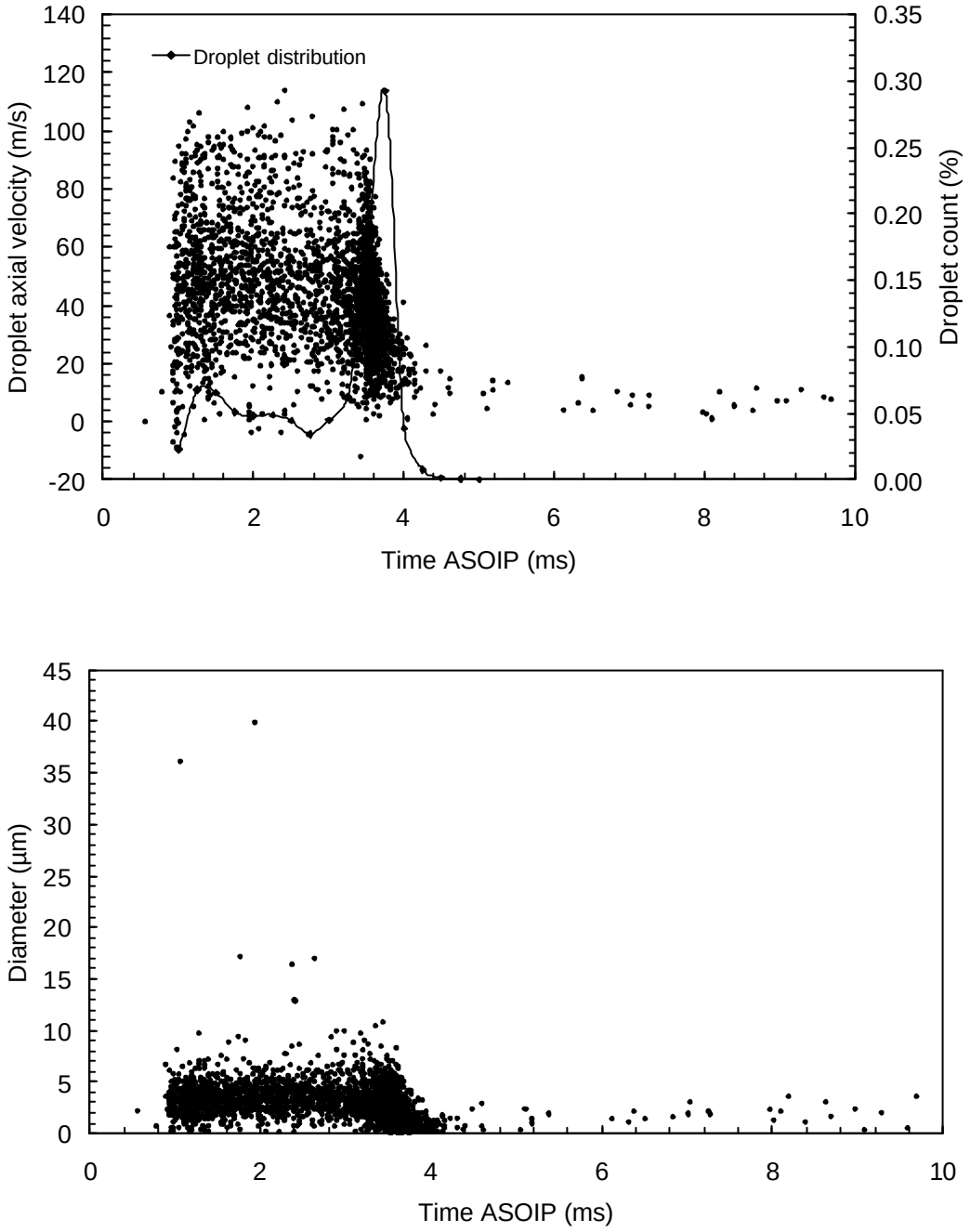

Figure 6-10: Time resolved axial droplet velocities and sizes at 30 mm from the nozzle on the spray axis (r = 0 mm); 684 K TDC temperature, 160 MPa injection pressure and 4 MPa in-cylinder pressure.

Figure 6-9 and Figure 6-10 show the effect of increasing the air intake temperature on the spray droplets velocities and diameters. At 30 mm from the nozzle on the spray axis, the air intake temperature was found to have an effect on the measured velocities. Increasing the air intake temperature from 572K to

684K resulted in a 25 % increase of the droplet velocities. As expected, higher air intake temperature produces smaller droplets diameter, due to increased evaporation, both in the low and high injection pressure cases. Most of the droplets are found to be in the range of 2-15 µm for an injection pressure of 60 MPa and 2-5 µm for an injection pressure of 160 MPa. A few ghost droplets are observed around 40 µm for both low and high injection pressure cases. Despite the effects of the surrounding air temperature on the droplet velocity and diameter, no influence of temperature could be seen from the droplet distribution in the core region of the spray (spray axis measurement). The core region seems to be less affected by the higher temperatures of the surrounding air, probably because the core region is denser and greater spray cooling takes place.

Droplet formation and size are influenced by various factors such as spray and droplet break-up mechanism, coalescence and evaporation, which are a function of time.

6.2.2 Effect of in-cylinder pressure

The effects of ambient pressure on the spray characteristics are analysed within a range from 2 MPa to 6 MPa (Figure 6-11). The effects of in-cylinder pressure were studied under two different injection pressures 60 MPa and 160 MPa.

PDA measurements of Diesel sprays show that increasing the in-cylinder pressure can dramatically slow droplets down. At high in-cylinder pressures the difference in droplet velocity profile between the head and the tail of the spray becomes small at low injection pressures. The ambient pressure also has an effect on the measured diameter; measurements undertaken at 50 mm from the nozzle and at 60 and 160 MPa showed a decrease in the droplet diameter with an increased in-cylinder pressure. This seems to contradict the observation of Hiroyasu and Arai (1990) and Koo and Martin (1990) where diameters increase as the in-cylinder pressure increased. Their data revealed that the increase in droplet diameter is caused by the coalescence effect.

In completely atomised sprays, an increase in the ambient pressure should result in an increase of the mean diameter due to a higher droplet concentration

(Hiroyasu and Arai (1990) and Payri et al. (1996)). It is believed that these discrepancies can be explained by the fact that for the elevated in-cylinder pressures used in this study, the shear and aerodynamic forces are more significant than the coalescence effects.

For comparison, Figure 6-12 show the same data as Figure 6-11, but with an in-cylinder temperature of 684K. For an increase in in-cylinder pressure (or density since the intake temperature is fixed), a decrease in droplet velocity and diameter is also observed. This confirms the hypothesis made by Crua (2002), where the increase of ignition delay with increase in in-cylinder pressure was attributed to enhanced droplet break up. The velocity and diameter profile for an in-cylinder pressure of 6 MPa could not be displayed, because at such a pressure and such a distance from the nozzle tip (50mm), the spray has completely evaporated. The increase of droplets velocities at higher in-cylinder temperature are believed to be caused by the reduction of in-cylinder density. Therefore, droplets travelling on the spray axis will be less decelerated by shear between the air and the spray envelope. The velocity and diameter profiles are similar at both in-cylinder temperatures.

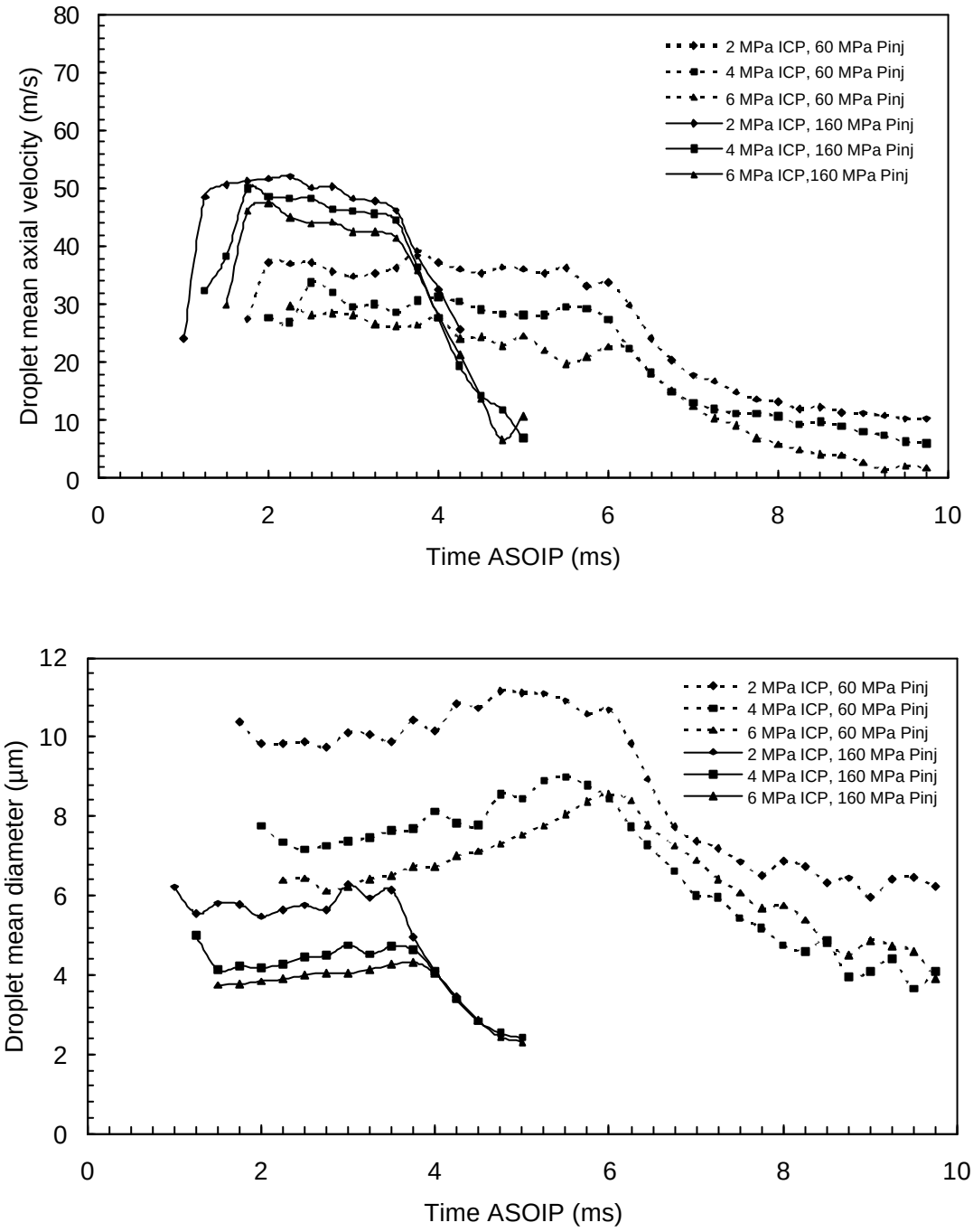

Figure 6-11: Mean droplet axial velocity and diameter profiles at 50 mm from the nozzle on the spray axis for injection pressure ranging from 60 to 160 MPa and in-cylinder pressure ranging from 2 to 6 MPa, 572K TDC temperature.

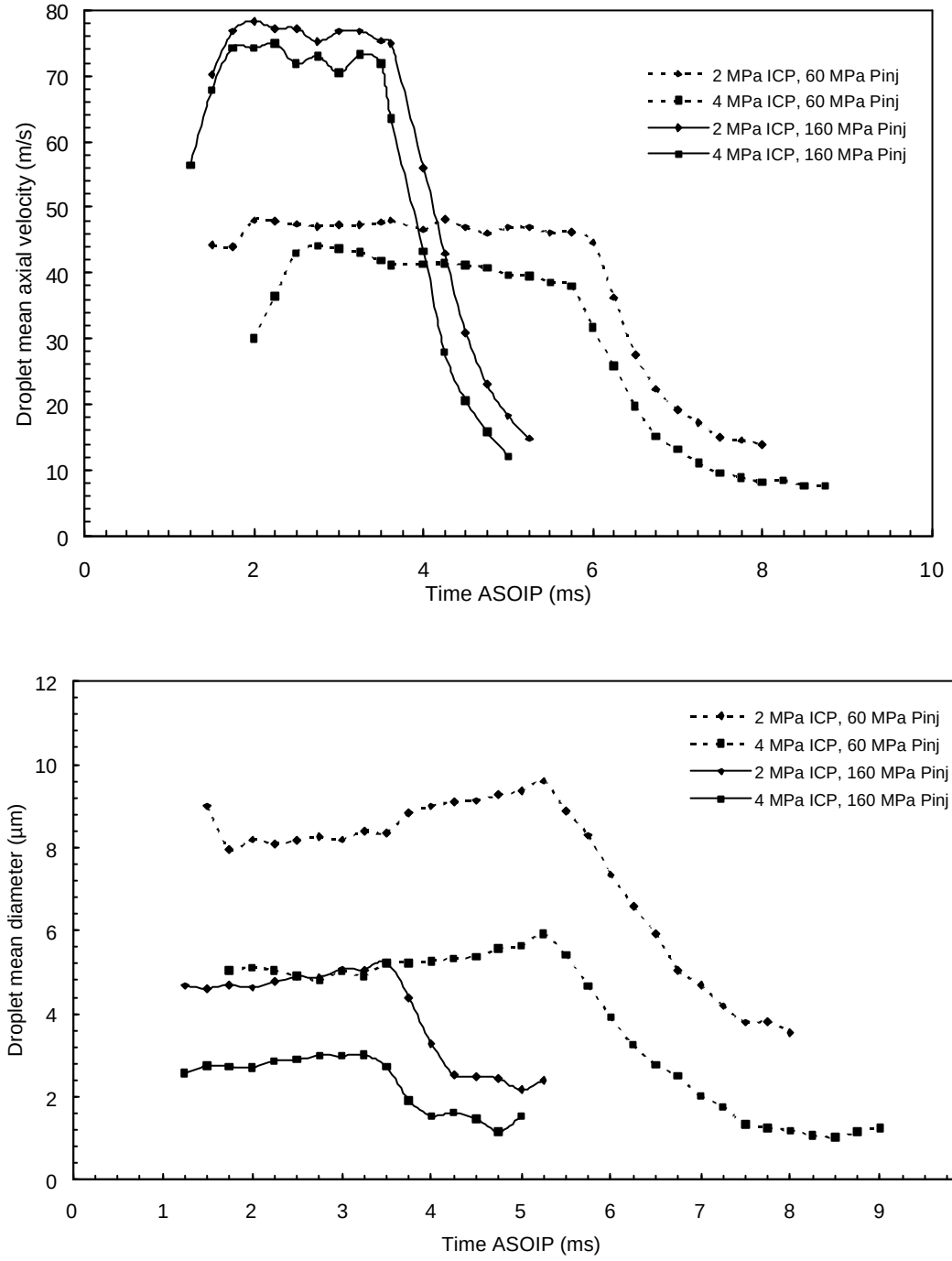

Figure 6-12: Mean droplet axial velocity and diameter profiles at 50 mm from the nozzle on the spray axis for injection pressure ranging from 60 to 160 MPa and in-cylinder pressure ranging from 2 to 4 MPa, 684K TDC temperature.

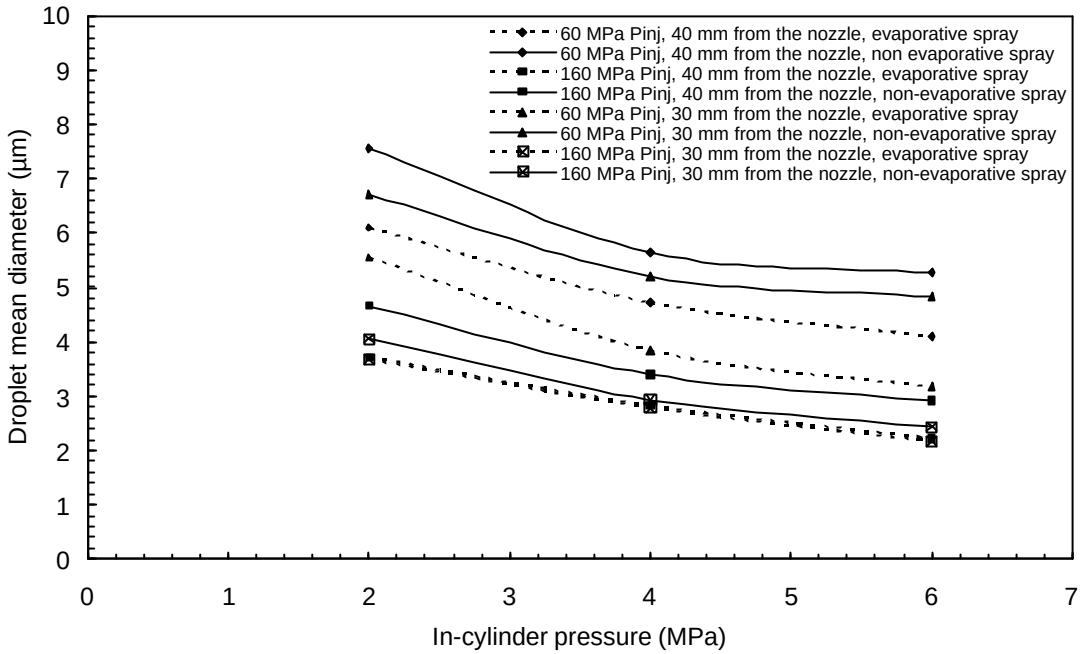

Figure 6-13: Effects of injection, in-cylinder pressure and temperature on the droplet mean diameter measured on the spray axis (evaporative spray: in-cylinder temperature of 684K and non-evaporative spray: in-cylinder temperature of 572K)

When comparing the evolution of the droplet diameters with injection and in-cylinder pressures (Figure 6-13), in-cylinder temperature seems to have larger influence on the low injection pressure sprays. At 40 mm from the nozzle and at low injection pressure, the droplet mean diameter decreases by 1.4 µm when the in-cylinder temperature is increased, while at high injection pressure it decreases only by 0.4 µm. The effect of ambient temperatures on the droplet mean diameters is greater at low injection pressure, probably because the Diesel spray is less dense than at high injection pressure (Ficarella et al., 1997); thermal interactions between the droplets and the surrounding is increased resulting in increased evaporation. Also, higher injection pressures increase the rate of fuel delivery and generate smaller droplets; together these affect the rate of evaporation and heat transfer thus reducing local temperature along the liquid core. It is believed this surrounding colder vapour region can partially "protect" the liquid core from the convection effect and subsequent droplet evaporation is decreased.

The droplet mean diameters are shown to be dependent upon both injection and in-cylinder pressures. However, at high in-cylinder temperature, the effects of the injection pressure on the droplet mean diameter is reduced as the in-cylinder pressure is increased. A deeper study for in-cylinder pressures above 6 MPa would be necessary to confirm the observed trend. Unfortunately, this is not possible with the current technology, where PDA measurements are not yet possible ate elevated in-cylinder pressure.

6.2.3 Effect of axial position

Figure 6-14 shows the velocity and the diameter profiles for the spray axis locations at 30 mm, 40 mm, 50 mm and 55 mm from the nozzle. Velocity and diameter profiles measured on the spray axis at 40 mm from the nozzle appear similar to the one measured at 50 mm and 55 mm. For an increasing distance from the nozzle, an increase in droplet mean velocity and mean diameter is observed. The evolution of the droplet sizes can be explained by different processes. Coalescence of droplets is due to collisions; small droplets can gather together to create large ones. At such in-cylinder conditions (4 MPa in-cylinder pressure and 540 K in-cylinder temperature), droplets will be subjected to evaporation therefore droplets with small diameters will have completely evaporated at 55 mm from the nozzle. In Figure 6-14, a diameter increase can be observed in the spray head, while the diameter decreases towards the end of the injection. The aerodynamic drag effect will cause droplets with small diameters to suffer more retardation than the large ones; these will then reach the measurement point later.

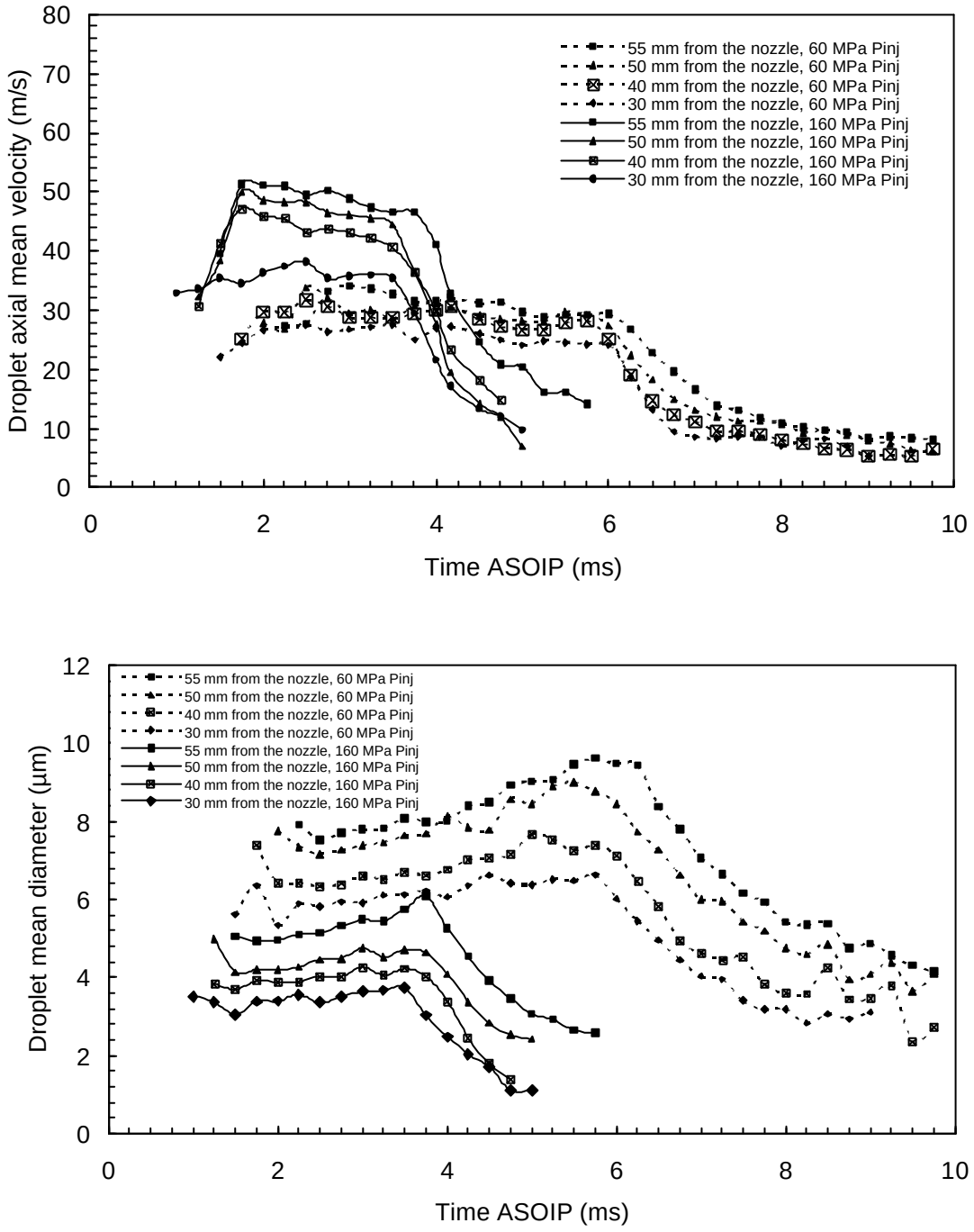

Figure 6-14: Mean droplet axial velocity and diameter profiles at 4 MPa in-cylinder, at 30, 40, 50 and 55 mm from the nozzle, for injection pressure ranging from 60 to 160 MPa, 572K TDC temperature

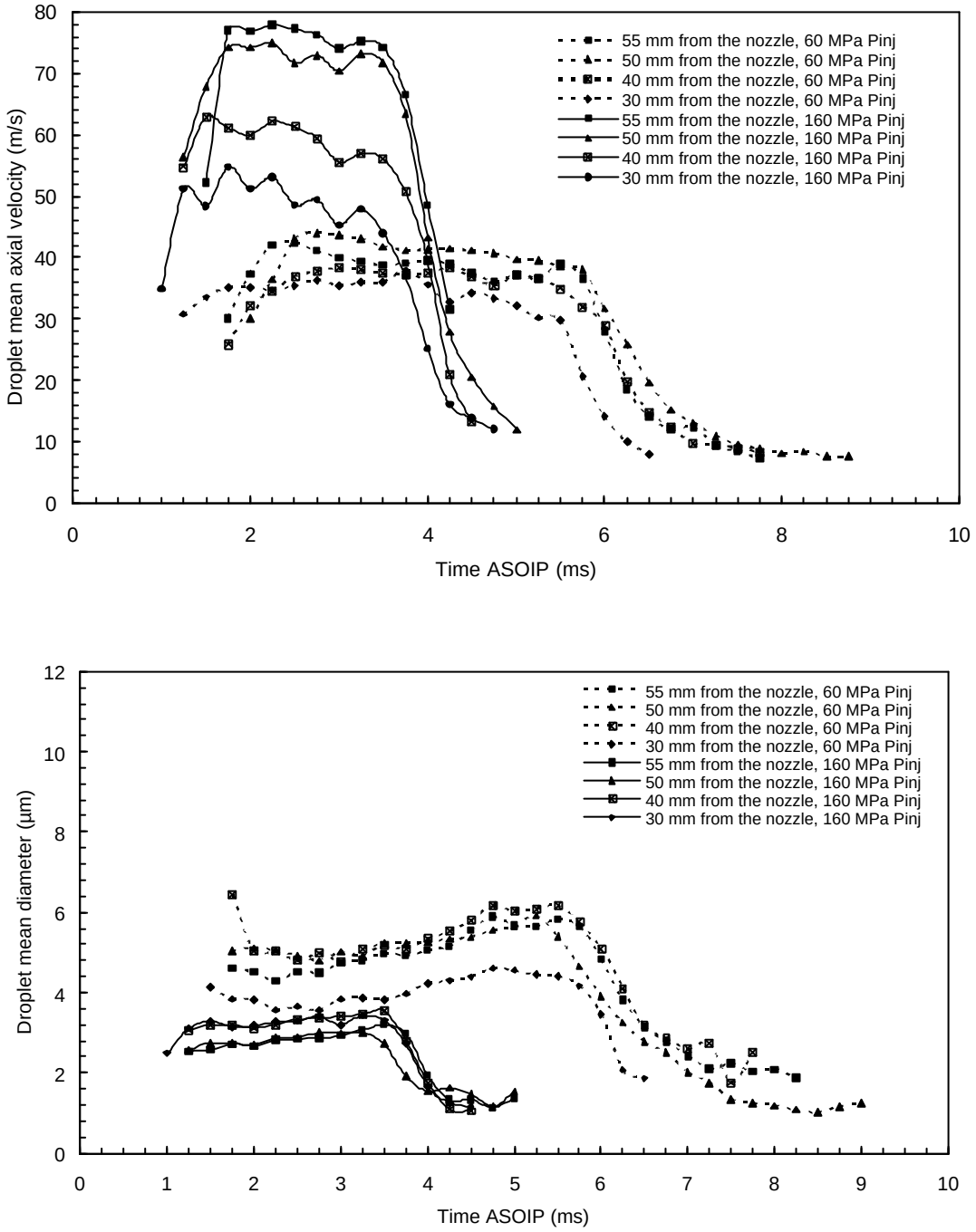

Figure 6-15: Mean droplet axial velocity and diameter profiles at 4 MPa in-cylinder, at 30, 40, 50 and 55 mm from the nozzle, for injection pressure ranging from 60 to 160 MPa, 684K TDC temperature.

Figure 6-15 shows the mean droplet axial velocity and diameter profiles for the same location as Figure 6-14 in the high in-cylinder temperature spray. The spray general profile is similar for both the non-evaporative and evaporative sprays. Droplet velocities and diameters both drop off rapidly at the transition

between the head and the tail. Observing more closely, an increase in droplet mean diameter is found when the distance from the nozzle tip is increased. In contrast to the non-evaporative spray where the enhancement in droplet diameter is noticed at all the locations (from 30 mm to 55 mm), in the evaporative spray the increase in diameter is only observed on the first part of the spray (from 30mm to 40mm). The droplets then decrease in size towards the spray the tip. Coalescence of droplets on the first 40 mm must be the predominant phenomena, hence explaining the evolution of the droplet sizes. Using a Schlieren video imaging technique, Crua (2002) showed that at approximately 55 mm from the nozzle hole and equivalent in-cylinder conditions (4 MPa and 684 k), the liquid phase of the spray turned to vapour. The transition to vapour is preceded by a phase of evaporation, explaining the decrease in droplet diameter towards the end of the spray. Moreover, the droplets velocity increases with axial distance, increasing the heat transfer by convection. An increase in droplet velocity is observed when the in-cylinder temperature is increased. The spray will be less affected by the shear between the spray envelope and the air, as the cylinder density is lower.

Figure 6-16 shows the peak velocities at four different axial distances from the nozzle, different in-cylinder pressure and temperature and different injection pressures. It is noticed from this figure that the peak velocity is affected by ambient conditions (in-cylinder pressure and temperature) and injection pressure. It reveals a tendency of gradual increase with increasing axial distance until it stabilise around 50 mm from the nozzle. This seems to contradict the observations made by Koo and Martin (1990) where the peak velocities reduce as the axial distance from the nozzle is increased from 10 to 120 mm. However, their data reported that the peak velocity remained almost the same at axial locations of 10 and 30 mm were compared. A study by Levy et al. (1997) showed an increase in velocities with the distance from the nozzle. This was justified by the jet widening.

In this case, the following explanation can be made. The first droplets to enter the high ambient pressure chamber at very high initial velocity as the particles travel through the air, they accelerate the surrounding air. As a result of the

local velocity component of the gas, the droplets coming out of the nozzle hole will experience less deceleration because of the reduced relative velocity between the fuel and the gas. These droplets will then catch up with those firstly injected and overtake them. Once at the top of the spray, these droplets will be entering again the quiescent surrounding and be decelerated rapidly. Repetition of this process during the injection may lead to the increase of the axial velocity component of air along the droplet trajectories. As a result the droplet injected at the time of the peak injection rate might be slightly accelerated as they travel along the centre line resulting in higher values over the range of axial distances considered in this study.

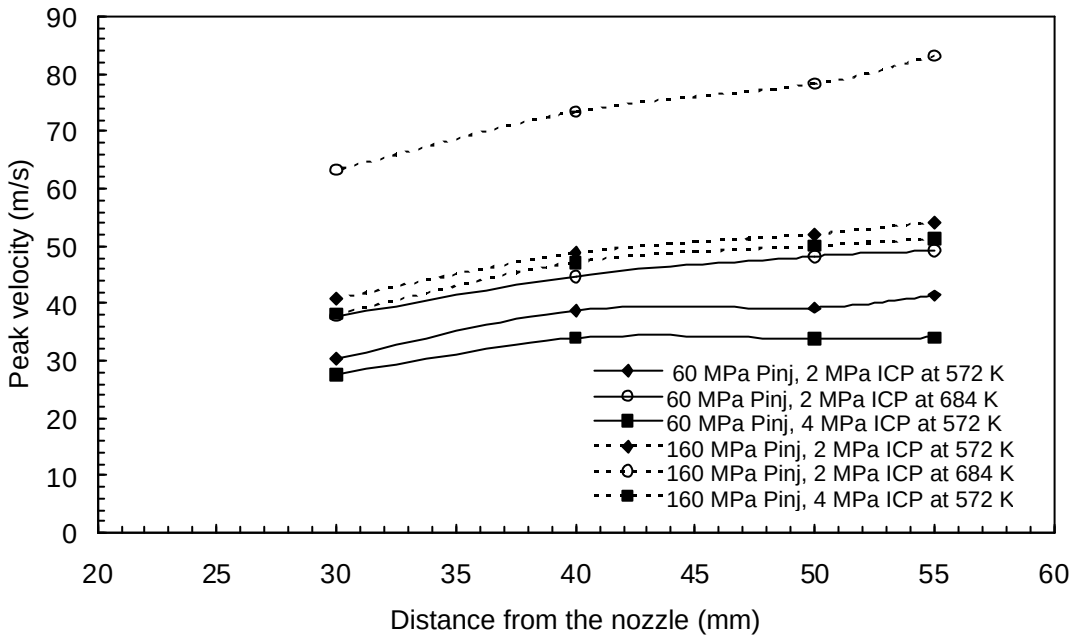

Figure 6-16: Peak axial velocities on the spray axis for injection pressures ranging from 6 to 160 MPa, in-cylinder pressures from 2 to 4 MPa and TDC temperatures from 572 K to 684 K.

6.2.4 Effect of radial position

Results presented in Figure 6-17 and Figure 6-18 demonstrate the evolution of the spray droplet velocities and sizes from five radial locations along the spray axis at 40 mm from the nozzle. Droplet velocity and diameter are time resolved with the origin on the time axis corresponding to the injector pulse.

Droplet velocity and diameter distribution both show strong dependence on the radial position in the spray. This is illustrated in Figure 6-17 and Figure 6-18. The velocity profiles show that droplets measured on the periphery of the spray have smaller velocities than those measured on the spray axis. Consequently, particles travelling on the edge of the spray will be more affected by shear between the air and the spray envelope, after the disintegration of the liquid column emerging from the nozzle. The generated droplets may breakup into smaller ones as they progress into the surrounding gas. Droplets located on the spray periphery may also be subjected to evaporation as in-cylinder temperatures at top dead centre reaches 540 K. This is confirmed by the diameter distribution, for both non-evaporative and evaporative spray, where a reduction in droplet diameter is observed with an increase in radial distance.

A diameter increase in the spray head on the periphery can be observed over time for the non-evaporative spray (Figure 6-17). This diameter increase over time is much reduced for the evaporative spray (Figure 6-18), as the increasing induced gas flow in the spray is counterbalanced by increasing evaporation rate, and therefore the influence of the droplet coalescence is smaller due to the lower droplet number density.

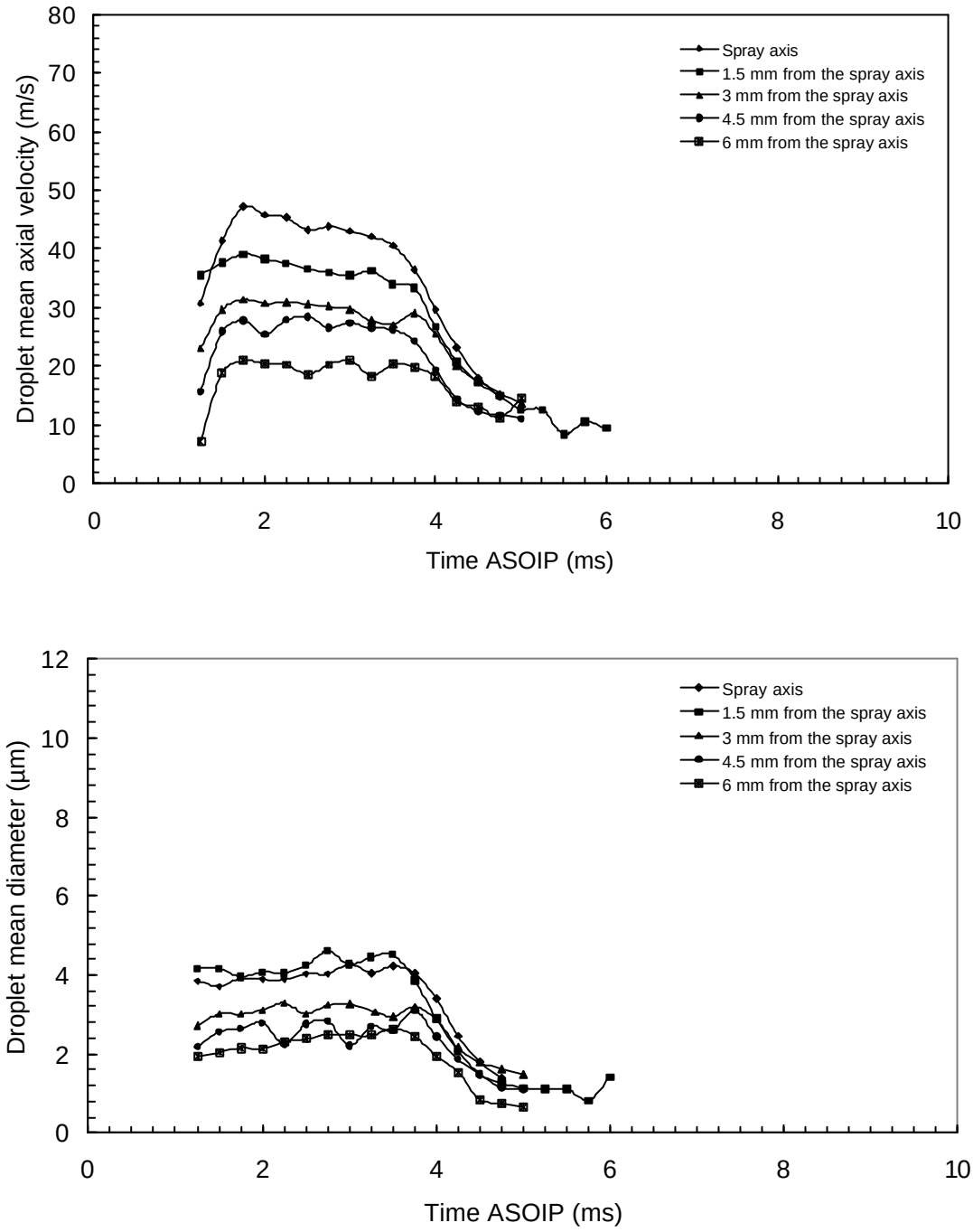

Figure 6-17: Mean droplet axial and velocity profiles at 40 mm from the nozzle, 160 MPa injection pressure, 4 MPa in-cylinder pressure and 572 K TDC temperature for radial position ranging from 0 to 6 mm from the spray axis.

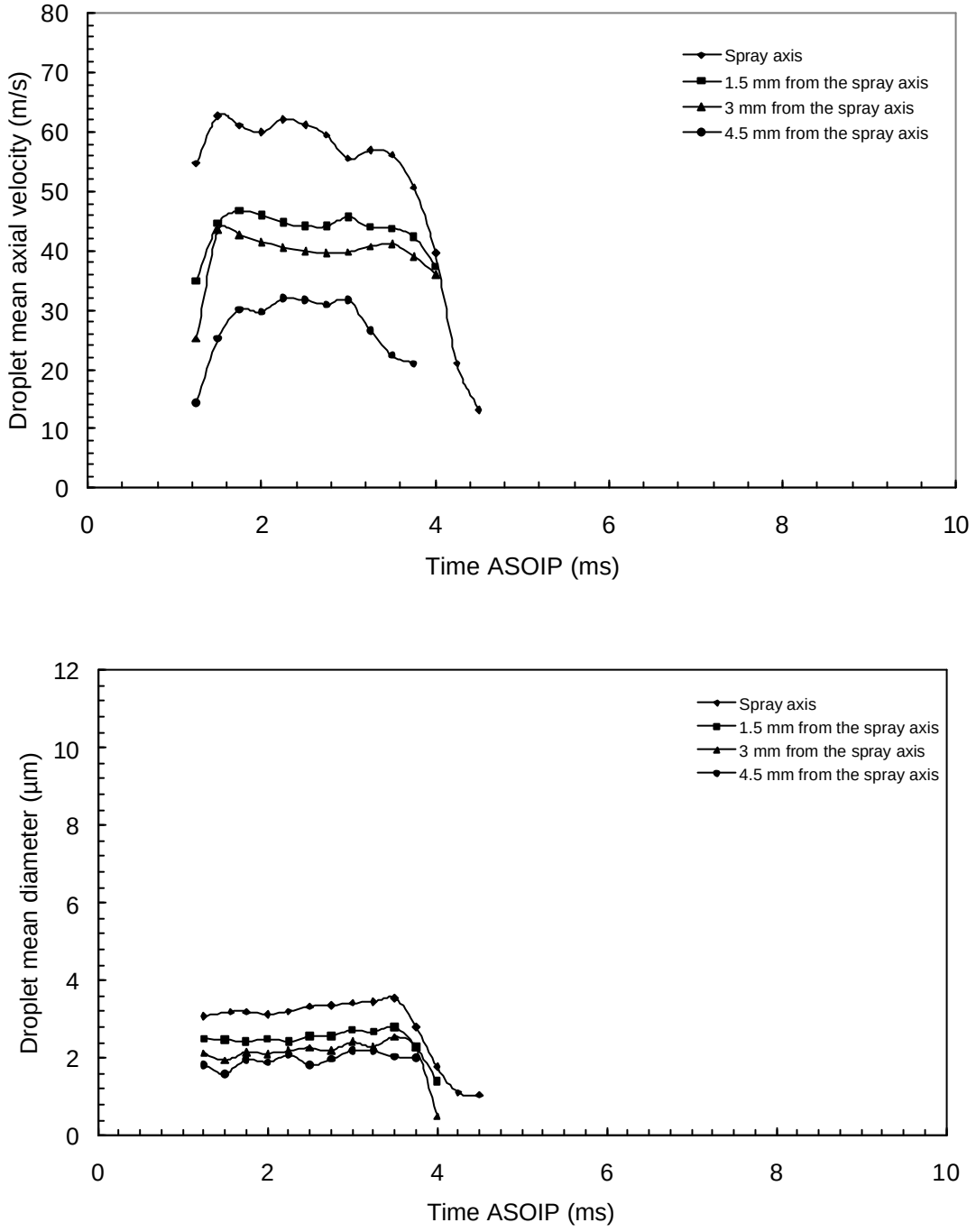

Figure 6-18: Mean droplet axial and velocity profiles at 40 mm from the nozzle, 160 MPa injection pressure, 4 MPa in-cylinder pressure and 684 K TDC temperature for radial position ranging from 0 to 6 mm from the spray axis.

Figure 6-19 shows the spray droplet mean axial velocity at different radial positions and at two different injection and in-cylinder pressures. As can be seen, the high injection pressure spray has a “top hat” velocity profile unlike the low injection pressure spray. This can be explained by the increased mass flux

at the edge of the spray which increases momentum in that region and maintains higher velocities, despite the decelerating effect of the high density air. Evidence for such an increase in mass flux would be an actual measurement using the PDA system; unfortunately such measurements, although possible, are unreliable in such dense sprays (Domnick, 1997). However, the increased mass flux can be inferred by considering the fact that the cone angle does not significantly increase at higher injection pressures (Crua, 2002). Clearly if more mass is being delivered through the nozzle, and the average velocities is higher. Then simple conservation of mass says that the average mass flux of the spray must be higher. If there is an increase in the mass flux in the middle of the spray, then higher velocities would be found on the spray axis; as this is the case the increased mass flux must be towards the spray's edges.

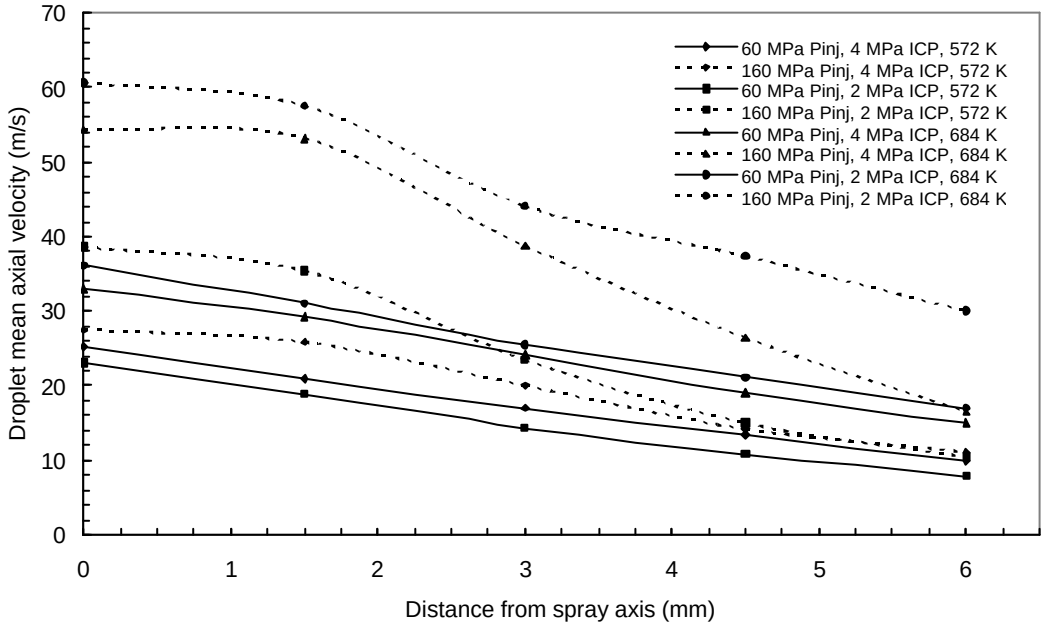

Figure 6-19: Effect of the radial distance on droplet axial mean velocity at 40 mm from the nozzle for injection pressures ranging from 60 to 160 MPa, in-cylinder pressures from 2 to 4 MPa and TDC temperatures from 572 K to 684 K.

6.3 Velocity-diameter correlation

The droplet data acquired can be compared with droplet breakup criteria (or stability criteria) and give indications of the susceptibility of the droplets to aerodynamic breakup processes. The droplet breakup criteria are functions of non-dimensional parameters, specially the droplet Weber number. The droplet Weber number, We_D, is defined as:

$$We_D = \frac{r_g d u_d^2}{s_l} \tag{6.1}$$

where ρ_g is the density of the gas surrounding the droplet, d is the droplet diameter, u_d is the relative velocity of the droplet, and σ_l is the surface tension of the droplet fluid. The droplet Weber number is the ratio of disruptive hydrodynamic force to the force of surface tension.

Following Reitz and Diwakar (1987), the criterion for bag breakup of a droplet is $We_D > 12$. Droplets not meeting this criterion are assumed to be stable.

In the droplet Weber number and calculations, the droplet velocity is the relative velocity with respect to the surrounding gas.

Since the velocity of the surrounding gas is an unknown, it is impossible to calculate the true Weber number. In the past, some people (Koo and Martin, 1991) have used the velocity of the smallest droplets to approximate the gas velocity, but droplets measurements near the nozzle often show droplet velocities are independent of size. Consequently, this would mean that all the droplets are aerodynamically stable since the estimated gas velocity would equal the droplet velocity.

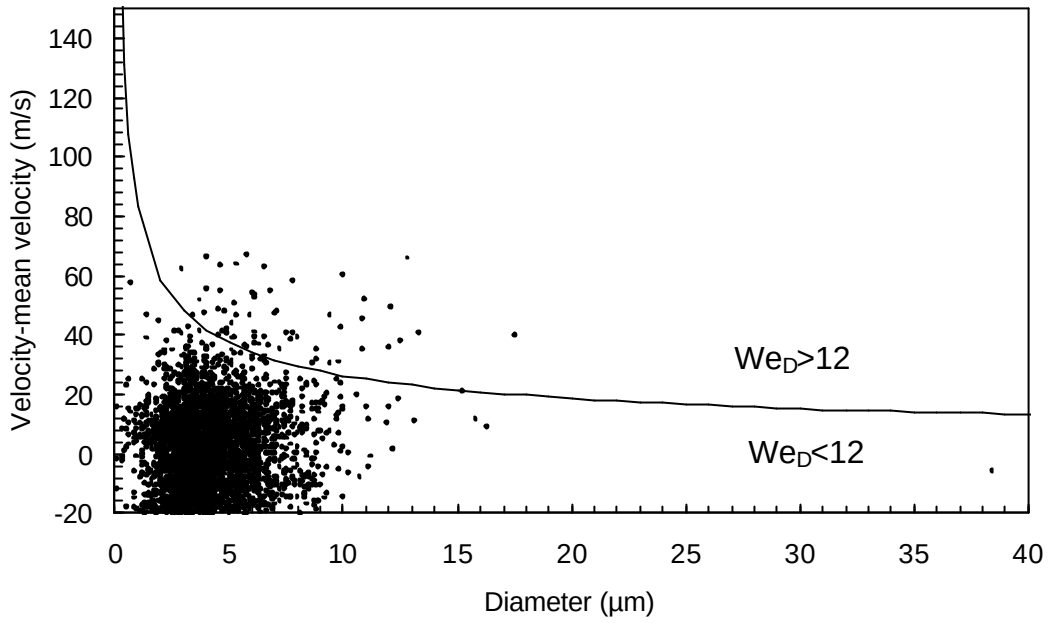

Figure 6-20: Comparison of 160 MPa injection pressure and 4 MPa in-cylinder pressure droplet data, on the spray axis at 30 mm from the nozzle tip, with droplet breakup criteria. The droplet relative velocity is assumed as the absolute value of the droplet velocity minus the average droplet velocity at that time in the spray.

To overcome the lack of knowledge of the true relative velocity of the droplets, two different estimates of relative velocity are made to bound the problem. The first method is to simply use the measured velocity for the relative velocity. This assumes a stagnant gas velocity, making the estimate high in areas where surrounding gas possesses velocity from the entrainment process. The second is to assume that the gas velocity is equal to the mean droplet velocity at that point in time and space. Then one can take the droplet relative velocity as equal to the absolute value of the droplet velocity minus the average droplet velocity. This method tends to under predict the relative velocity, but it is more accurate than the first method in areas such as the spray core where droplets would have imparted a non-zero velocity to the surrounding gas. The true relative velocity would lie in between the two estimates.

Figure 6-20 is a relative velocity-diameter plot of droplet data for the high-pressure case, on the spray axis at 30 mm from the nozzle. The plot also

includes break-up criteria boundary. The bag break up criteria is represented by the line.

Figure 6-20 shows several droplets above the bag break up criteria. These would be subject to bag break up. The droplet relative velocity is taken as the difference between the droplet velocity and the average droplet velocity for that point in time of the spray. For this location, this method probably gives a better estimate of the true relative velocity. The true relative velocity would likely be somewhat higher, so more droplets than what are shown would exceed the break up criteria.

In comparison, Figure 6-21 shows the same data as Figure 6-20 but the surrounding gas velocity assumed negligible. With this assumption, many of the droplets would be subjected to bag break up. For the core of the spray, these relative velocities would be too high, but this figure gives some perspective on where the true relative velocity might lie.

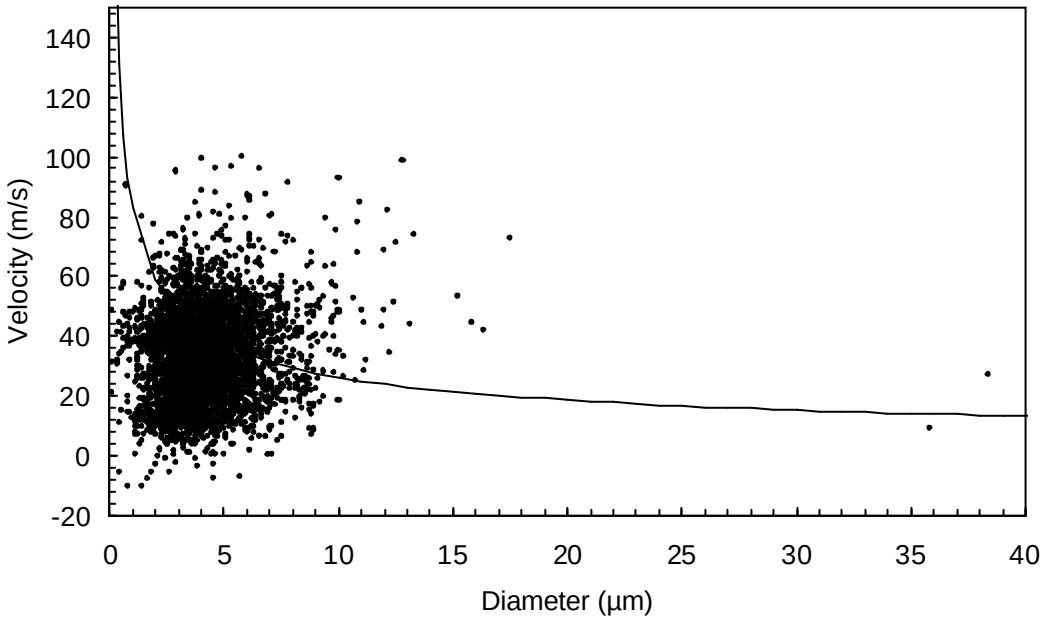

Figure 6-21: Comparison of 160 MPa injection pressure and 4 MPa in-cylinder pressure droplet data, on the spray axis at 30 mm from the nozzle tip, with droplet breakup criteria. The surrounding gas velocity is assumed to be zero.

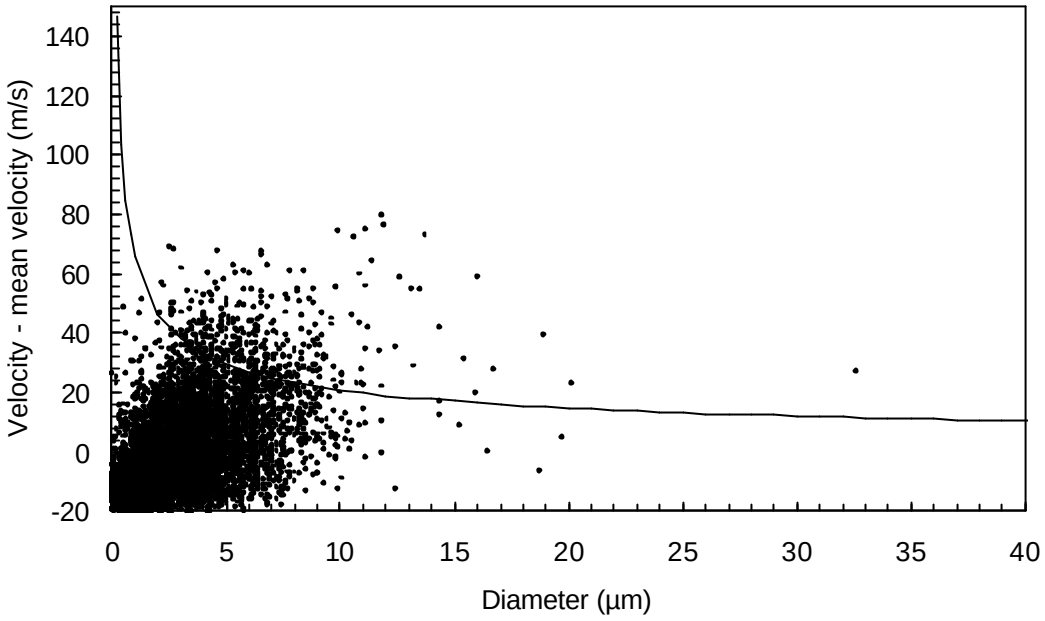

Figure 6-22: Comparison of 160 MPa injection pressure and 4 MPa in-cylinder pressure droplet data, on the spray axis at 40 mm from the nozzle tip, with droplet breakup criteria. The droplet relative velocity is assumed as the absolute value of the droplet velocity minus the average droplet velocity at that time in the spray.

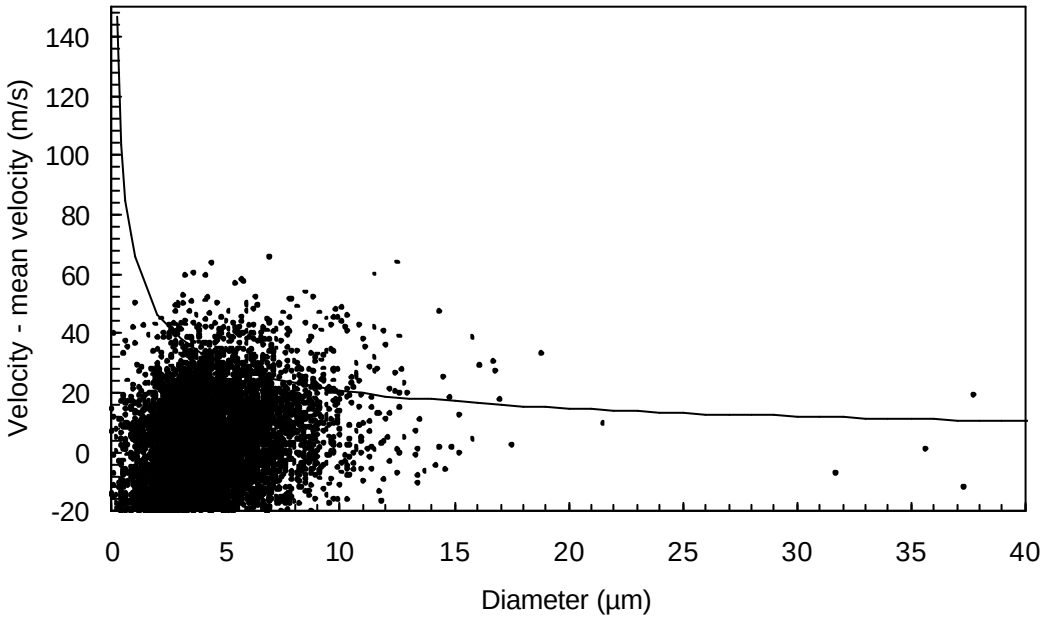

Figure 6-23: Comparison of 160 MPa injection pressure and 4 MPa in-cylinder pressure droplet data, on the spray axis at 50 mm from the nozzle tip, with droplet breakup criteria. The droplet relative velocity is assumed as the absolute value of the droplet velocity minus the average droplet velocity at that time in the spray.

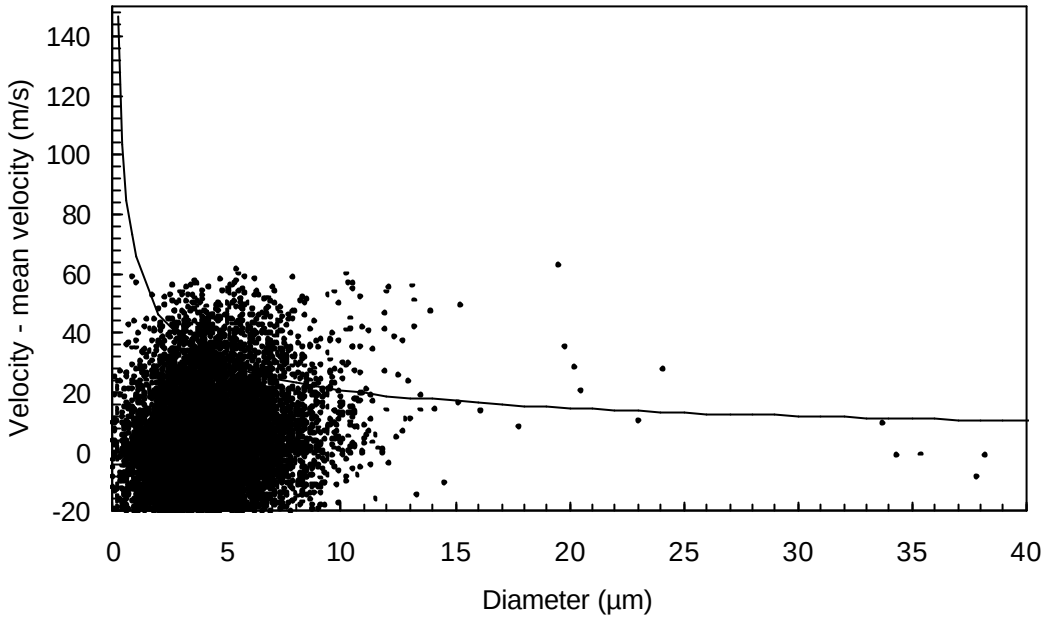

Figure 6-24: Comparison of 160 MPa injection pressure and 4 MPa in-cylinder pressure droplet data, on the spray axis at 55 mm from the nozzle

Figure 6-22, Figure 6-23 and Figure 6-24 show the progression of the spray along the axis at z=40 mm, 50 mm and 55 mm, respectively. In these plots, one noticeable trend is the decline of small droplets with axial distance. The droplet mean diameter increased from 3.02 to 3.68 µm, when the distance from the nozzle was increased from 40 to 55 mm.

Again, for a perspective view, Figure 6-25, Figure 6-26 and Figure 6-27 show the same data as Figure 6-22, Figure 6-23 and Figure 6-24, respectively, but with the assumption of negligible surrounding gas velocity. These plots show the increase in large droplets with axial distance. They also show that the velocity range is maintained. While the numbers of fast droplets increase with axial distance, numerous droplets maintain velocities of 100 $m.s^{-1}$. This slow increase of droplet velocities is also noted in figure and figure. In each graph, several droplets consistently exceed the droplet breakup criteria.

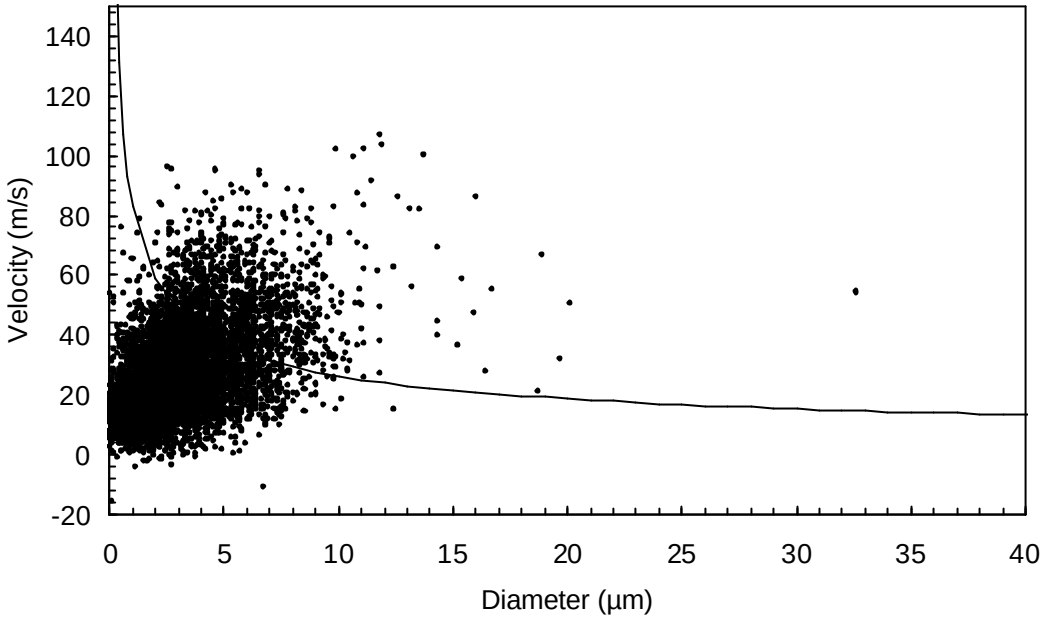

Figure 6-25: Comparison of 160 MPa injection pressure and 4 MPa in-cylinder pressure droplet data, on the spray axis at 40 mm from the nozzle tip, with droplet breakup criteria. The surrounding gas velocity is assumed to be zero.

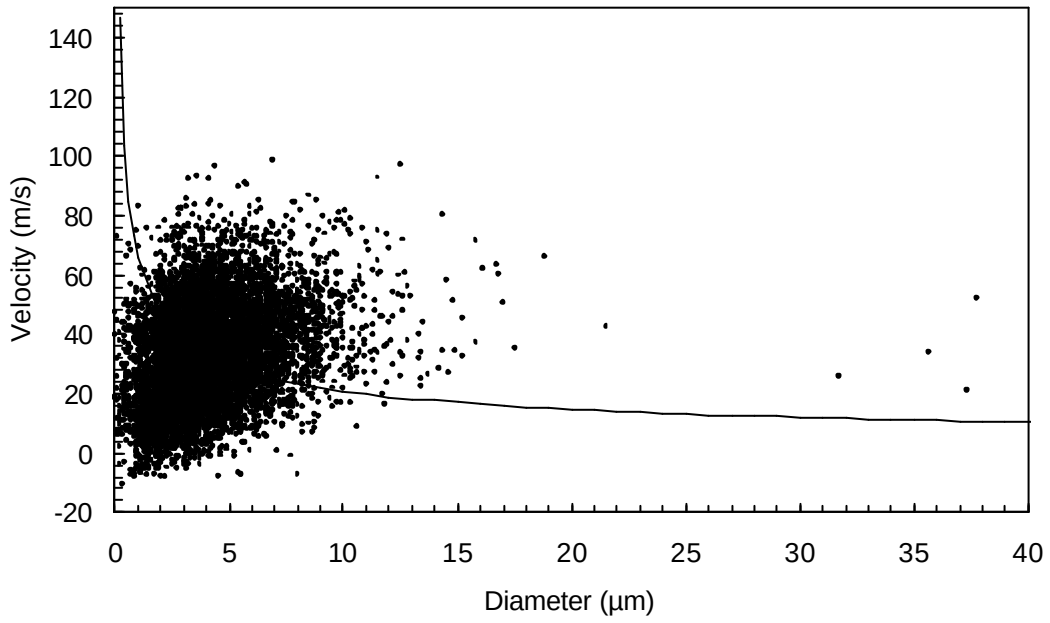

Figure 6-26: Comparison of 160 MPa injection pressure and 4 MPa in-cylinder pressure droplet data, on the spray axis at 50 mm from the nozzle tip, with droplet breakup criteria. The surrounding gas velocity is assumed to be zero.

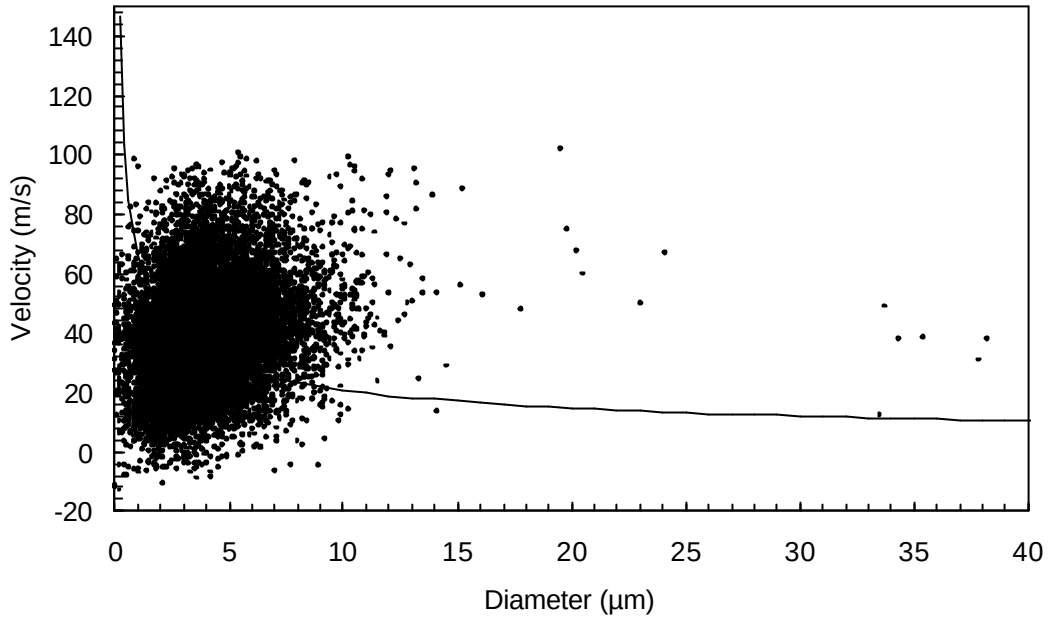

Figure 6-27: Comparison of 160 MPa injection pressure and 4 MPa in-cylinder pressure droplet data, on the spray axis at 55 mm from the nozzle tip, with droplet breakup criteria. The surrounding gas velocity is assumed to be zero.

Off-axis data is shown in Figure 6-28 for high pressure spray together with breakup criteria boundary. The droplet data was taken at the location z=30mm, r=4mm. The surrounding gas velocity is assumed to be zero, although the spray would have imparted some velocity to the gas despite the off-axis location. The plot shows that almost all the droplets are stable. Only a few surpass the bag breakup criteria.

Figure 6-29 represents the low pressure Diesel spray of Figure 6-28. The low pressure case only has a few droplets in excess of the bag breakup criteria. The rest of the droplets are stable as in the high pressure case. Both graphs show how the data lay with respect to the breakup criteria. In Figure 6-29, all the droplets are stable. The droplet data in either figure does not exhibit any visible velocity-diameter correlation.

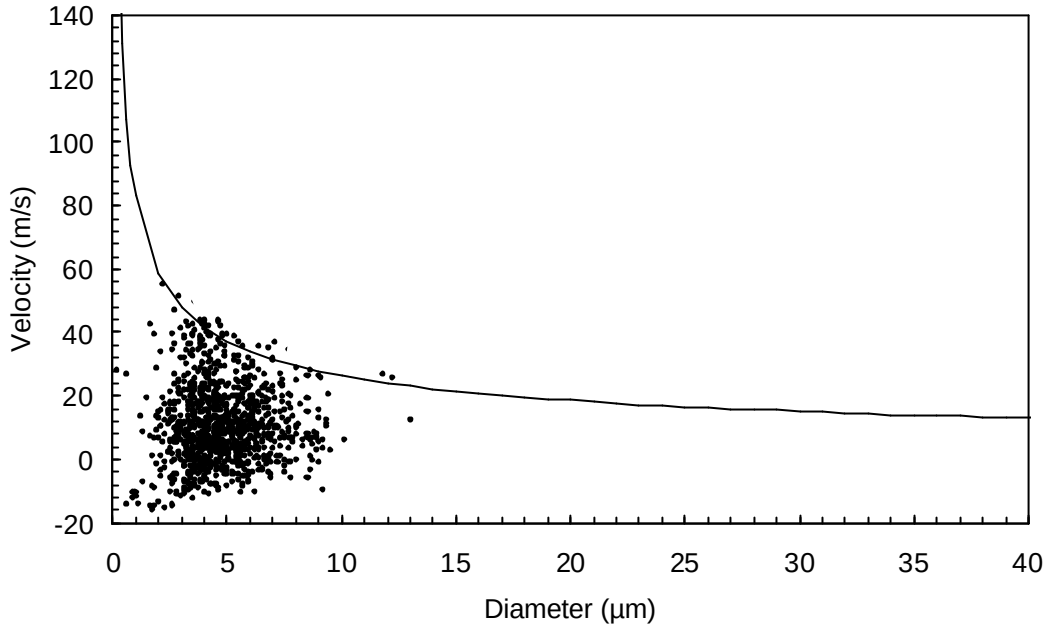

Figure 6-28: Comparison of 160 MPa injection pressure and 4 MPa in-cylinder pressure droplet data, at 4 mm from the spray axis and 30 mm from the nozzle tip, with droplet breakup criteria. The surrounding gas velocity is assumed to be zero.

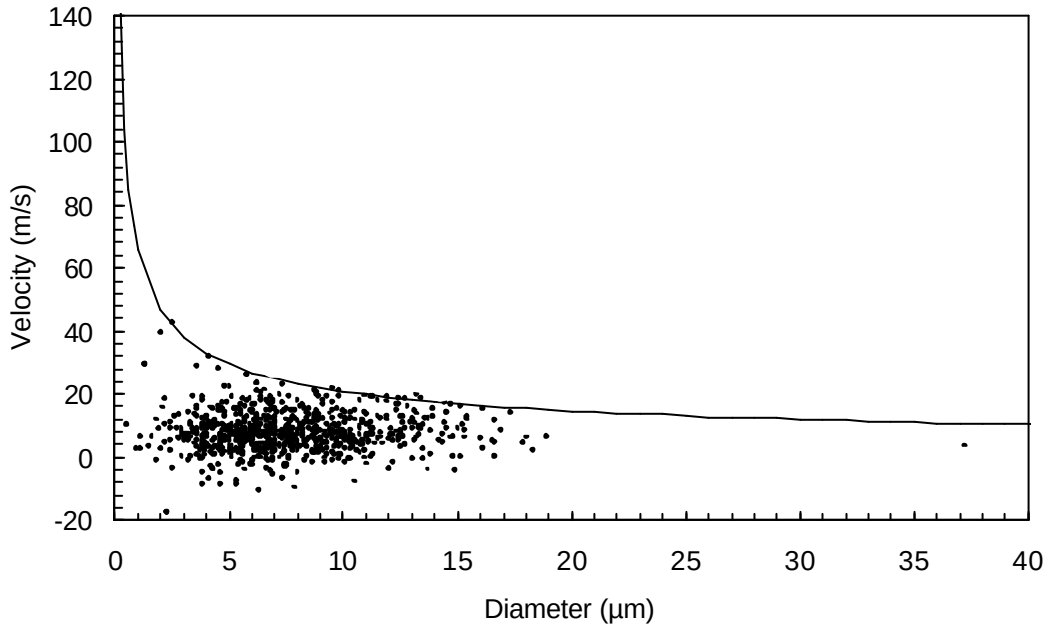

Figure 6-29: Comparison of 60 MPa injection pressure and 4 MPa in-cylinder pressure droplet data, at 4 mm from the spray axis and 30 mm from the nozzle tip, with droplet breakup criteria. The surrounding gas velocity is assumed to be zero.

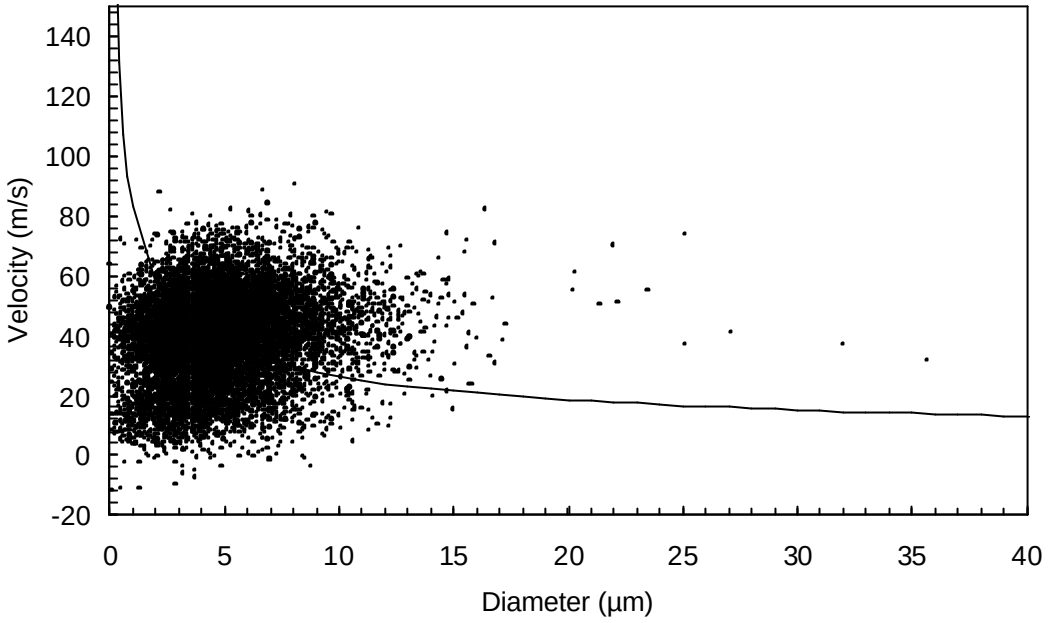

Figure 6-30: Comparison of 60 MPa injection pressure and 4 MPa in-cylinder pressure droplet data, on the spray axis and 40 mm from the nozzle tip and 684K TDC temperature, with droplet breakup criteria.

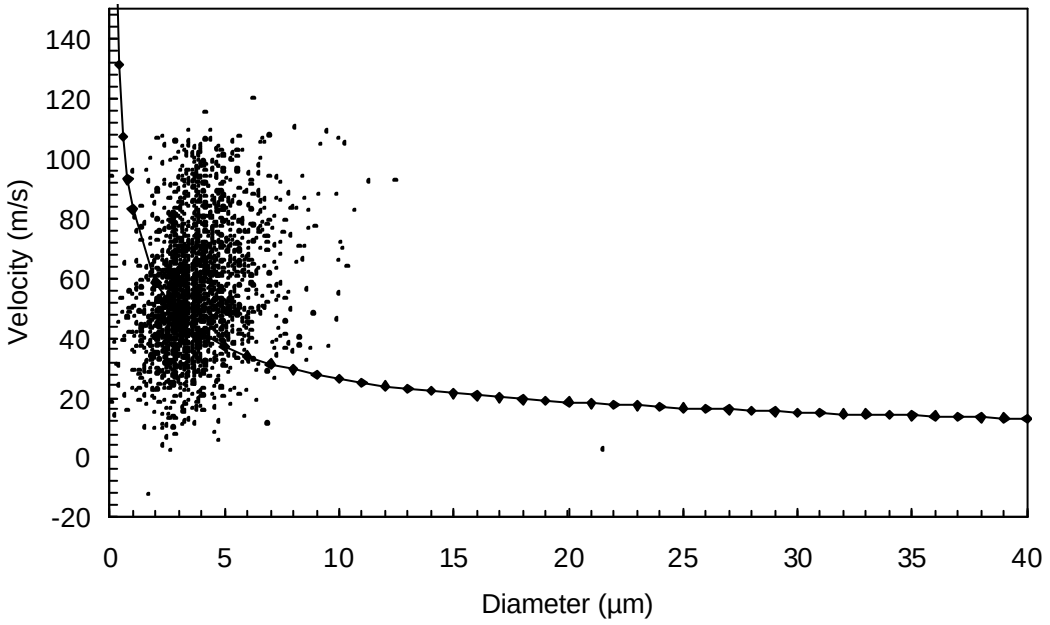

Figure 6-31: Comparison of 160 MPa injection pressure and 4 MPa in-cylinder pressure droplet data, on the spray axis and 40 mm from the nozzle tip and 684K TDC temperature, with droplet breakup criteria.

Figure 6-30 and Figure 6-31 show the droplet measurements relative to bag breakup. Most of the droplets are unstable and exceed the breakup criteria. Droplet to droplet interaction can explain this phenomenon. Although, the measured droplets are smaller at higher in-cylinder temperature than at low in-cylinder pressure, the coalescence effects may be greater.

6.4 Spray droplet Sauter mean diameter and correlation with empirical model

Figure 6-32 and Figure 6-33 show the injection pressure and the radial position effects on the overall spray SMD. Three observations can be made:

- There is a decreasing trend in the spray tail.
- The diameter distribution shows a dependence on the radial position in the spray. Larger Sauter mean diameters are observed on the spray axis, observations already made Koo and Martin (1990) and Arcoumanis et al. (1997).
- The overall spray SMD of high injection pressure sprays is smaller than that of low injection pressure spray. This indicates that high injection pressure is beneficial to spray atomisation.

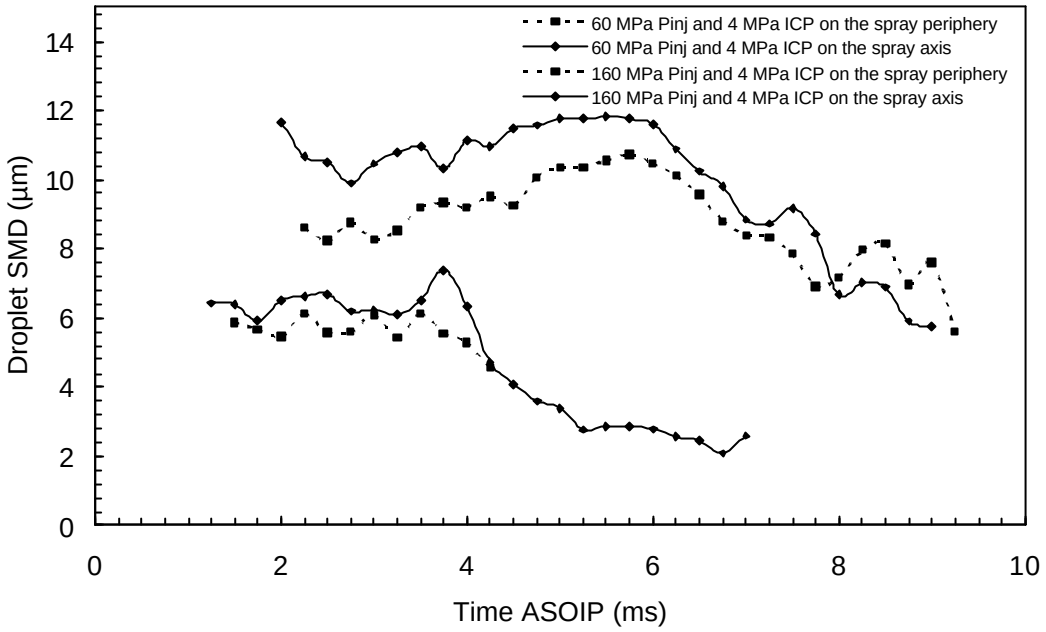

Figure 6-32: Droplet Sauter Mean Diameter at 50 mm from the nozzle on the spray axis and the spray periphery for injection pressure ranging from 60 to 160 MPa at an in-cylinder pressure of 4 MPa, 572K TDC temperature.

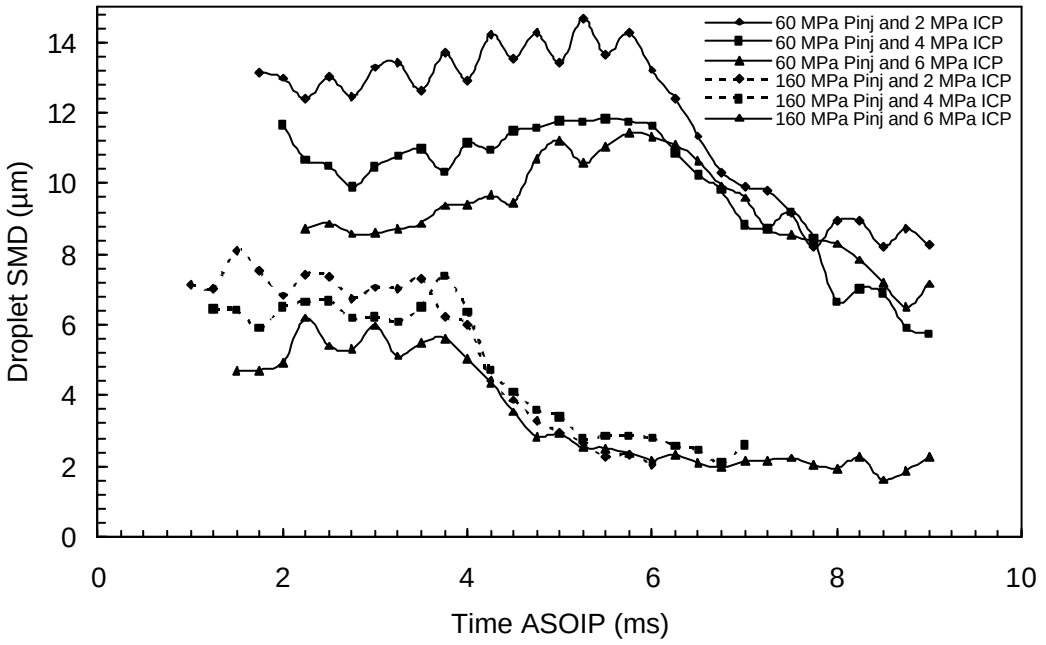

Figure 6-33: Droplet Sauter Mean Diameter at 50 mm from the nozzle on the spray axis for injection pressure ranging from 60 to 160 MPa and in-cylinder pressure ranging from 2 to 6 MPa, 572K TDC temperature.

Referring to the present correlations for the spray overall SMD, the following equations proposed by Hiroyasu et al. (1990) and Elkotb (19820, respectively, will be used to compare with the results obtained in this study.

Hiroyasu et al. :

$$d_{32} = 2.33 \times 10^{3} (?P)^{-0.135} (?_{g})^{0.121} (Q)^{0.131} \quad (6.2)$$

Elkotb:

$$d_{32} = 3.08 \times 10^{6} (?P)^{-0.54} (?_{g})^{0.06} (?_{l})^{0.737} (u_{l})^{0.385} (s)^{0.737} \quad (6.3)$$

where d_{32} (μm) is the Sauter Mean Diameter (SMD), ?P (Pa) is the pressure difference between the injection pressure and the ambient pressure, $?_a$ (kg/m^3) is the air density, Q (m^3/inj) is the injection quantity, $?_l$ (kg/m^3) is the fuel density, $?_l$ (m^2/s) is the kinematic viscosity of fuel and s (N/m) is the surface tension.

Pressure difference (Pa)	58×10^6	158×10^6	56×10^6	156×10^6
Ambient density (kg/m^3)	23.7		47.5	
Fuel delivery (m^3/inj)	3×10^{-8}			
Fuel density (kg/m^3)	668			
Kinematic fuel viscosity (m^2/s)	2.85×10^{-6}			
Surface tension (N/m)	1.43×10^{-2}			
SMD prediction using Eq. 6.2 (μm)	31.6	27.6	34.6	30.1
SMD prediction using Eq. 6.3 (μm)	9.3	5.4	9.9	5.7
SMD from PDA measurements	11.8	5.5	9.9	4.7

Table 6-1: Experimental and theoretical SMD values based on Hiroyasu and Elkotb equations

Table 6-1 presents the experimental results and the correlations' predictions under the current experimental conditions. Two different injection and in-cylinder pressures were used. The accuracy of measurements of spray Sauter mean diameter was estimated to be ± 0.2 μm.

Hiroyasu et al's prediction, Equation 6.2, on the high injection pressure case (?P=158×10^6) and the low injection pressure (?P=58×10^6) case are 27.6 μm and 31.6μm, respectively. Elkotb's predictions, Equation 6.3, on high and low injection pressure cases are 5.4 μm and 9.3μm, respectively. Comparing the experimental results and considering the measurement error, the Elkotb's

correlation seems to be good for the high injection and high in-cylinder pressure cases. However, the calculated Sauter mean diameter from Equation 6.2 with injection pressure of 60 MPa is far larger than the actual measured data, which may indicate that the model does not apply to high injection pressure system.
Nevertheless, Hiroyasu et al's and Elkotb predictions show an increase in SMD with an increase in in-cylinder pressure, which is contrary to our observations.
Therefore, a thorough study, which is beyond the scope of this work, should be necessary to establish a new SMD correlation that takes into account all the parameters of a modern Diesel injection system.

6.5 Effect of nozzle hole diameter on the structure of a Diesel spray

The effects of the nozzle hole diameter on the spray characteristics were analysed by using two single-hole VCO nozzles of different hole diameters (0.1 mm vs. 0.2 mm). In order to isolate the effects of nozzle diameter, the other geometric configurations of the nozzle tip were kept constant. The effect of the nozzle hole diameter was studied at 40 mm from the nozzle at two different injection pressures (60 MPa and 160 MPa) and one in-cylinder pressure (2 MPa).
Figure 6-34 displays the effects of nozzle hole diameter on the droplet axial mean velocity and the droplet mean diameter. It is interesting to note that both velocity profiles exhibit a similar trend, while the diameter profiles show different behaviour. The spray head diameter increase for a 0.1 mm VCO nozzle is more pronounced than for the 0.2 mm VCO nozzle.

PDA measurements of Diesel sprays show that reducing the nozzle hole size can increase the droplet velocity and reduce the droplet diameter. Reducing the nozzle hole diameter may result in an increase in cavitation, leading to higher turbulence and velocities in the nozzle hole. This may result in a better spray breakup which ultimately leads to smaller droplets in the spray.
The trends observed are consistent with other publications reported in the literature (Minami et al., 1990 and Varde, 1991).

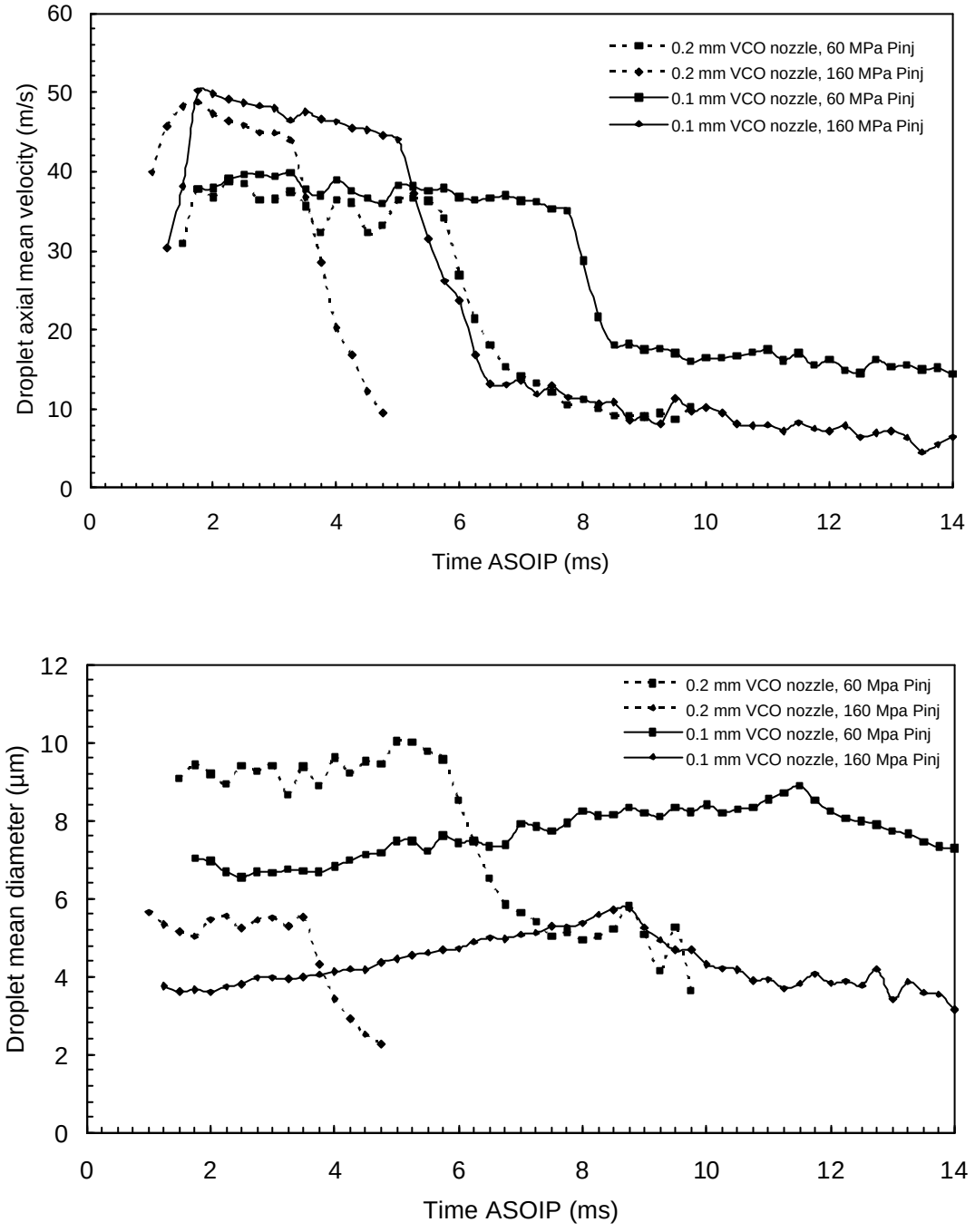

Figure 6-34: Mean droplet axial velocity and diameter profiles for a 0.1 mm and 0.2 mm VCO nozzle at 40 mm from the nozzle on the spray axis for injection pressure ranging from 60 to 160 MPa and an in-cylinder pressure of 4 MPa, 572K TDC temperature.

6.6 Conclusions

High injection pressure had several effects upon the droplet behaviour. They can be briefly summarised as follow:

- The droplet velocity and diameter profiles were shown to be dependent upon the position in the spray (axially and radially), the injection pressure, the in-cylinder pressure and the in-cylinder temperature.
- An increase in droplet velocity was observed when injection pressure or axial distance was increased.
- Increasing the cylinder pressure reduced the droplet velocities and droplet diameters.
- Increasing the cylinder temperature reduced the droplet diameters and increased the droplet velocities.
- The injection pressure effect upon the droplet diameter showed similar trend to those reported in the literature.

7 CONCLUSION AND SUGGESTIONS FOR FURTHER WORK

7.1 Conclusion

An experimental study on the Diesel spray characteristics was performed with an advanced direct injection system (common rail injection system). High speed photography was employed to record the transient high injection pressure Diesel sprays in a rapid compression machine (Proteus). For the study of the spray, the images taken with a high speed video camera were processed and analysed. The results include the analysis of the time delay, the initial spray hesitation, the spray characteristics at the end of the injection and the spray tip penetration of different types of nozzle.

The effects of the phase Doppler anemometry setting parameters were studied and tailored to allow the measurements of dense Diesel sprays. The effects of injection and cylinder pressures and cylinder temperature on the droplet behaviour were using phase Doppler anemometry.

This investigation found the following:

- A study of the PDA system parameters (laser power, photomultiplier voltage and measurement volume size) is required to tailor the system to the measurement of dense sprays.
- The photomultiplier voltage, the laser power and the size of measurement volume all show significant effects on measured droplet diameters.
- The droplet velocity and diameter profiles were shown to be dependent upon the position in the spray (radially and axially), the injection and in-cylinder pressures. An increase in mean droplet velocity was seen when the injection pressure or axial distance from the nozzle was increased.
- Increasing the cylinder pressure reduced the droplet velocities.
- Increasing the injection and cylinder pressures improved the spray atomisation.

7.1.1 High injection pressure Diesel spray characteristics

Varying the injection pressure from 60 MPa to 160 MPa influenced the injection delay. However, the injection delay was independent from in-cylinder charge density and nozzle type. The spray characteristics at the end of injection were shown to be strongly dependent upon nozzle hole dimensions and geometry (VCO or mini-sac nozzle). In the close-up visualisation, liquid ligaments were observed at the end of injection that could affect the engine emission. This phenomenon was caused by the bouncing of the needle.

Variations of spray penetration were observed at different injection and cylinder pressures were attributed to needle eccentricity and variation in hydrodynamic behaviour between each hole.

7.1.2 Phase Doppler anemometry set-up

The Diesel spray of a common rail system proved to be a challenging environment for the PDA measurement. The photomultiplier voltage, the laser power and the size of the measurement volume all show significant effects on the detected droplet diameters. The study of the PDA operating parameters had proved to be necessary to optimise the system for the measurement of dense sprays. The accuracy of the PDA was checked by comparing the spray tip penetration obtained from the high speed video photography.

7.1.3 Injection and cylinder pressures effects on droplet behaviour

PDA measurements of dense sprays proved to be possible only when the measurement volume was moved 30 mm away from the injector nozzle tip. This occurred for the low and high injection pressure measurement. It is probable that the lack of data was due to a high optical dense region. High number density can cause measurement rejections by introducing multiple droplets within the measurement volume, increasing the probability of non-sphericity through droplet-droplet interactions and attenuating PDA beam intensity and signal strength with droplets locating outside the measurements volume.

High injection pressure had several effects upon the droplets behaviour. In comparison with the low injection pressure spray, droplet velocities were typically 35 $m.s^{-1}$ higher than those of the low injection pressure cases. A better spray atomisation was observed at higher injection pressure. The observations made by Ficarella et al. (1997) and Zhou et al. (2000), that the droplet diameter were smaller at higher injection pressure, were corroborated by the results presented in this thesis. Higher air intake temperature also proved to have significant effect on the droplet behaviours as smaller particles were measured. This droplet size reduction was due to evaporation, both in the low and high injection pressure cases.

The droplet velocity and diameter profiles were shown to be dependent upon the location (axially and radially) in the spray. An increase in mean droplet velocity was observed when the axial distance from the nozzle was increased. This was caused by the constant increase of air entrainment along the spray axis. The velocity profiles show that droplets measured on the periphery of the spray have smaller velocities than those measured on the spray axis. Consequently, particles travelling on the edge of the spray were more affected by shear between the air and the spray envelope, generating smaller droplets.

With high velocities due to increased injection pressure, the droplets far from the nozzle were susceptible to aerodynamic break-up. The evolution of the droplet sizes was concluded to be raised by the coalescence of droplets and the evaporation of small ones.

PDA measurements of Diesel sprays showed that reducing the nozzle hole diameter can increase the droplet velocity and reduce the droplet diameter. Reducing the nozzle hole diameter may result in an increase in cavitation, leading to higher turbulence and velocities at the nozzle exit.

7.2 Suggestions for further work

This research highlights several areas for further research. First, the study of the Diesel sprays behaviour for in-cylinder pressures above 6 MPa. The PDA system and especially the photomultipliers used in this study were not capable

of dealing with the light scattered from the droplets at such high cylinder pressure.

The results of this research suggest that the nozzle hole diameter and shape play an important role on the spray and droplet behaviour. Some work in this area has been started (e.g. characterisation of the spray from a 0.1 mm VCO nozzle) and needs to be continued. Further investigations could be conducted, with the phase Doppler anemometry, to study the effect of the nozzle K factor on the droplet behaviour.

Furthermore, a study of the effect of pilot (injection of a small quantity of fuel in the cylinder to precondition the combustion chamber) and staged injection on fuel spray formation could be undertaken. This process has been shown to reduce vehicle emissions, however the exact mechanisms and effect on spray dynamics is not fully understood.

The PDA technique could also be used to analyse the effect of different fuel blends on the spray shape, droplet velocity and size. High-speed photography may also be used to observe the spray.

REFERENCES

Arai, M., Shimizu, M., Hiroyasu, H., (1985) *"Break-Up Length and Spray Angle of High Speed Jet"*, ICLASS-85

Arai, M., Shimizu, M., Hiroyasu, H., (1985) *"Break-Up and Spray Angle of High Speed Jet"*, ICLASS 85, 3rd International Conference on Liquid Atomisation and Spray Systems

Araneo, L., Coghe, A., (2002) *"Effect of Injection Conditions on Penetration and Drop Size of HCCI Diesel Sprays"*, THIESEL, Conference on Thermo- and Fluid Dynamic Processes in Diesel Engines

Araneo, L., Tropea, C., (2000) *"Improving Phase Doppler Measurements in a Diesel Spray"* SAE Paper 2000-01-2047

Arcoumanis, C., Cossali, E., Paal, G., Whitelaw, J. H., (1990) *"Transient Characteristics of Multi-Hole Diesel Sprays",* SAE Paper 900480

Arcoumanis, C., Gavaises, M., French, B., (1997) *"Effect of Fuel Injection Processes on the Structure of Diesel Sprays",* SAE Paper 970799

Arcoumanis, C., Whitelaw, J. H., (2000) *"Is Cavitation Important in Diesel Engine Injectors?",* THIESEL 2000, Thermofluidynamic Processes in Diesel Engine, pp. 57-66

Bachalo, W. D., (1994) *"The Phase Doppler Method: Analysis, Performance Evaluations, and Applications"*, Particle & Particle Systems Characterization, v 11, n 1, p 73-83

Bachalo, W. D., (2000) *"Spray Diagnostics for the Twenty-first Century",* Atomisation and Sprays, vol.10, pp. 439-474

Bachalo, W. D., Houser, M. J., (1984) *"Development of the Phase/Doppler Spray Analyser for Liquid Drop Size and Velocity Characterisations",* Proc. AIIA/SAE/ASME 20th Joint Propulsion Conference, Cincinnati, Ohio

Badock, C., Wirth, R., Fath, A., Leipertz A., (1999) *"Investigation of Cavitation in Real Size Diesel Injection Nozzles",* International Journal of Heat and Fluid Flow, Vol. 20, pp. 538-544

Bae, C. H., Kang, J., (2000) *"Diesel Spray Characteristics of Common-Rail VCO Nozzle Injector"*, THIESEL 2000, Thermofluidynamic Processes in Diesel Engines, pp. 57-66

Baritaud, T. A., Heinze, T. A., Le Coz, J. F. (1994) *"Spray and Self-Ignition Visualisation in a DI Diesel Engine"*, SAE Paper 940681

Birch, S., (1990) *"Fuel Injection: The Inside Story"*, Technical Briefs, Available from www.sae.org

Bosch, R., (1999) *"Diesel-engine management"*, Society of Automotive Engineers Publisher, 2nd edition

Bruneaux, G., Verhoeven, D., Baritaud, T. (1999) *"High Pressure Diesel Spray and Combustion Visualisation in a Transparent Model Diesel Engine"*, SAE Paper 1999-01-3648

Bruneaux, G. (2001) *"Spray Structure in Common Rail Diesel injection System"*, Atomisation and Spray, Vol.1, No.5, pp. 533-556

Cao, Z. M., Nishino, K., Mizuno, S., Torii, K., (2000) *"Spray Structure and Associated Droplet Velocity in the Initial Stage of Diesel Fuel Injection"*, JSME International Journal, Series B, Vol. 43, No. 4, pp. 582-589

Chang, C. T., Farrel, P.V., (1997) *"A Study on the Effects of Fuel Viscosity and Nozzle geometry on High Injection Pressure Diesel Spray Characteristics",* SAE Paper 970353

Chigier, N., (1993) *"Spray Science and Technology",* Fluid Mechanics and Heat Transfer in Sprays, FED-Vol. 178/HTD-Vol. 270, pp 1-18, ASME 1993

Crua, C. (2002) *"Combustion Processes in a Diesel Engine"*, Ph. D. Thesis, University of Brighton, U. K.

DANTEC, 2001, BSA Flow Software Guide

Dec, J. (1997) *"A Conceptual Model of DI Diesel Engine"*, SAE Paper 970873

Dent, J. C., (1971) *"A Basis for the Comparison of Various Experimental Methods for Studying Spray Penetration",* SAE Paper 710571

Dieselnet (2002), "European emissions legislation for passenger cars", available from www.Dieselnet.com/standards/eu/ld.html

Dodge, L. G., (1984) *"Change of Calibration of Diffraction Based Particle Sizes in Dense Spray"*, Opt. Eng., Vol. 23, No. 5, pp. 626-630

Domann, R., Hardalupas, Y., (2002) *"Quantitative Measurement of Planar Droplet Sauter Mean Diameter in Spray Using Planar Droplet Sizing"*, 11th International Symposium on Application of Laser Techniques to Fluid Mechanics, Lisbon, Portugal

Domnick, J., (1997) *"Some Comments Concerning the State-of-the-art of Phase Doppler Anemometry Applied to Liquid Sprays"*, Proceedings of 13th Annual Conference on Liquid Atomisation and Spay Systems

Dust, F., Melling, A., Whitelaw, J. H., (1981) *"Principles and Practice of Laser-Doppler Anemometry"*, Academic Press, London (2nd edition)

Eckbreth, A. C., (1996) *"Laser Diagnostics for Combustion Temperature and Species"*, Gordon and Breach Publishers (2nd edition)

Elkotb, M. M., (1982) *"Fuel Atomisation for Sprays modelling"*, Prog. Energy Combust. Sci., Vol. 8, pp. 61-91

Faeth, G. M., Hsiang, L. P., Wu, P. K., (1995) *"Structure and Breakup Properties of Sprays"*, International Journal of Multiphase Flow, Vol. 21, pp. 99-127

Farmer, W. M., (1972) *"Measurement of Particle Size, Number Density, and Velocity Using a Laser Interferometer"*, Applied Optics, Vol. 11, No. 44, pp. 2603-2612

Farrar-Khan, J. R., Andrews, G. E., Williams, P. T., (1992) *"Influence of Nozzle Sac Volume on Diesel Spray Droplet Sizes"*, Proceeding of the Institution of Mechanical Engineers, Vol. 206, pp.239-248.

Farrel, P. V., (1999) *"Droplet Sizing in High Pressure High Density Sprays"*, Proceeding of SPIE-The Internal Society for Optical Engineering, Vol. 3783, pp. 274-285.

Farrugia, N. Kanne, S., Greenhalgh, D. A., (1995) *"Three Pulses Digital PIV"*, Opt. Lett., Vol. 20, No. 17, pp. 1827-1829.

Faure, M. A., (1997) *"Particle Image Velocimetry Measurements of In-Cylinder Flows"*, Ph. D. Thesis, University of Brighton, U. K.

Felton, P. G., (1978), *"In-stream Measurement of Particle Size Distribution"*, Computer Physics Communication, v. 1

Ficarella, A., Laforgia, D., (1998) *"Experimental and Numerical Investigation on Cavitating Flows in Diesel Injection Systems"*, Meccanica, v 33, n 4, p 407-425

Ficarella, A., Laforgia, D., Starace, G., Damiani, V., (1997) *"Experimental Investigation of the Sprays of an Axi-Symmetric Nozzle of a Common-Rail High Pressure Electro-Injector"*, SAE Paper 970054

Fujimoto, H., Tanaka, T., Ashida, K., Yeom, J. K., Senda, J., (2000) *"Flow Characterisations inside Liquid Phase in an Evaporating Spray by means of PIV"*, 10th International Symposium on Applications of Laser Techniques to Fluid Mechanics, Lisbon

Grehan, G., Gouesbet. G., Naqwi. A., Durst. F., (1993) *"Trajectory Ambiguities in Phase Doppler Systems: Study of a Near Forward and a Near Backward Geometry"*, Particle & Particle Systems Characterization, v 11, n 1, p 133-144

Gülder, O. L. (1994) *"Transmission and Tomographic Analysis of the Internal Structure of the Transient and Dense Diesel Sprays"*, International Symposium on Advanced Spray Combustion, Hiroshima, Japan

Gupta, S., Poola, R., Sekar, R., (2000) *"Injection Parameter Effects on Diesel Spray Characteristics"*, SAE Paper 2000-01-1626

Hao, L., Fushui, L., Yulin, L., Jumei, S., (1999) *"Study of Diesel Spray Particle Velocity Field Using a Particle Image Velocimetry Set-up"*, Journal of Beijing Institute of Technology, vol. 8, No. 2, pp. 201-206

Hardalupas, Y., Taylor, A. M. K. P., Whitelaw, J. H., (1992) *"Characteristics of the Spray from a Diesel Injector"*, International Journal of Multiphase Flow, Vol. 18, No.2, pp. 159-179

Hardalupas, Y., Liu, C. H., (1997) *"Implications of the Gaussian Intensity Distribution of Laser Beams on the Performance of the Phase Doppler Technique Sizing Uncertainties"*, Progress in Energy and Combustion Science, v 23, n 1, pp. 41-63

Hattori, H., Naruyima, K., Tsue, M., Kadota, T., (2002) *"Photographical Analysis of the Initial Breakup Process of Diesel Spray"*, THIESEL 2002, Conference on Thermo- and Fluid-Dynamic Process in Diesel Engines.

Hay, N., Jones, P. L., (1972) *"Comparison of the Various Correlations for Spray Penetration"*, SAE Paper 720776

Hiroyasu, H., Kadota, T., (1974) *"Fuel Droplet Size Distribution in Diesel Combustion Chamber"*, SAE Paper 740715

Hiroyasu, H., Arai, M., (1990) *"Structures of Fuel Sprays in Diesel Engines"*, SAE Paper 900475

Hiroyasu, H., (1998) *"The Structure of Fuel Sprays and he Combustion Processes in Diesel Engines"*, American Society of Mechanical Engineers, Internal Combustion Engine Division (Publication) ICE, v 31, n 1, pp. 3-15

Hosoya, H., Obokata, T., (1993) *"Effect of Nozzle Configuration on Characteristics of Steady-State Diesel Spray"*, SAE Paper 930593

Huh, J. C., Lee, G. Y., Yang, O. Y., (1991) *"An experimental Study on Initial Behaviour of Diesel Fuel Spray Characteristics",* Proc. ICLASS 91, Nat. Inst. Standards Technology, pp. 283-290

Jawad, B. A., (1997) *"Effect of Injection Pressure on Spray Atomisation",* ASME Fluids Engineering Division Summer Meeting, FEDSM97-3106, pp. 1-8

Jeong, D. Y., Park, S. J., Lee, J. T. (2003) *"An Analysis on the Suitable Injection Pressure of Diesel Injection with High Pressure"*, 9th International Conference on Liquid Atomisation and Spray Systems, Sorrento, Italy

Jimenez, J., Castro, F., Tinaut, F., Gimenez, B., (2000) *"The Tip Evolution of an Evaporative Intermittent Fuel Spray"*, THIESEL 2000, Thermofluidynamic Processes in Diesel Engines, pp. 67-74.

Jones, A. R., (1977) *"A Review of Drop Size Measurement-The Application of Techniques to Dense Fuel Sprays"*, Prog. Energy Combust. Sci., Vol. 3, pp. 225-234.

Kato, T., Tsujimara, K., Shintani, M., Minami, T., Yamaguchi, L., (1989) *"Spray Characteristics and Combustion Improvement of a D.I. Diesel Engine with High Pressure Fuel Injection"*, SAE Paper 890265.

Kennaird, D., Crua, C., Heikal, M., Morgan, R., Bar, F., Sapsford, S., (2000) *"A New High-Pressure Diesel Spray Research Facility"*, International Conference on Computational and Experimental Methods in Reciprocating Engines, C587/040/2000, pp.179-188.

Kennaird, D. A., Crua, C., Lacoste, J., Heikal, M., Gold, M. R., Jackson, N. S., (2002) *"In-Cylinder Penetration and Break-Up of Diesel Sprays Using a Common-Rail Injection System"* SAE Paper 2002-01-1626.

Kneer, R., Will mann, M., Scheider, M., Hirleman, D., Koch, R., Wittig, S. (1994) *"Theoretical Studies on the Influence of Refractive Index Gradients within Multicomponent Droplets on Size Measurements by Phase Doppler Anemometry"*, ICLASS-94, Paper IV-10, pp.451-458.

Koo, J. H., Hong, S. T., Shakal, J. S., Goto, S., (1997) *"Influence of Fuel Injector Nozzle Geometry on Internal Flow Characteristics",* SAE Paper 970354.

Koo, J. Y., Martin J. K., (1990) *"Droplet Sizes and Velocities in a Transient Diesel Fuel Spray"*, SAE Paper 900397.

Koo, J. Y., Martin J. K., (1991) *"Comparison of Measured Drop Sizes and Velocities in a Transient Fuel Spray with Stability Criteria and Computed PDF's"*, SAE Paper 910179.

Lacoste, J., Crua, C., Heikal, M., Kennaird, D., Gold, M. (2003) *"PDA Characterisation of Dense Diesel Sprays Using a Common-Rail Injection System"*, SAE Paper 2003-01-3085

Lefebvre, A. H., (1989) *"Atomisation and Sprays"*, Taylor and Francis.

Le Gal, P. Farrugia, N., Greenhalgh, D. A., (1999) *"Laser Sheet Dropsizing of Dense Sprays"*, ELSEVIER, Optics & Laser Technology, vol. 31, pp. 75-83.

Levy, N., Amara, S., Champoussin, J. C., Guerrassi., (1997) *"Non-Reactive Diesel Spray Computations Supported by PDA Measurements"*, SAE Paper 970049.

Mimani, T., Yamaguchi, I., Tsujimura, K., Suzuki, T., (1990) *"Analysis of Fuel Spray Characteristics and Combustion Phenomena under High Pressure Fuel Injection",* SAE Paper 900438.

Morgan, R., Wray, J., Kennaird, D., Crua, C. Heikal, M. (2001), *"The Influence of Injector Parameters on the Formation and Break-Up of a Diesel Spray"*, SAE Paper 2001-01-0529

Mugele, R., Evans, H. D., (1951) *"Droplet Size Distribution in Sprays"*, Ind. Eng. Chem., Vol. 43. No. 6, pp. 1317-1324.

Naber, J. D., Siebers, D. L., (1996) *"Effects of Gas Density and Vaporization on Penetration and Dispersion of Diesel Sprays"*, SAE Paper 960034.

Naqwi, A., Durst. F., Kraft. G., (1991) "Sizing of Submicrometer Particles Using a Phase-Doppler System", Applied Optics, vol. 30, No. 33, pp. 4903-4913.

Payri, F., Desantes, J. M., Arrègle, J., (1996) *"Characterization of D.I. Diesel Sprays in High Density Conditions"*, SAE Paper 960774.

Pitcher, G., Wigley, G., (1994) *"Two Component Velocity and Size Measurements for a Non-Combusting Fuel Spray in a Diesel Swirl Combustion*

Chamber", Sixth International Conference on liquid atomisation and spray system, Rouen, France.

Pitcher, G., Wigley, G., Saffman, M., (1990) *"Velocity and Drop Size Measurement in Fuel Sprays in a Direct Injection Diesel Engine"*, Particle & Particle Systems Characterization, v 7, p 160-168.

Pitcher, G., Wigley, G., (1991) *"The Droplet Dynamics of Diesel Fuel Sprays under Ambient and Engine Conditions"*, ASME, Vol. 2, pp. 571-586.

Reitz, R. D., Diwakar, R., (1987) *"Structure of High-Pressure Fuel Sprays"* SAE Paper No. 870598.

Sankar, S. V., Bachalo, W. D., (1991) *"Response Characteristics of the Phase Doppler Particle Analyser for Sizing Spherical Particles Larger that the Light Wavelength"*, Applied Optics, Vol. 30, No. 12, pp. 1487-1496.

Sankar, S. V., Weber, B. J., Kamemoto, D. Y., Bachalo, W. D., (1991) *"Sizing Fine Particles with the Phase Doppler Interferometric Technique"*, Applied Optics, Vol. 30, No. 33, pp. 4914-4920.

Sankar, S. V., Maher, K. E., Robart, D. M., Bachalo, W. D., (1999) *"Rapid Characterisation of Fuel Atomisers Using an Optical Patternator"*, Journal of Engineering for Gas Turbines and Power, vol. 21, pp. 409-414.

Sanchez, M. L., Castro, F., Tinaut, F. V., Melgar, A., (2000) *"Considerations on the Gas-Phase Velocity Field in a Non-evaporating Diesel Spray"*, Atomisation and Sprays, vol.10, pp.529-543.

Schneider, M., Dan Hirleman, E., (1994) *"Influence of Internal Refractive Index Gradients on Size Measurements of Spherically Symmetric Particles by Phase Doppler Anemometry"*, Applied Optics, Vol. 33, No. 44, pp. 2379-2388.

Shimizu, M., Arai, M., Hiroyasu, H., (1984) *"Measurements of Breakup Length in High Speed Jet"*, Bulletin of JSME, Vol. 27, No. 230, pp. 1709-1715.

Smallwood, G. J., Gülder, O. L., (2000) *"Views on the Structure of Transient Diesel Sprays"*, Atomisation and Sprays, vol. 10, pp. 355-386.

Soteriou, C., Andrews, R., Smith, M., (1995) *"Direct Injection Diesel Sprays and the Effect of Cavitation and Hydraulic Flip on Atomisation",* SAE Paper 950080.

Su, T. F., El-Beshbeeshy, M. S., Corradini, M. L., Farrell, P. V., (1995) *"Light Extinction Method on High-Pressure Diesel Injection"*, Proceedings of SPIE - The International Society for Optical Engineering, v 2546, p 490-501.

Tabata, M., Fujii, H., Arai, M., Hiroyasu, H., (1991) *"Mean Drop Diameter of a Diesel Spray in a Vaporizing process",* JSME International Journal, Series II, Vol. 34, No.3, pp 369-378.

Tamaki, N., Shimizu, M., Nishida, K., Hiroyasu, H., (1998) *"Effects of Cavitation and Internal Flow on Atomisation of a Liquid Jet"*, Atomisation and Sprays, vol. 8, pp. 179-197.

Tropea, C., (1995) *"Laser Doppler Anemometry: Recent Developments and Future Challenges"*, Measurement Science Technology, vol.6, pp. 605-619.

Varde, K. S., (1991) *"Effects of Injection Parameters on Droplet Sizes in a High Pressure, Intermittent Diesel Spray",* SAE Paper 912458.

Warrick, C. B., Su, T. F., Farrel, P.V., (1996) *"Temperature Effects on Fuel Sprays from a Multi-Hole Nozzle Injector",* SAE Paper 962005.

Whitelaw, J., Payri, F., Desantes, J. M., (2001) *"Thermo and Dynamics Processes in Diesel Engines"*, Experiments on Applicability of Different Laser Diagnostics, Springer.

Wigley, G., Pitcher, G., (1997) *"The Effect of Fuel Line Pressure and Injection Duration on Diesel spray Formation and Structure"*, Proc ILASS-98, pp.83-88.

Yeh, Y., Cummins, H. Z., (1964), Applied Physics Letters, vol. 4, pp. 176-178.

Yoda, T., Tsuda, T., (1997) *"Influence of Injection Nozzle Improvement on DI Diesel Engine"*, SAE Paper 970356.

Yule, A. J., Filipovic, I., (1991) *"Correlations for Diesel Spray Penetration Including the Effect of the Break-Up Zone",* Proc. ICLASS-91, Nat. Inst. Standards Technology, pp. 267-274.

Yule, A. J., Filipovic, I., (1992) *"On the Break-Up Lengths of Diesel Sprays",* International Journal of Heat and Fluid Flow, vol. 10, No. 2.

Yule, A. J., Salters, D. G., (1995) *"On the Distance Required to Atomise Diesel Sprays Injected from the Orifice-Type Nozzles"*, Proceeding of the Institution of Mechanical Engineers, vol. 209, pp.217-226.

Zhou, P., Wang, Y., Roskilly, A. P., (2000) *"An Investigation of Droplet Size and Velocity in DI Diesel Sprays Using Laser PDA and Mathematical Regression Technique"*, International Maritime Technology, vol. 112, n 3-4, pp 103-113.

PAPERS PUBLISHED BY THE AUTHORS

Journals

Lacoste, J., Crua, C., Kennaird, D., Heikal, M., Gold, M. (2003) *"PDA Characterisation of Dense Diesel Sprays Using a Common-Rail Injection System"* SAE 2003-01-3085, Journal of Fuels and Lubricants

Conferences

Kennaird, D.A., Crua, C., Lacoste, J., Heikal, M.R., Gold, M.R., Jackson, N.S., (2002) *"In-Cylinder Penetration and Break-Up of Diesel Sprays Using a Common-Rail injection System"*, *SAE 2002 Spring Fuels & Lubricants Meeting*, Reno, USA, 6-9 May 2002, SAE paper no. 2002-01-1626.

Laguitton, O., Gold, M., Kennaird, D., Crua, C., Lacoste, J., Heikal, M., (2002) *"Spray Development and Combustion Characteristics for Common Rail Diesel Injection Systems"*, Fuel Injection Systems, I.Mech.E. Conference transactions, London, UK, 26-27 November 2002.

Lacoste, J., Kennaird, D., Begg, S., Heikal, M. (2002) *"Phase Doppler Anemometry Measurements of a Diesel Spray"*, Total Vehicle |Technology conference, University of Sussex 11-12 Nov 2002

Lacoste, J., Crua, C., Kennaird, D., Heikal, M., Gold, M. (2003) *"PDA Characterisation of Dense Diesel Sprays Using a Common-Rail Injection System"* SAE 2003-01-3085, SAE Powertrain & Fluid Systems Conference & Exhibition, October 2003, Pittsburgh, PA, USA,